Universidad Autónoma de Madrid
Departamento de Física Teórica
Instituto de Física Teórica UAM-CSIC

The Quest for the Origin of Neutrino Masses

Memoria de Tesis Doctoral realizada por
Josu Hernández García,
presentada ante el Departamento de Física Teórica
de la Universidad Autónoma de Madrid
para la obtención del Título de Doctor en Ciencias.

Tesis dirigida por el
Investigador Enrique Fernández Martínez,
del Departamento de Física Teórica
y miembro del Instituto de Física Teórica, IFT-UAM/CSIC
de la Universidad Autónoma de Madrid.

Madrid, 26 de junio de 2017

Contents

Resumen y Motivaciones

La gran mayoría de procesos físicos fundamentales pueden describirse a través de unas pocas "piezas de contrucción": las partículas elementales, cuyas interacciones están gobernadas por cuatro fuerzas. El Modelo Estándar de Física de Partículas (SM) es el marco teórico que describe estas partículas elementales y tres de las cuatro fuerzas. Las tres fuerzas fundamentales descritas por el SM son el electromagnetismo, la fuerza débil y la fuerza fuerte. La gravedad, la más débil de las cuatro fuerzas, no está descrita por el SM. Desarrollado a principios de los años 70 [1–5], el SM ha predicho una amplia variedad de fenómenos que han sido testados experimentalmente hasta una increíble precisión de 10^{-8}.

La última pieza del SM en ser esclarecida ha sido el mecanismo que está detrás del origen de las masas de los bosones de gauge Z y $W^{\pm}$ que median las interacciones débiles, así como las masas de la mayoría de constituyentes elementales del SM. El mecanismo de ruptura de la simetría electrodébil (EWSB) también conocido como mecanismo de Higgs [6–8] proporciona un marco consistente para explicar dichas masas observadas empíricamente. El mecanismo de Higgs también predice la existencia de una partícula escalar, el denominado bosón de Higgs, que finalmente fue descubierto en 2012 por los experimentos de ATLAS [9] y CMS [10] del Gran Colisionador de Hadrones (LHC) en el CERN.

Sin embargo, todavía hay algunos problemas que no se explican con el SM y que representan nuestra mejor ventana hacia una teoría más fundamental de la Naturaleza. Uno de estos problemas sin resolver, que implica que el contenido de partículas del SM está incompleto, es la evidencia de Materia Oscura (DM). Varias observaciones tales como las lentes gravitacionales, las curvas de rotacíon de galaxias, o las medidas del Fondo Cósmico de Microondas (CMB) por WMAP [11] y Planck [12] apuntan hacia la existencia de una nueva especie de materia no bariónica en el SM.

La asimetía bariónica observada en el Universo (BAU) [12] es otra evidencia de la existencia de una teoría fundamental subyacente más allá del SM. Esta asimetría entre materia y antimateria podría haber sido generada dinámicamente en el Universo primitivo a través de procesos que violan el número bariónico B. Este fenómeno se conoce como bariogénesis [13]. Las condiciones de Sakharov [14] necesarias para crear la asimetría bariónica son: interacciones que violen B, violación de las simetrías C y CP, y desviación del equilibrio térmico. Sin embargo, el SM por sí mismo no produce la suficiente violación de CP necesaria para explicar la asimetría bariónica observada [15], y la transición de fase EW no es suficientemente fuerte como para bariogénesis EW [16].

Finalmente, los experimentos con neutrinos solares [17–34], con neutrinos atmosféricos [35–45], con neutrinos producidos en reactores [46–50], y con neutrinos producidos en aceleradores y detectados a largas distancia [51–59], indican que el cambio de sabor neutrínico a través del fenómeno de oscilación de neutrinos, está causado por masas de neutrinos no nulas y mezcla leptónica. Las evidencias experimentales muestran que, al menos, dos de los autoestados de masa de los neutrinos tienen que ser masivos y no degenerados. Sin embargo, el SM no puede explicar estas masas a través del mecanismo de Higgs debido a que los neutrinos dextrógiros no forman parte de su contenido de partículas. Además, la pequeñez de la masa de los neutrinos hace que el origen del patrón de las masas y mezclas de todos los fermiones sea aún más fascinante. En el SM, los quarks y leptones cargados obtienen sus masas a través de las interacciones de Yukawa con el bosón de Higgs. Por lo tanto, los correspondientes acoplos de Yukawa son "números fijados" de forma que reproduzcan las masas de las partículas medidas. Estos números van desde $\sim \mathcal{O}(10^{-6})$ para el Yukawa del electrón (o $\sim \mathcal{O}(10^{-12})$ si los neutrinos son partículas de Dirac) hasta $\sim \mathcal{O}(1)$ para el Yukawa del top. Hoy en día, no se ha encontrado una explicación teórica para esta distribución de Yukawas ni para el sorprendente desigual patrón de la mezcla de quarks y leptones. A este problema se le refiere comúnmente como rompecabezas del sabor.

Es más, la existencia de Nueva Física acarrea otro problema teórico, la inestabilidad de la masa del bosón de Higgs bajo correcciones radiativas de la posible Nueva Física a una escala de energías Λ grande, conocido como problema de las jerarquías [60]. Debido a que éstas correcciones a la masa escalar M_h^2 van con Λ^2, la masa del bosón de Higgs podría obtener correcciones radiativas enormes si la escala de la Nueva Física está considerablemente por encima de la escala electrodébil (EW). Por ello, con el fin de reproducir el valor de $M_h \sim 126$ GeV medido, se requiere una

cancelación muy precisa entre el valor de la masa a nivel árbol y las contribuciones de los loops. Otros problemas teóricos que surgen del SM incluyen el problema CP fuerte, la Energía Oscura o Unificación, y que también dan a entender la existencia de una teórica subyacente más fundamental.

Actualmente hay un gran esfuerzo diseñando y construyendo experimentos de física de partículas de alta tecnología para búsqueda de Nueva Física en las dos posibles fronteras. Los experimentos en la Frontera de Energía exploran las partículas elementales en colisionadores. Los experimentos de ATLAS y CMS están poniendo las cotas a búsquedas directas más actualizadas con las colisiones protón-protón a $\sqrt{s} = 14$ TeV en el LHC. Los experimentos en la Frontera de Intensidad o Precisión usan haces de partículas muy intensos y detectores de sensitividad muy alta para explorar partículas que interaccionan poco, procesos que violan sabor leptónico (LFV), así como violación de CP en los sectores de quarks y leptones. Los experimentos de oscilaciones de neutrinos como NOνA, IceCube y T2K, los experimentos de detección de DM como XENON1T, LUX, CDMS, o los experimentos de sabor tales como LHCb, Belle, MEG or Mu2e obtienen actualmente las medidas de mayor precisión de los distintos procesos.

De entre los problemas sin resolver del SM, las únicas evidencias experimentales de Nueva Física que existen son las masas de los neutrinos distintas de cero, la observada BAU, y la existencia de DM que el SM no puede acomodar. En concreto, esta tesis se centrará en ciertas consecuencias fenomenológicas de las extensiones del SM capaces de explicar las masas de los neutrinos y las mezclas observadas, con el fin de probar su existencia.

Debido a que el SM fue formulado con el contenido mínimo de partículas para explicar los fenómenos observados, y a que para entonces no había evidencias experimentales de la existencia de masas para los neutrinos, no se incluyeron neutrinos dextrógiros (ni ninguna otra posible partícula extra necesaria para generar las masas de los neutrinos). Consecuentemente, el contenido de partículas del SM debe ser ampliado. Varias extensiones del SM capaces de explicar las masas de los neutrinos, requieren la incorporación de neutrinos dextrógiros. En estas extensiones, los neutrinos adquieren masas de Dirac después de la EWSB vía interacciones de Yukawa con el bosón de Higgs. Sin embargo, el patrón de masas de neutrinos observado experimentalmente, pone una cota a estos acoplos de Yukawa $\sim \mathcal{O}(10^{-12})$. Esta supresión forzada de los acoplos de Yukawa de los neutrinos, comparada con aquellos del resto de fermiones del SM, sugiere que el mecanismo detrás del origen de la masa de los neutrinos sea distinto al mecanismo de Higgs. Además, como los neu-

trinos dextrógiros son singletes bajo todo el grupo de simetría de gauge del SM; un término de masa Majorana para estos fermiones está permitido en el Lagrangiano. Debido a que esta nueva escala no está relacionada con el mecanismo de Higgs, ni con ninguna otra escala fundamental del SM, podría ser mucho más grande que la escala EW. En concreto, si la escala de Majorana es suficientemente alta, entonces la pequeñez de las masas observadas de los neutrinos se vuelve natural, debido a la supresión de esta escala de masa de Majorana tan grande, en el denominado mecanismo del Seesaw [61–77]. En el SM ampliado con sólo tres neutrinos masivos, la matriz de mezcla que relaciona los autoestados de masa y de sabor, y que explica la oscilación de neutrinos, se denomina matriz de Pontecorvo-Maki-Nakagawa-Sakata (PMNS). La matriz PMNS es por lo tanto la matriz de mezcla leptónica que aparece en las interacciones de corrientes cargadas (CC), en analogía a la matriz de mezcla de Cabibbo-Kobayashi-Maskawa (CKM) del sector de los quarks. Otra consecuencia de aumentar el contenido de neutrinos con neutrinos de Majorana es que la matriz de mezcla es ampliada. Como consecuencia, el sub-bloque 3×3 de la matriz de mezcla que corresponde a la mezcla de los neutrinos levógiros, el cual interviene en las interacciones de CC, deja de ser unitaria. Por lo tanto, estas desviaciones de la unitariedad de la matriz de mezcla leptónica pueden usarse para testar la mezcla de los neutrinos pesados.

En la presente tesis se ha estudiado la no unitariedad de la matriz de mezcla leptonica después de incluir neutrinos dextrógiros adicionales, con el fin de explicar las masas observadas de los neutrinos. Se ha derivado el conjunto de cotas más riguroso, actualizado, y general sobre la mezcla de los neutrinos pesados (con masas por encima de la escala EW) del Seesaw con los leptones cargados a través de un ajuste global a los datos actuales de medidas de sabor y medidas de precisón electrodébiles. Dos escenarios distintos han sido explorados y comparados: un escenario completamente general donde un número arbitrario de neutrinos dextrógiros pesados son tratados desde la teoría efectiva, sin ninguna otra suposición, y otro escenario más constreñido en el cual sólo son considerados tres estados pesados adicionales. Las suposiciones del segundo escenario implican correlaciones no triviales con el fin de reproducir el patron de masas y mezclas observado en experimentos de oscilaciones de neutrinos. El conjunto de procesos relevantes analizados en el ajuste global incluye: búsquedas de desintegraciones con LFV, test de universalidad de interacciones débiles, cotas de unitariedad de la CKM, y medidas de precisión electrodébiles. En concreto, se ha realizado un estudio exhaustivo y comparativo de la sensitividad actual y futura de los diferentes experimentos de búsqueda de desintegraciones con

LFV.

Además, las partículas pesadas con acoplos de Yukawa grandes pueden inducir correcciones radiativas relevantes. Por ello, se ha estudiado la importancia de las correcciones de orden superior, que vienen de los loops de neutrinos dextrégiros, cuando se derivan las cotas de su mezcla con los estados ligeros. Para el análisis se ha elegido el escenario con tres singletes pesados adicionales y con una simetría $B-L$ aproximada. Las expresiones a 1-loop de los observables dominantes usados en el ajuste global han sido calculadas y normalizadas. Todas la amplitudes a 1-loop y los contratérminos necesarios para su renormalización han sido calculados para esta tesis. Se ha abordado la posible cancelación entre las correcciones a nivel loop y las contribuciones a nivel árbol a la no unitariedad de la matriz de mezcla leptónica, y se ha discutido el impacto en las cotas derivadas a través del ajuste global tras incluir dichas correcciones.

Finalmente, se ha estudiado el impacto en las probabilidades de oscilación de los neutrinos cuando el SM es extendido con neutrinos dextrógiros. Las manifestaciones fenomenológicas de estas extensiones son distintas dependiendo de si los neutrinos adicionales son accesibles cinemáticamente o no. Como resultado, se han abordado dos escenarios distintos, con neutrinos dextrógiros ligeros (por debajo de la masa del π) y con neutrinos pesados (por encima de la masa del π), respectivamente. Se han explorado las diferencias y similitudes entre el impacto en la búsqueda de oscilaciones de neutrinos de los dos escenarios, y ambos límites han sido descritos en el práctico lenguaje de las interacciones no estándar (NSI). Para finalizar, se han comparado las cotas de los dos escenarios con las sensitividades esperadas en un experimento futuro de oscilación de neutrinos, tomando la propuesta de DUNE como punto de referencia para la discusión. Para neutrinos por encima de la escala EW, las cotas derivadas en la primera parte de esta tesis aplican; y por lo tanto, el impacto de estos neutrinos pesados adicionales en experimentos de oscilaciones queda limitado.

Esta tesis se organiza de la siguiente manera. En el Capítulo 1 se introduce el SM. También se discute el fenómeno de oscilación de neutrinos, y por qué su descubrimiento implica la existencia de neutrinos masivos no degenerados y mezcla leptónica no nula. Finalmente, se hace un resumen de las extensiones del SM capaces de acomodar las masas de los neutrinos, con especial énfasis en el Seesaw Tipo I. Los siguientes capítulos contienen el trabajo principal de esta tesis, el cual está basado en los resultados publicados en los artículos [78], [79], y [80]. En el Capítulo 2, se realiza el ajuste global a los datos actuales de medidas de sabor y medidas de precisión electrodébiles, y se derivan las cotas generales a la no unitariedad de la matriz de mezcla

leptónica. En el Capítulo 3, se estudia la importancia de las correcciones a 1-loop de los neutrinos dextrógiros pesados cuando se derivan las cotas a su mezcla a través de un ajuste global. En el Capítulo 4 se estudia el impacto en las búsquedas de oscilaciones de neutrinos cuando el SM es extendido con neutrinos dextrógiros, tomando para el análisis la propuesta de DUNE como punto de referencia. Finalmente, el capitulo *Conclusiones y Perspectivas* resume las conclusiones más importantes del presente trabajo. Tambin se resaltan las contribuciones de esta tesis a la situación actual del área de investigación, y se presenta una discusión sobre cómo arrojar luz sobre los actuales problemas sin resolver del SM, y por lo tanto cómo progresar en la comprensión de la teoría fundamental subyacente más allá del SM.

Overview and Motivations

Most fundamental physical processes can be described though a few building blocks: the elementary particles, whose interactions are governed by four forces. The Standard Model of Particle Physics (SM) is the theoretical framework that describes these elementary particles and three of the four forces. The three fundamental forces accounted for by the SM are electromagnetism, the weak and the strong forces. Gravity, the weakest of the four forces, is not described by the SM. Developed in the early 1970s [1–5], the SM has predicted a wide variety of phenomena that have been tested experimentally to an incredible precision of 10^{-8}.

The last piece of the SM to be clarified was the mechanism behind the origin of the observed masses of the Z and $W^{\pm}$ gauge bosons that mediate the weak interactions, as well as the masses for most of the elementary constituents of the SM. The mechanism of electroweak symmetry breaking (EWSB) also known as the Higgs mechanism [6–8] provides a consistent framework to explain these masses. It also predicted the existence of a physical scalar particle, the so-called Higgs boson, that was finally discovered in 2012 by the Large Hadron Collider (LHC) ATLAS [9] and CMS [10] experiments at CERN.

Nevertheless, there are still some open problems which are not explained by the SM and that represent our best window to a more fundamental theory of Nature. One of these problems, which implies that the SM particle content is incomplete, is the evidence for Dark Matter (DM). Several observations such as gravitational lensing, rotation curves of galaxies or measurements of the Cosmic Microwave Background (CMB) by WMAP [11] and Planck [12] point to the existence of a new species of non-baryonic matter not presented in the SM.

The observed baryon asymmetry of the Universe (BAU) [12] is another evidence of a more fundamental underlying theory beyond the SM. This matter-antimatter asymmetry could be dynamically generated in the early Universe via processes that

violate baryon number B. This phenomenon is known as baryogenesis [13]. The necessary Sakharov conditions [14] to create the baryon asymmetry are: $B-$violating interactions, violation of the C and CP symmetries, and departure from thermal equilibrium. However, the SM itself does not provide the sufficient CP violation as to explain the observed baryon asymmetry [15], and the EW phase transition is not strong enough for EW baryogenesis [16].

Finally, experiments with solar [17–34], atmospheric [35–45], reactor [46–50], and long-baseline accelerator [51–59] neutrinos indicate that neutrino flavor change through the neutrino oscillation phenomenon is caused by non-zero neutrino masses and lepton mixings. The experimental evidences show that at least two of the three neutrino mass eigenstates have to be massive and non-degenerate. However, the SM cannot account for these masses through the Higgs mechanism since right-handed neutrinos are not included in its particle content. Moreover, the smallness of neutrino masses makes the origin of the pattern of all fermion masses and mixings even more intriguing. In the SM, quarks and charged leptons obtain their masses trough the Yukawa interaction with the Higgs boson. Therefore, the corresponding Yukawa couplings are "fixed numbers" tuned so as to reproduce the measured masses of the particles. These numbers range from $\sim \mathcal{O}(10^{-6})$ for the electron Yukawa (or $\sim \mathcal{O}(10^{-12})$ if neutrinos are Dirac particles) to $\sim \mathcal{O}(1)$ for the top Yukawa. Nowadays, no theoretical explanation is found for these Yukawa ordering nor for the strikingly dissimilar pattern of quark and lepton mixings. This problem is commonly dubbed flavor puzzle.

Furthermore, the existence of New Physics carries another theoretical problem, the instability of the mass of the Higgs boson under radiative corrections from possible New Physics at a high energy scale Λ, known as the hierarchy problem [60]. Since these corrections to the scalar mass M_h^2 go with Λ^2, the mass of the Higgs boson would get huge radiative corrections if the scale of New Physics is significantly above the electroweak (EW) scale. Therefore, in order to reproduce the measured $M_h \sim 126$ GeV, a fine-tuned cancellation between the tree level mass and the loop contributions is required. Other theoretical problems that arise from the SM include the strong CP, Dark Energy or Unification, and also hint to the existence of a underlying more fundamental theory.

Nowadays, there is a huge effort designing and building high-technology particle physics experiments to look for New Physics at the two possible frontiers. Experiments at the Energy Frontier explore elementary particles at colliders. ATLAS and CMS experiments are setting the most updated bounds on direct searches with

$\sqrt{s} = 14$ TeV proton-proton collisions at LHC. The Intensity or Precision Frontier experiments use very intense particle beams and highly sensitive detectors to explore rarely interacting particles, lepton flavor violating (LFV) processes, as well as CP violation in the lepton and quark sectors. Neutrino oscillation experiments such as NOνA, IceCube and T2K, DM detection experiments like XENON1T, LUX, CDMS, or flavor experiments such as LHCb, Belle, MEG or Mu2e set the most precise measurements of the different processes.

Among the SM open problems, the only existing experimental evidences for New Physics are the non-zero neutrino masses, the observed BAU, and the existence of DM that the SM cannot accommodate. In particular, this thesis will focus on certain phenomenological consequences from SM extensions able to explain the observed neutrino masses and mixings, so as to probe for their existence.

Since the SM was formulated with a minimum content of particles to account for the observed phenomena, and no experimental evidence of neutrino masses existed at the time of its formulation, right-handed neutrinos (nor other possible extra particle necessary to generate neutrino masses) were included. Consequently, the SM particle content must be extended. Several extensions of the SM to account for neutrino masses require the addition of right-handed neutrinos. In these extensions, the neutrinos acquire Dirac masses after EWSB through the Yukawa interaction with the Higgs boson. However, the observed experimental pattern of neutrino masses sets a bound on these Yukawa couplings $\sim \mathcal{O}(10^{-12})$. This unnatural suppression of the neutrino Yukawa couplings compared to the ones of other fermions of the SM suggests a different mechanism behind the origin of neutrino masses, different from the Higgs mechanism. In addition, since right-handed neutrinos are singlets under all the SM gauge symmetry, a Majorana mass term for these fermions is therefore allowed in the Lagrangian. Since this new mass scale is not related to the Higgs mechanism, nor to any other fundamental scale of the SM, it could be much larger than the EW scale. In particular, if the Majorana mass is sufficiently large, then the smallness of the observed neutrino masses becomes natural, due to the suppression of this large Majorana mass scale, in the so-called Seesaw mechanism [61–77]. In the SM extended with just three massive neutrinos, the unitary mixing matrix that relates the flavour and mass eigenstates, and which accounts for neutrino oscillations, is called Pontecorvo-Maki-Nakagawa-Sakata (PMNS) matrix. This PMNS matrix is therefore the lepton mixing matrix that appears in the charged current (CC) interactions in analogy to the Cabibbo-Kobayashi-Maskawa (CKM) mixing matrix of the quark sector. Another consequence of enlarging the neutrino content with Majorana

neutrinos is that the mixing matrix is enlarged. And as a result, the 3×3 sub-block of the mixing matrix that corresponds to the left-handed lepton mixing, and which is involved in the CC interactions, is not longer unitary. Therefore, these deviations from unitarity of the leptonic mixing matrix can be used to probe for the heavy neutrino mixing.

In the present thesis, the non-unitarity of the leptonic mixing matrix upon inclusion of extra right-handed neutrinos in order to explain the observed neutrino masses has been studied. The most stringent, updated and general set of constraints on the mixing of the heavy Seesaw neutrinos (with masses above the EW scale) to the charged leptons has been derived from a global fit to present flavor and electroweak precision data. Two different scenarios are explored and compared: a completely general scenario where an arbitrary number of heavy right-handed neutrinos are integrated out without any further assumption, and a more constrained scenario where only 3 additional heavy states are considered. The assumptions of the second scenario imply non-trivial correlations in order to reproduce the observed pattern of neutrino masses and mixings in neutrino oscillation experiments. The relevant set of processes analyzed in the global fit includes: searches for LFV decays, probes of the universality of weak interactions, CKM unitarity bounds and electroweak precision data. In particular, a comparative and detailed study of the present and future sensitivity of the different LFV experiments has been performed.

Moreover, heavy particles with large Yukawa couplings can induce sizable radiative corrections. Therefore, the importance of higher order corrections from right-handed neutrino loops when deriving bounds on their mixing with the light active states has been studied. The scenario of 3 additional heavy singlets with an approximate $B-L$ symmetry has been chosen for the analysis. The 1-loop expressions of the dominant observables used for the global fit have been computed and renormalized. All the 1-loop amplitudes and the necessary counterterms for the renormalization have been derived for this thesis. The possible cancellation between the loop-level corrections and the tree-level contributions to the non-unitarity of the leptonic mixing matrix has been addressed, and the impact on the bounds derived through the global fit upon their inclusion has been discussed.

Finally, the impact on neutrino oscillation probabilities when the SM is extended with right-handed neutrinos has been studied. The phenomenological manifestation of these extensions is different depending in whether the extra neutrinos are kinematically accesible or not. As a result, two different scenarios with light (bellow the π mass) and heavy (above the π mass) right-handed neutrinos respec-

tively have been addressed. The differences and similitudes between the impact of the two scenarios at neutrino oscillation searches have been explored, and both limits have been described in the practical language of non-standard interactions (NSI). To conclude, the bounds of both scenarios have been compared with the expected sensitivities of a future neutrino oscillation experiment, taking the DUNE proposal as a benchmark for the discussion. For neutrinos above the EW scale, the bunds derived in the first part of this thesis apply, and thus limit the impact of these extra neutrinos at oscillation experiments.

The thesis is organized as follows. In Chapter 1 the SM is introduced. The neutrino oscillation phenomenon is also discussed, and why its discovery implies the existence of non-degenerate neutrino masses and non-zero lepton mixing. Finally, extensions of the SM able to accommodate neutrino masses are outlined with emphasis in the Type-I Seesaw. The following chapters contain the central work of this thesis which is based on the results published in the articles [78], [79] and [80]. In Chapter 2 the global fit to present flavor and electroweak precision data is performed, and the general bounds to the non-unitarity of the leptonic mixing matrix are derived. In Chapter 3 the importance of the 1-loop heavy right-handed neutrino corrections when deriving bounds on their mixing trough a global fit is studied. In Chapter 4 the impact on neutrino oscillation searches when the SM is extended with right-handed neutrinos is studied taking the DUNE proposal as a benchmark for the analysis. Finally, the chapter *Conclusions and Outlook* summarizes the main conclusions of the present work. The contributions of this thesis to the present situation of the field are highlighted and a discussion on how to shed light on the present open problems of the SM and thus progress in the understanding of an underlying fundamental theory beyond are presented.

Chapter 1

The Standard Model and its limitations

The SM [1–5] is based in the gauge group $\mathrm{SU}(3)_c \times \mathrm{SU}(2)_L \times \mathrm{U}(1)_Y$, where c stands for the color of the strong force (c =red, green, blue), L represents left-handed chirality and Y the hypercharge. Its particle content can be split into two groups: particles with fractional spin called fermions and those with integer spin dubbed bosons. The fermions form the visible matter of the Universe while the bosons carry the fundamental forces. Quarks and leptons are organized in 3 families or generations with identical quantum numbers that determine their interactions but different masses. The two heavier generations are unstable and decay into the first generation. Altogether, there are 6×3 quarks and 6 leptons. In terms of their left-handed and right-handed components, the fermionic particle content of the SM is then summarized in Table 1.1.

The 8 gluons G^a_μ, which are in the adjoint representation of $\mathrm{SU}(3)_c$, are the vector particles responsible for the strong interaction. Gluons couple to quarks with a coupling of strength g_s. The three color charges of the quarks form the fundamental representation of the non-Abelian $\mathrm{SU}(3)_c$ symmetry. The generators of this representation are the 8 3×3 Gell-Mann matrices λ_a, with the algebra

$$\left[\frac{\lambda_a}{2}, \frac{\lambda_b}{2}\right] = i f_{abc} \frac{\lambda_c}{2}\,, \tag{1.1}$$

where f_{abc} are the structure constants. Neither quarks nor gluons can be isolated as free particles. Quarks are confined together into $\mathrm{SU}(3)_c$-singlet combinations of two or three quarks called mesons or baryons respectively.

	Leptons		Quarks		
1^{st} generation	$\begin{pmatrix} \nu_{eL} \\ e_L \end{pmatrix}$	e_R	$\begin{pmatrix} u_L \\ d_L \end{pmatrix}$	u_R	d_R
2^{nd} generation	$\begin{pmatrix} \nu_{\mu L} \\ \mu_L \end{pmatrix}$	μ_R	$\begin{pmatrix} c_L \\ s_L \end{pmatrix}$	c_R	s_R
3^{rd} generation	$\begin{pmatrix} \nu_{\tau L} \\ \tau_L \end{pmatrix}$	τ_R	$\begin{pmatrix} t_L \\ b_L \end{pmatrix}$	t_R	b_R
$(\text{SU}(3)_c, \text{SU}(2)_L)$	$(1,2)$	$(1,1)$	$(3,2)$	$(3,1)$	$(3,1)$

Table 1.1: Fermionic content of the 3 generations of the SM and their representations under the $\text{SU}(3)_c$ and $\text{SU}(2)_L$ gauge groups.

The $\text{SU}(2)_L \times \text{U}(1)_Y$ electroweak interaction are given by three vector fields W^i_μ coupled to the weak isospin current J^i_μ, and a vector field B_μ coupled to the weak hypercharge current j^Y_μ. Similarly to the $\text{SU}(3)_c$ case, the generators of the representation of the weak isospin, T^i, are the three 2×2 Pauli matrices σ_i that satisfy the equivalent algebra of that given by Eq. (1.1). And finally, the weak hypercharge Y encodes the strength of the coupling of each fermion to the vector field B_μ. The different quantum numbers associated to the charges of the electroweak interaction of the 1^{st} generation of the SM are summarized in Table 1.2. Since the second and third generations of fermions are copies of the 1^{st} generation but with different masses, their charges can be derived from the same Table 1.2. With these ingredients the gauge invariant Lagrangian that describes the kinetic energies as well as the strong and electroweak interactions of quarks and leptons can be built

$$\mathcal{L} = \underbrace{-\frac{1}{4} F_{\mu\nu} F^{\mu\nu}}_{\substack{W^i_\mu,\ B_\mu,\ \text{and}\ G^a_\mu \\ \text{kinetic energies and} \\ \text{self-interactions}}} + \underbrace{\overline{\psi}_{L,R} \not{D} \psi_{L,R}}_{\substack{\text{fermion kinetic energies} \\ \text{and their interactions} \\ \text{with}\ W^i_\mu,\ B_\mu,\ \text{and}\ G^a_\mu}} , \tag{1.2}$$

where the interaction states $\psi_{L,R} = \frac{1}{2}\left(1 \mp \gamma_5\right)\psi \equiv P_{L,R}\psi$ are the left-handed or right-handed components of a given fermion ψ in the Weyl representation, $F_{\mu\nu}$ represents the three field strengths $W^i_{\mu\nu}$, $B_{\mu\nu}$, and $G^a_{\mu\nu}$, $\not{D} \equiv \gamma^\mu D_\mu$, and D_μ the covariant

	Leptons			Quarks			
	ν_e	e_L	e_R	u_L	d_L	u_R	d_R
T	1/2	1/2	0	1/2	1/2	0	0
T^3	1/2	-1/2	0	1/2	-1/2	0	0
Y	-1	-1	-2	1/3	1/3	4/3	-2/3
Q	0	-1	-1	2/3	-1/3	2/3	-1/3

Table 1.2: Quantum numbers of the 1st generation of the SM. The other two generations have the same charges of the equivalent particle of the 1st generation.

derivative for left-handed or right-handed fermions given by

$$D_\mu = i\partial_\mu \underbrace{-g\frac{\sigma_i}{2}W_\mu^i}_{\substack{\neq 0 \text{ only} \\ \text{for } \psi_L}} - g'\frac{Y}{2}B_\mu \underbrace{-g_s\frac{\lambda_a}{2}G_\mu^a}_{\substack{\neq 0 \text{ only if} \\ \psi_{L,R} = q_{L,R}}}, \tag{1.3}$$

where g, g', and g_s are the strength of the two weak currents and strong forces, respectively. Notice that gauge invariance does not allow including a gauge boson mass term of the form $-m_B^2 B^\mu B_\mu$ nor a fermion mass term $-m_f\overline{\psi}\psi$ in the Lagrangian of Eq. (1.2). As a consequence all the particles and mediators of the three forces described by that Lagrangian are massless. However, this is in conflict with empirical evidence since masses for the different fermions as well as for the $W^\pm$ and Z gauge bosons have been observed in different experiments.

Therefore, the electroweak symmetry $\mathrm{SU}(2)_L \times \mathrm{U}(1)_Y$ is broken to $\mathrm{U}(1)_{\mathrm{em}}$ in such a way that the physical $W^\pm$ and Z gauge bosons of the charged (CC) and neutral (NC) weak current interactions, respectively, become massive, while the photon that mediates the electromagnetic (em) interaction remains massless. Thus, the generator of the electromagnetic interaction, Q, is the only charge conserved in the broken phase and which can be expressed as a combination of the generators of the $\mathrm{SU}(2)_L \times \mathrm{U}(1)_Y$ symmetry, T^3 and Y

$$Q \equiv T^3 + \frac{Y}{2}\,. \tag{1.4}$$

The Lagrangian that describes the electroweak interaction in the unbroken phase

$$\mathcal{L}_{\mathrm{EW}} = -igJ^{i\mu}W_\mu^i - i\frac{g'}{2}j^{Y\mu}B_\mu\,, \tag{1.5}$$

gives rise to the Lagrangians of the three currents after EWSB

$$\begin{aligned}
\mathcal{L}_{\rm em} &= e j^{\rm em}_\mu A^\mu = e\overline{\psi}\gamma^\mu Q\psi A_\mu \,, \\
\mathcal{L}_{\rm NC} &= \frac{g}{\cos\theta_{\rm W}} J^{\rm NC}_\mu Z^\mu = \frac{g}{\cos\theta_{\rm W}}\overline{\psi}\gamma^\mu \left(T^3 P_L - Q\sin^2\theta_{\rm W}\right)\psi Z_\mu \,, \\
\mathcal{L}_{\rm CC} &= \frac{g}{\sqrt{2}} J^{\rm CC\dagger}_\mu W^{-\mu} + \text{h.c.} = \frac{g}{\sqrt{2}}\overline{\psi}_L\gamma^\mu\psi_L W^-_\mu + \text{h.c.} \,,
\end{aligned} \tag{1.6}$$

where T^3 and Q are the different fermionic charges given in Table 1.2, and where $\theta_{\rm W}$ is the Weinberg angle that defines the mixing among the weak interaction fields and the physical states

$$\begin{aligned}
A_\mu &= B_\mu\cos\theta_{\rm W} + W^3_\mu\sin\theta_{\rm W} \,, \\
Z_\mu &= -B_\mu\sin\theta_{\rm W} + W^3_\mu\cos\theta_{\rm W} \,, \\
W^\pm_\mu &= \frac{1}{\sqrt{2}}\left(W^1_\mu \mp i W^2_\mu\right) \,,
\end{aligned} \tag{1.7}$$

where the following relation among the strength of the two weak currents g and g', and the electric charge of the electromagnetic current has been used to define the three currents

$$g\sin\theta_{\rm W} = g'\cos\theta_{\rm W} \equiv e \quad \Rightarrow \begin{cases} j^{\rm em}_\mu \equiv J^3_\mu + \dfrac{1}{2} j^Y_\mu \\ J^{\rm NC}_\mu \equiv J^3_\mu - \sin^2\theta_{\rm W} j^{\rm em}_\mu \\ J^{\rm CC}_\mu \equiv J^+_\mu = \dfrac{1}{2}\left(J^1_\mu + i J^2_\mu\right) \end{cases} . \tag{1.8}$$

Notice that the CC interaction of Eq. (1.6) only involves left-handed fermions. Therefore, C symmetry is violated within the SM. A mechanism that breaks $\mathrm{SU}(2)_L\times\mathrm{U}(1)_Y$ in order to build the Lagrangian that represents the behavior of the different massive particles under the weak interactions. And here is where the Higgs mechanism enters.

1.1 Masses in the SM: the Higgs mechanism

The Higgs mechanism was first introduced in 1964 by R. Brout and F. Englert [6], by P. Higgs [7], and by G. Guralnik, C. R. Hagen, and T. Kibble [8] to explain why the Z and $W^\pm$ gauge bosons are massive while the photon remains massless.

In order to do this, four scalar fields ϕ_i are introduced in such a way that the new $\mathrm{SU}(2)_L \times \mathrm{U}(1)_Y$ gauge invariant piece added to the Lagrangian of Eq. (1.2) is

$$\mathcal{L}_{\text{Higgs}} = \left| \left(i\partial_\mu - g\frac{\sigma_i}{2} W_\mu^i - g'\frac{Y}{2} B_\mu \right) \phi \right|^2 - V(\phi) \,, \tag{1.9}$$

where ϕ denotes the Higgs, a complex doublet of $\mathrm{SU}(2)_L$ with a weak hypercharge $Y = 1$ that contains four scalar fields ϕ_i

$$\phi = \begin{pmatrix} \phi^+ \\ \phi^0 \end{pmatrix} \quad \text{with} \quad \begin{cases} \phi^+ \equiv \dfrac{1}{\sqrt{2}} (\phi_1 + i\phi_2) \\ \phi^0 \equiv \dfrac{1}{\sqrt{2}} (\phi_3 + i\phi_4) \end{cases} . \tag{1.10}$$

The Higgs potential, $V(\phi)$, of Eq. (1.9) is given by

$$V(\phi) = \mu^2 \phi^\dagger \phi + \lambda \left(\phi^\dagger \phi \right)^2 . \tag{1.11}$$

For $\mu^2 > 0$ the potential has a paraboloid shape with the minimum in $\phi_0 = 0$ (see Figure 1.1). However, when $\mu^2 < 0$ and $\lambda > 0$ the potential exhibits a "Mexican-hat" shape with a non-zero vacuum expectation value (vev), ϕ_0, of $\phi(x)$

$$\phi_0 = \frac{1}{\sqrt{2}} \begin{pmatrix} 0 \\ v_{\text{EW}} \end{pmatrix} \quad \text{with} \quad v_{\text{EW}} \equiv \sqrt{-\frac{\mu^2}{\lambda}} = 246 \text{ GeV} \,. \tag{1.12}$$

Notice that the above choice of ϕ_0, with $T = 1/2$, $T^3 = -1/2$, and $Y = 1$ breaks both $\mathrm{SU}(2)_L$ and $\mathrm{U}(1)_Y$ gauge symmetries. However, since ϕ^0 is the neutral Higgs component that develops a vev, the $\mathrm{U}(1)_{\text{em}}$ symmetry with generator $Q = T^3 + Y/2$ remains unbroken. The vacuum is thus invariant under $\mathrm{U}(1)_{\text{em}}$ transformations while the symmetry associated to the other three generators of $\mathrm{SU}(2)_L \times \mathrm{U}(1)_Y$ is broken. Consequently, the photon remains massless while the breaking generates three massive Goldstone bosons [81–83]. These Goldstone bosons become the longitudinal components of the Z and $W^\pm$ gauge bosons, and masses for them are thus induced as explained in the following Section 1.1.1. That is, after spontaneous symmetry breaking, of the four scalar fields, the only physical field that remains is the Higgs field h

$$\phi = \begin{pmatrix} \phi^+ \\ \phi^0 \end{pmatrix} \xrightarrow[\text{EWSB}]{\text{after}} \phi = \frac{1}{\sqrt{2}} \begin{pmatrix} 0 \\ v_{\text{EW}} + h \end{pmatrix} , \tag{1.13}$$

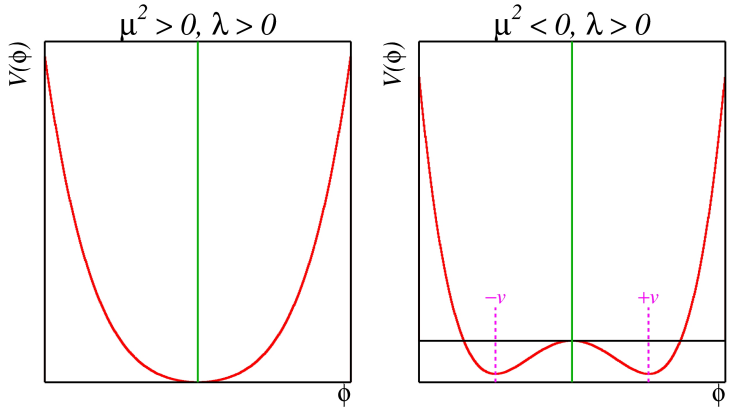

Figure 1.1: Higgs potential $V(\phi)$ for a complex scalar field for $\lambda > 0$ and $\mu^2 > 0$ (left panel) with zero vev and for $\mu^2 < 0$ (right panel) with non-zero vev.

where the Higgs boson h is the scalar (spin 0) particle associated to this new filed and whose bare mass is related to the parameter λ of the Higgs potential

$$M_h = v_{\rm EW}\sqrt{2\lambda} = \sqrt{-2\mu^2}\,. \tag{1.14}$$

1.1.1 Gauge boson masses

The masses of the gauge bosons arise from the first term of the Higgs Lagrangian Eq. (1.9) when the Higgs develops a vacuum expectation value of ϕ_0

$$\begin{aligned}\left|\left(g\frac{\sigma_i}{2}W_\mu^i + \frac{g'}{2}B_\mu\right)\phi_0\right|^2 &= \frac{v_{\rm EW}^2 g^2}{8}\left(\left[\left(W_\mu^1\right)^2 + \left(W_\mu^2\right)^2\right] + \left[\left(W_\mu^3\right)^2 - \frac{2g'}{g}W_\mu^3 B^\mu + \frac{g'^2}{g^2}B_\mu^2\right]\right) \\ &= \left(\frac{1}{2}v_{\rm EW}g\right)^2 W_\mu^+ W^{-\mu} + \frac{1}{2}\left(\frac{1}{2}v_{\rm EW}\sqrt{g^2+g'^2}\right)^2 Z_\mu Z^\mu\end{aligned} \tag{1.15}$$

where the relations among the interaction fields and the physical states given by Eq. (1.7) have been used. One can therefore identify the coefficients of the first and second terms of Eq. (1.15) as the masses of the $W^\pm$ charged gauge bosons and of the Z neutral gauge boson, respectively. And as expected, since no $A_\mu A^\mu$ term is generated in Eq. (1.15), the photon is massless

$$M_W = \frac{1}{2}v_{\rm EW}g = \cos\theta_{\rm W} M_Z\,, \quad M_Z = \frac{1}{2}v_{\rm EW}\sqrt{g^2+g'^2} \quad \text{and} \quad M_\gamma = 0. \tag{1.16}$$

Thus we have succeed to break $\mathrm{SU}(2)_L \times \mathrm{U}(1)_Y$ in such a way that the three Goldstone bosons that arise from the breaking give masses to the Z and $W^\pm$ gauge bosons, while the photon remains massless.

1.1.2 Fermion masses through the Yukawa interaction

As mentioned before, due to gauge invariance, a fermion mass term $-m_f\overline{\psi}\psi$ was not included in the first Lagrangian Eq. (1.2). Nevertheless, the beauty of the Higgs mechanism is that the same Higgs field that is responsible for breaking $\mathrm{SU}(2)_L \times \mathrm{U}(1)_Y \to \mathrm{U}(1)_{\mathrm{em}}$, giving masses to the $W^\pm$ and Z, is also capable to give masses to the quarks and leptons through the so called Yukawa interaction. One can therefore build the third $\mathrm{SU}(2)_L \times \mathrm{U}(1)_Y$ gauge invariant piece of the Lagrangian

$$\begin{aligned}\mathcal{L}_{\text{Yukawa}} &= -\overline{L}_{Li}y'^{\ell}_{ij}\ell_{Rj}\phi - \overline{Q}_{Li}y'^{d}_{ij}q^{d}_{Rj}\phi - \overline{Q}_{Li}y'^{u}_{ij}q^{u}_{Rj}\tilde{\phi} + \text{h.c.} \\ &= -\frac{y^{\ell}_{\alpha}v_{\text{EW}}}{\sqrt{2}}\overline{\ell_\alpha}\ell_\alpha - \frac{y^{q}_{\beta}v_{\text{EW}}}{\sqrt{2}}\overline{q_\beta}q_\beta - \frac{y^{\ell}_{\alpha}}{\sqrt{2}}\overline{\ell_\alpha}\ell_\alpha h - \frac{y^{q}_{\beta}}{\sqrt{2}}\overline{q_\beta}q_\beta h\,,\end{aligned} \tag{1.17}$$

where $\tilde{\phi} = -i\sigma_2\phi^*$, and where y'^{ℓ}_{ij}, y'^{u}_{ij} and y'^{d}_{ij} are the Yukawa couplings for leptons, up-type quarks and down-type quarks respectively. The second line of Eq. (1.17) is rewritten in the physical basis in which the Yukawas are real and diagonal, and where one can therefore identify the coefficient of the first two terms as

$$m_{\ell_\alpha} = \frac{v_{\text{EW}}}{\sqrt{2}}y^{\ell}_{\alpha} \quad \text{and} \quad m_{q_\beta} = \frac{v_{\text{EW}}}{\sqrt{2}}y^{q}_{\beta}\,, \tag{1.18}$$

with $\ell_\alpha = e, \mu, \tau$ and $q_\beta = u, d, c, s, b, t$. Since the same Yukawa couplings that define the masses of the fermions enter in their interaction with the Higgs boson, the more massive a fermion is, the stronger its interaction with the Higgs boson. However, Yukawa couplings are not predicted but free parameters of the theory.

Notice that since the SM does not contain right-handed neutrinos (nor other possible extra field necessary to generate neutrino masses), there is no Yukawa interaction term in Eq. (1.17) for the neutrinos. And thus, within the SM, the neutrinos are strictly massless particles at any order in perturbation theory.

1.1.3 The discovery of the Higgs boson and beyond

The Higgs mechanism explains the masses of all the massive gauge bosons and fermions, however the theory needed the discovery of this scalar particle in order

to be verified. From the late 1980s to 2010s, the experiments of the Large Electron-Positron collider (LEP) at CERN and Tevatron at Fermilab, searched for the Higgs boson without any evidence. Later, on the 4$^{\text{th}}$ of July of 2012, the ATLAS and CMS experiments of CERN's Large Hadron Collider (LHC) announced the discovery of a new particle in the mass region of ~ 126 GeV consistent with the SM Higgs boson. Figure 1.2 shows the preliminary results of the discovery announcement of both ATLAS [9] and CMS [10] experiments. The data shown in both experiments correspond to the reconstruction of the Higgs boson mass m_h from the golden decay channel $h \to \gamma\gamma$. Finally, in 2013 the Nobel Prize in physics was awarded jointly to F. Englert and P. Higgs for the theoretical discovery of a mechanism behind the origin of the mass of elementary particles.

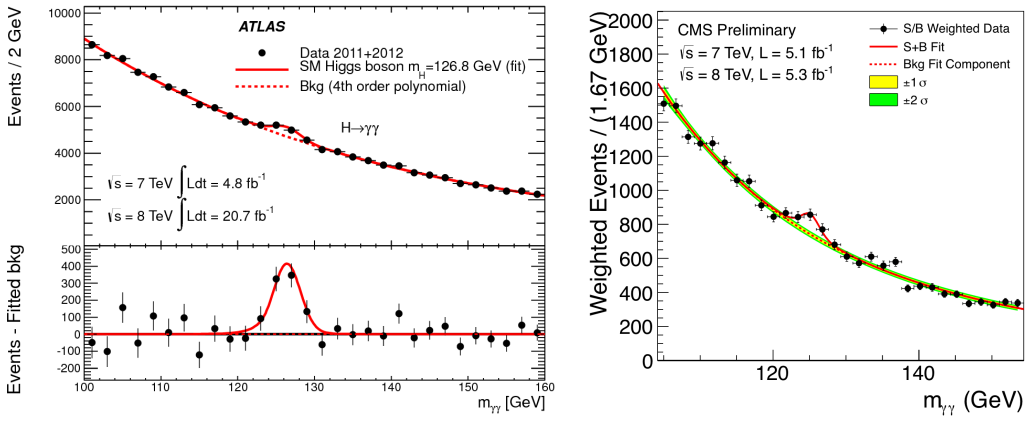

Figure 1.2: Di-photon ($\gamma\gamma$) invariant mass distribution for the ATLAS (left panel) and CMS (right panel) data of 2011 and 2012 (black points with error bars). The data are weighted by the signal to background ratio for each subcategory of events. The solid red line shows the fit result for signal plus background; the dashed red line shows only the background. From [9, 10].

After the Higgs boson discovery, the last piece of the SM was assembled and one can therefore build the Lagrangian that describes the observed strong and electroweak interactions as well as the masses of the SM fermions and gauge bosons. The SM Lagrangian $\mathcal{L}_{\text{SM}}$ is thus the sum of Eq. 1.2, 1.9 and 1.17 rewritten in a compact

form as

$$\begin{aligned}\mathcal{L}_{\rm SM} &= \mathcal{L} + \mathcal{L}_{\rm Higgs} + \mathcal{L}_{\rm Yukawa} \\ &= -\frac{1}{4}F_{\mu\nu}F^{\mu\nu} + i\overline{\psi}\not{D}\psi + \left(\overline{\psi}_i y_{ij}\psi_j\phi + \text{h.c.}\right) + |D_\mu\phi|^2 - V(\phi)\,.\end{aligned} \tag{1.19}$$

1.2 Neutrino oscillations and the leptonic mixing matrix

In this section it is shown that if neutrinos are massive and they mix in analogy to their quark counterparts, then leptonic flavor change is possible trough the neutrino oscillation phenomenon. The neutrino oscillation probabilities, both in vacuum and in presence of mater will be derived and discussed.

1.2.1 The leptonic mixing matrix: $U_{\rm PMNS}$

If neutrinos are massive, in all generality their mass and flavor eigenstates will not coincide and will be related to each other via an analogous unitary matrix to the Cabibbo-Kobayashi-Maskawa (CKM) mixing matrix [84, 85]. Thus, the three neutrino fields ν_α (associated to the charged leptons ℓ_α via the CC interactions) are linear combinations of three mass eigenstates ν_i with masses m_i. In the basis in which charged lepton Yukawas are diagonal

$$\nu_\alpha = \left(U_{\rm PMNS}\right)_{\alpha i}\,\nu_i\,, \tag{1.20}$$

where $\alpha = e,\ \mu,\ \tau$ and $i = 1,\ 2,\ 3$ are flavor and mass eigenstates indices respectively. The $U_{\rm PMNS}$ is a CKM-like Pontecorvo-Maki-Nakagawa-Sakata (PMNS) [86–89], a 3×3 unitary mixing matrix that relates the two different basis.

In the mass basis the leptonic NC and CC interactions of Eq. (1.6) are therefore given by

$$\begin{aligned}\mathcal{L}_{\rm NC} &= \frac{g}{2c_{\rm W}}\left\{\overline{\nu_i}\gamma^\mu P_L\nu_i - \overline{\ell_\alpha}\gamma^\mu P_L\left(1-2s_{\rm W}^2\right)\ell_\alpha\right\}Z_\mu\,, \\ \mathcal{L}_{\rm CC} &= \frac{g}{\sqrt{2}}\overline{\ell_\alpha}\gamma^\mu P_L\left(U_{\rm PMNS}\right)_{\alpha i}\,\nu_i W_\mu^- + \text{h.c.}\,,\end{aligned} \tag{1.21}$$

where the unitary relation $\sum\left(U_{\rm PMNS}^\dagger\right)_{i\alpha}\left(U_{\rm PMNS}\right)_{\alpha j} = \delta_{ij}$ has been used in the NC interaction. This means that the NC are diagonal and that $U_{\rm PMNS}$ is the unitary leptonic mixing matrix that appears in CC interactions.

The PMNS matrix can be parametrized by the usual Chau-Keung representation [90] trough three angles, θ_{ij}, and a CP violation phase, δ, called Dirac phase[1]

$$U_{\text{PMNS}} = \begin{pmatrix} c_{12}c_{13} & s_{12}c_{13} & s_{13}e^{-i\delta} \\ -s_{12}c_{23} - c_{12}s_{23}s_{13}e^{i\delta} & c_{12}c_{23} - s_{12}s_{23}s_{13}e^{i\delta} & s_{23}c_{13} \\ s_{12}s_{23} - c_{12}c_{23}s_{13}e^{i\delta} & -c_{12}s_{23} - s_{12}c_{23}s_{13}e^{i\delta} & c_{23}c_{13} \end{pmatrix}, \tag{1.22}$$

where $c_{ij} = \cos\theta_{ij}$ and $s_{ij} = \sin\theta_{ij}$ have been used in order to shorten the notation.

1.2.2 Neutrino oscillations in vacuum

The amplitude for a neutrino in the mass eigenstate i to interact as a neutrino of flavor α is given by the mixing matrix element $(U_{\text{PMNS}})_{\alpha i}$, therefore a ν_α originally produced in association with a given charged lepton ℓ_α will evolve in a non-trivial way[2]

$$\begin{aligned} |\nu_\alpha(L,t)\rangle &= (U_{\text{PMNS}})^*_{\alpha i}\, e^{-i(E_i t - p_i L)} |\nu_i\rangle \overset{t\simeq L}{\simeq} (U_{\text{PMNS}})^*_{\alpha i}\, e^{-i(E_i - p_i)L} |\nu_i\rangle \\ &\simeq (U_{\text{PMNS}})^*_{\alpha i}\, e^{-i\frac{\Delta m_i^2 L}{2E}} |\nu_i\rangle , \end{aligned} \tag{1.23}$$

where L is the distance traveled by the neutrino between production and detection. Therefore there is a non-zero oscillatory probability of detecting the neutrino ν_β associated with ℓ_β

$$P_{\alpha\beta} \equiv P(\nu_\alpha \to \nu_\beta) = |\langle \nu_\beta | \nu_\alpha(L)\rangle|^2 = \left| \left(U_{\text{PMNS}} e^{-iHL} U^\dagger_{\text{PMNS}} \right)_{\beta\alpha} \right|^2 , \tag{1.24}$$

where the Hamiltonian H in vacuum will be given by

$$H = \frac{1}{2E} \begin{pmatrix} 0 & 0 & 0 \\ 0 & \Delta m^2_{21} & 0 \\ 0 & 0 & \Delta m^2_{31} \end{pmatrix} \quad \text{with} \quad \Delta m^2_{ij} \equiv m^2_j - m^2_i . \tag{1.25}$$

[1] As will be discussed in Section 1.3, neutrino masses could be of the Majorana kind, in which case two other physical masses could be present in the PMNS matrix.

[2] For a more consistent computation in the wave pocket formalism, without using the plane wave approximation, see for instance [91–93].

Then, starting form Eq. (1.24) the neutrino (anti-neutrino) oscillation probabilities in vacuum reduces to

$$\begin{aligned} P_{\alpha\beta}\left(\overline{P_{\alpha\beta}}\right) = \delta_{\alpha\beta} - 4\sum_{i>j} \mathrm{Re}\left[U_{\alpha i}U^*_{\beta i}U^*_{\alpha j}U_{\beta j}\right]\sin^2\left(\Delta_{ij}\right) \\ + (-)\,2\sum_{i>j} \mathrm{Im}\left[U_{\alpha i}U^*_{\beta i}U^*_{\alpha j}U_{\beta j}\right]\sin\left(2\Delta_{ij}\right)\,, \end{aligned} \tag{1.26}$$

where $U \equiv U_{\mathrm{PMNS}}$ and $\Delta_{ij} \equiv \Delta m^2_{ij} L/4E$ have been used to shorten notation, and where $\overline{P_{\alpha\beta}}$ stands for the anti-neutrino oscillation probability $P\left(\overline{\nu}_\alpha \to \overline{\nu}_\beta\right)$.

Notice that the observation of flavor change in the neutrino sector given by Eq. (1.26) implies both $\Delta m^2_{ij} \neq 0$ and $\left(U_{\mathrm{PMNS}}\right)_{\alpha i} \neq \delta_{\alpha i}$. That is, the observations of neutrino oscillation requires to non-degenerate neutrino mass eigenstates and non-trivial mixing in the leptonic sector. Moreover, if U_{PMNS} is a complex matrix, then $P_{\alpha\beta}$ and $\overline{P_{\alpha\beta}}$ will be different.

Neutrino oscillations given by Eq. (1.26) do not depend on the mass eigenvalues themselves but in the two mass squared splittings, Δm^2_{ij}. As a result, no information on the absolute neutrino mass scale is obtained trough neutrino oscillation measurements.

1.2.3 Neutrino oscillations in matter

When neutrinos travel trough matter they can undergo coherent scattering with the particles that form the atoms. Two kind of interactions can take place. Coherent scatterings of ν_e (or $\overline{\nu}_e$) with the electrons in the medium via $W^\pm$ exchange giving rise to an extra CC interaction potential V_{CC}

$$V_{\mathrm{CC}} = \pm\sqrt{2}G_F n_e \tag{1.27}$$

where $G_F \equiv$ is the Fermi constant, and n_e is the electron density of the matter where the neutrinos are propagating. The $+(-)$ sign is for neutrino (anti-neutrino) propagation. The second mater interaction is that of neutrinos with electrons, protons and neutrons via exchange of Z bosons. For neutral matter, the interaction with electrons cancels with that with protons and as a result, the NC interaction potential V_{NC} only depends on the flavor-blind neutron contribution

$$V_{\mathrm{NC}} = \mp\frac{\sqrt{2}}{2}G_F n_n \tag{1.28}$$

where n_n is the matter neutron density, and again $-(+)$ corresponds to neutrino (anti-neutrino) propagation.

Then, the neutrino oscillation probability in matter is given by Eq. (1.24) but where the matter Hamiltonian, $H^{\rm m}$, will not only account for the vacuum neutrino evolution but also for the new CC and NC interactions

$$H^{\rm m} = \frac{1}{2E}\begin{pmatrix} 0 & 0 & 0 \\ 0 & \Delta m^2_{21} & 0 \\ 0 & 0 & \Delta m^2_{31} \end{pmatrix} + U^{\dagger}_{\rm PMNS}\begin{pmatrix} V_{\rm CC}+V_{\rm NC} & 0 & 0 \\ 0 & V_{\rm NC} & 0 \\ 0 & 0 & V_{\rm NC} \end{pmatrix} U_{\rm PMNS}\,. \tag{1.29}$$

For approximately constant matter density, the matter Hamiltonian of Eq. (1.29) can by diagonalized getting as a result *effective* mass eigenstates, $\tilde{\Delta}_{ij}$, that will enter in the neutrino oscillation probability in matter given by

$$\begin{aligned} P^{\rm m}_{\alpha\beta}\left(\overline{P^{\rm m}_{\alpha\beta}}\right) = \delta_{\alpha\beta} - 4\sum_{i>j}{\rm Re}\left[\tilde{U}^*_{\alpha i}\tilde{U}_{\beta i}\tilde{U}_{\alpha j}\tilde{U}^*_{\beta j}\right]\sin^2\left(\tilde{\Delta}_{ij}\right) \\ + (-)\,2\sum_{i>j}{\rm Im}\left[\tilde{U}^*_{\alpha i}\tilde{U}_{\beta i}\tilde{U}_{\alpha j}\tilde{U}^*_{\beta j}\right]\sin\left(2\tilde{\Delta}_{ij}\right)\,, \end{aligned} \tag{1.30}$$

where $\tilde{U}$ is the unitary matrix that diagonalizes the matter Hamiltonian of Eq. (1.29).

In the simple two-family approximation, in which only two mass eigenstates, ν_1 and ν_2, and therefore two corresponding flavor states, ν_e and ν_μ, are significant, then there is only one squared-mass splitting $\Delta m^2 \equiv m^2_2 - m^2_1$. Then, the mixing matrix, $U(\theta)$, is the rotation matrix between the mass and flavor basis. Therefore, the neutrino oscillation probability in matter given by Eq. (1.30) becomes

$$P^{\rm m}_{e\mu} = \sin^2 2\theta_{\rm m}\sin^2\frac{\Delta m^2_{\rm m}L}{4E} \tag{1.31}$$

where $\Delta m^2_{\rm m}$ is given by

$$\Delta m^2_{\rm m} \equiv \Delta m^2\sqrt{\sin^2 2\theta + (\cos 2\theta - x)^2} \tag{1.32}$$

and where $\theta_{\rm m}$ and x are given by

$$\sin^2 2\theta_{\rm m} \equiv \frac{\sin^2 2\theta}{\sin^2 2\theta + (\cos 2\theta - x)^2} \quad \text{with} \quad x \equiv \frac{V_{\rm CC}/2}{\Delta m^2/4E} = \frac{2\sqrt{2}G_F n_e E}{\Delta m^2}\,. \tag{1.33}$$

It is shown in Eq. (1.33) that for $x \simeq \cos 2\theta$, $\sin^2 2\theta_{\rm m}$ can be near unity even for very small vacuum mixing angle θ. This dramatic amplification of a small mixing angle in vacuum into a very large one in matter is the known as the resonant version of the Mikheev-Smirnov-Wolfenstein (MSW) effect [94, 95].

1.2.4 Measuring the neutrino oscillation parameters

The three angles θ_{ij} of the $U_{\rm PMNS}$, the Dirac CP phase δ, and the two mass splittings Δm^2_{21} and Δm^2_{31} (solar and atmospheric mass splittings, respectively) can be measured in neutrino oscillation experiments. Neutrino and antineutrino oscillations have been observed discovered with high significance in a number of observations involving both ($\nu_\alpha \to \nu_\beta$, with $\alpha \neq \beta$) and disappearance ($\nu_\alpha \to \nu_\alpha$) channels given by Eq. (1.26) using a variety of experiments:

- Atmospheric ν_μ and $\overline{\nu}_\mu$ disappearance at Super-Kamiokande (SK) [36, 39–41, 44], MINOS [53, 55], and IceCUBE [45].
- Accelerator ν_μ and $\overline{\nu}_\mu$ disappearance at long-baselines (LBL) of $L \sim 300/800$ km K2K [52], T2K [58, 59], MINOS [54], and NOνA [56] experiments.
- Accelerator $\nu_\mu \to \nu_e$ at LBL of $L \sim 300/800$ km T2K [58, 59], MINOS [55], and NOνA [57] experiments.
- Solar $\nu_e \to \nu_\mu/\nu_\tau$ at Chlorine [18], Gallex [31], SK [27, 28, 30], SNO [32], and Borexino [29, 33, 34] experiments.
- Reactor $\overline{\nu}_e$ disappearance at a LBL of $L \sim 200$ km at KamLAND [47].
- Reactor $\overline{\nu}_e$ disappearance at a middle-baseline (MBL) of $L \sim 1$ km at Double-Chooz [49], Daya Bay [50], and Reno [48].

Table 1.3 shows the leading and subleading dependences of these experiments to the different neutrino oscillation parameters. Therefore, the best-fit value of $\sin^2\theta_{12}$, $\sin^2\theta_{23}$, $\sin^2\theta_{13}$, $\Delta m^2_{\rm sol}$, and $|\Delta m^2_{\rm atm}|$ through the global fit, NuFIT 3.0 [96], to a complete set of neutrino oscillation experiments.

However there are still some unknown values for the neutrino oscillation parameters. Namely, the sign of the atmospheric mass spiting $|\Delta m^2_{\rm atm}|$ which gives rise to the two possible neutrino mass orderings. If $\Delta m^2_{\rm sol} \equiv \Delta m^2_{21} > 0$, then two different mass orderings can be defined: normal hierarchy (NH) when $\Delta m^2_{\rm atm} = \Delta m^2_{31} > 0$ or inverted hierarchy (IH) $\Delta m^2_{\rm atm} = \Delta m^2_{32} < 0$. These tow different situations are shown in Figure 1.3. Moreover, the octant of θ_{23} and δ are unknown neutrino oscillation parameters too. Even tough NOνA and T2K experiments already have

Neutrino oscillation experiment	Leading dependence	Subleading dependence
Solar experiments	θ_{12}	$\Delta m^2_{\rm sol}$ & θ_{13}
Reactor LBL	$\Delta m^2_{\rm sol}$	θ_{12} & θ_{13}
Reactor MBL	θ_{13}	$\lvert\Delta m^2_{\rm atm}\rvert$
Atmospheric experiments	θ_{23}	$\Delta m^2_{\rm atm}$, θ_{13} & δ
Acc. LBL ν_μ & $\overline{\nu}_\mu$ disappearance	$\lvert\Delta m^2_{\rm atm}\rvert$	θ_{23}
Acc. LBL ν_e appearance	θ_{13}	$\Delta m^2_{\rm atm}$, δ & θ_{23}

Table 1.3: Dominant and subdominant dependence of the different neutrino oscillation experiments on the oscillation parameters.

hints for δ close to maximal ($\delta \sim -\pi/2$) [57, 59], it is expected that next generation long baseline of neutrino oscillation experiments such as DUNE (Fermilab, USA) or T2HK (Japan) will determine the value the mass ordering and the δ CP phase.

Even though the absolute neutrino mass scale, m_1 (m_3) for NH (IH) (see Figure 1.3) cannot be stablished through neutrino oscillation experiments, direct bounds on the absolute neutrino mass scale could be probed trough kinematical searches in $\beta-$decay experiments or in Cosmology. Single $\beta-$decay experiments set an upper bound on the effective flavor mass defined by

$$m^2_{\nu_\alpha} \equiv \sum_i |\,(U_{\rm PMNS})_{\alpha i}\,|^2 m_i^2\,. \tag{1.34}$$

The most sensitive limits on the effective mass $m_{\nu_e} < 2.3$ eV and $m_{\nu_e} < 2.1$ eV at 95%CL comes from Mainz [97] and Troitsk [98] experiments, respectively. On the other hand, the measurements of the CMB made by Planck [12] set an upper bound on the sum of the light neutrino masses

$$\sum_i m_i < 0.23 \text{ eV (95\% CL)}. \tag{1.35}$$

The experimental evidence for neutrino flavour change through the neutrino oscillation phenomenon [17–59] requires left-handed neutrinos to be massive. Therefore, the SM must be extended to account for this overwhelming experimental evidence.

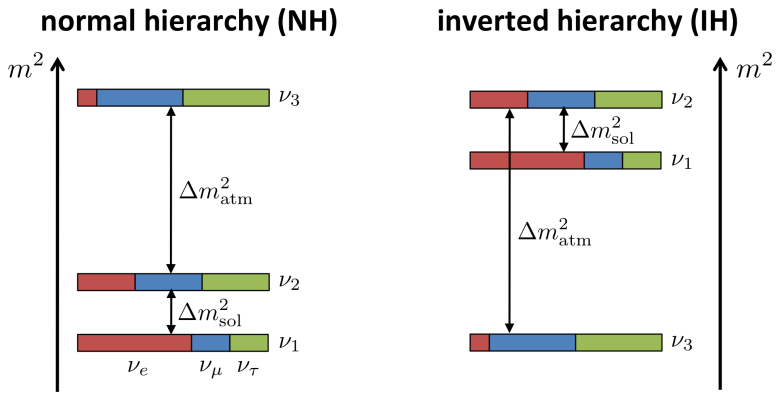

Figure 1.3: The two possible neutrino mass orderings. Normal hierarchy when $\Delta m^2_{\rm atm} = \Delta m^2_{31} > 0$ (left panel) and inverted hierarchy $\Delta m^2_{\rm atm} = \Delta m^2_{32} < 0$ (right panel). The absolute neutrino mass scale, m_1 (m_3) for NH (IH), is unknown and cannot be stablished trough neutrino oscillation experiments.

1.3 Neutrino masses and the Seesaw mechanism

Since neutrinos are the only neutral fermions of the SM, they are the only particles that can have either Dirac or Majorana mass terms. If the SM is extended with right-handed neutrinos ν_R, and under the *ad hoc* assumption that lepton number L is exactly conserved, a Dirac mass term $-m_D \overline{\nu}_L \nu_R$ for neutrinos can be added to the SM Lagrangian of Eq. (1.19). Analogous to the masses of charged leptons and quarks explained in Section 1.1.2, when the Higgs develops a vev, neutrinos would get Dirac masses trough the Yukawa interaction

$$m_D = \frac{v_{\rm EW}}{\sqrt{2}} y_N \,, \tag{1.36}$$

where y_N is the Yukawa interaction between the neutrinos and the Higgs field. However, the constraints on direct searches of neutrino masses of Eq. (1.35) set a bound on these Yukawa couplings $\sim \mathcal{O}(10^{-12})$ which is too small compared to the ones of the other fermions. This huge suppression of the neutrino Yukawa coupling suggest a different mechanism behind the origin of neutrino masses. On the other hand, a Majorana mass term for the left-handed neutrinos $-\hat{m}\overline{\nu^c_L}\nu_L$[3] is not allowed in the

[3]Where c stands for the charge-conjugate or particle-antiparticle operator defined by: $\hat{C} : \psi \to \psi^c \equiv i\gamma^0\gamma^2\overline{\psi}^T$

SM by gauge invariance. However, Majorana masses for the ν_L can be induced by the unique dimension 5 ($d = 5$) Weinberg operator [99] when the Higgs develops a non-zero vev

$$\frac{1}{2}c^{\mathrm{d=5}}_{\alpha\beta}\left(\overline{\ell_{\alpha L}^{c}}\tilde{\phi}^{*}\right)\left(\tilde{\phi}^{\dagger}\ell_{\beta_L}\right) + \text{h.c.} \xrightarrow[\text{EWSB}]{\text{after}} \frac{v_{\mathrm{EW}}^2}{2}c^{d=5}\overline{\nu_L^c}\nu_L\,, \tag{1.37}$$

and therefore, the Majorana mass generated for the left-handed neutrinos in terms of the coefficient of the Weinberg operator is given by

$$\hat{m} = -\frac{v_{\mathrm{EW}}^2}{2}c^{d=5}\,. \tag{1.38}$$

Since the Weinberg operator of Eq. (1.37) is a ($d = 5$) operator, this option implies that the SM is the low energy remanent of a higher energy theory. It should be effectively generated by some new particles extending the SM content. At tree level[4], only three different realizations of the Weinberg operator, which are characterized by the quantum numbers of the new mediators, exist:

- Type-I Seesaw [61–64]: the extension of the SM with heavy Majorana right-handed neutrinos N_R that are singlets under the SM gauge group.
- Type-II Seesaw [65–69]: Weinberg operator mediated by heavy $\mathrm{SU}(2)_L$ triplets of scalar fields Λ with hypercharge $Y = 2$.
- Type-III Seesaw [70–77]: Weinberg operator mediated by heavy $\mathrm{SU}(2)_L$ fermionic triplets Σ_R with zero hypercharge.

This thesis will be focussed on the study of the phenomenological implications of the Type-I Seesaw. The SM particle content is then enlarged by an arbitrary number of heavy right-handed singlets N_{Ri} and thus, the SM-Seesaw Lagrangian that describes the SM interactions with massive neutrinos and mixings is given by

$$\mathcal{L} = \mathcal{L}_{\mathrm{SM}} + i\overline{N_R}\not{\partial}N_R - \left(\frac{1}{2}\overline{N_{Ri}}(M_N)_{ij}N_{Rj}^{c} + (y_N)_{i\alpha}\overline{N_{Ri}}\phi^{\dagger}\ell_{L\alpha}\right) + \text{h.c.}\,, \tag{1.39}$$

where M_N is the Majorana mass allowed for the right-handed neutrinos N_{Ri} due to gauge invariance. Since N_R are singlets under the SM gauge group and have $Y = 0$, the covariant derivative reduces to $D_\mu = \partial_\mu$ in the kinetic term of Eq. (1.39).

Interestingly, if the SM neutrinos acquire Majorana masses via the Weinberg operator, additional physical phases can be present into the PMNS mixing matrix.

[4]For some pioneering works on radiatively induced neutrino masses see for instance [100, 101]

Contrary to the case of the CKM matrix of the quark sector, these two extra "Majorana phases" $\alpha_{1,2}$ cannot be reabsorbed in field redefinitions and therefore, they become physical. The two Majorana phases are encoded in the diagonal matrix V

$$V = \begin{pmatrix} e^{-i\frac{\alpha_1}{2}} & 0 & 0 \\ 0 & e^{-i\frac{\alpha_2}{2}} & 0 \\ 0 & 0 & 1 \end{pmatrix} . \tag{1.40}$$

Thus, the U_{PMNS} matrix that accounts for the possible Majorana nature of neutrinos is given by

$$U_{\text{PMNS}} = \begin{pmatrix} c_{12}c_{13} & s_{12}c_{13} & s_{13}e^{-i\delta} \\ -s_{12}c_{23} - c_{12}s_{23}s_{13}e^{i\delta} & c_{12}c_{23} - s_{12}s_{23}s_{13}e^{i\delta} & s_{23}c_{13} \\ s_{12}s_{23} - c_{12}c_{23}s_{13}e^{i\delta} & -c_{12}s_{23} - s_{12}c_{23}s_{13}e^{i\delta} & c_{23}c_{13} \end{pmatrix} \cdot V \,, \tag{1.41}$$

Since the PMNS matrix appears in the combination $\left(U_{\text{PMNS}}U^{\dagger}_{\text{PMNS}}\right)_{\alpha\beta}$ in the neutrino production and detection processes, the V part of Eq. (1.41) directly cancels making the experimental verification of the Majorana nature of the neutrinos not possible through oscillations. Nowadays, neutrinoless double beta ($0\nu\beta\beta$) decay experiments (CUORE, GERDA, KamLAND-Zen or EXO) are the best window to probe for the Majorana nature of neutrinos.

1.3.1 The Type-I Seesaw as a low energy EFT

When the masses of the new heavy states N_{Ri} are above the electroweak scale, the heavy fields can be integrated out, and the resulting effective field theory (EFT) can be used to study the low energy phenomenology encodes in a set of effective operators. Each of these effective operators is suppressed by a power of the energy scale $\Lambda \sim M_N$ until which the effective Lagrangian $\mathcal{L}_{\text{eff}}$ is valid

$$\mathcal{L}_{\text{eff}} = \mathcal{L}_{\text{SM}} + \frac{1}{\Lambda}\mathcal{L}^{d=5} + \frac{1}{\Lambda^2}\mathcal{L}^{d=6} + \cdots \simeq \mathcal{L}_{\text{SM}} + \delta\mathcal{L}^{d=5} + \delta\mathcal{L}^{d=6} \,, \tag{1.42}$$

where the series has been stoped at $d = 6$ since, in general, the effect of higher order operators is much more suppressed by the new heavy scale M_N.

$d = 5$ operator: neutrino masses through the Weinberg operator

The first effective operator, $\delta\mathcal{L}^{d=5}$, is the Weinberg operator of Eq. (1.37), which violates lepton number L by two units ($\Delta L = 2$). After the Higgs develops a vev the Weinberg operator induces Majorana masses for the light neutrinos. In the Seesaw limit $M_N \gg m_D$, these Majorana masses are given by

$$\hat{m} = -\frac{v_{\rm EW}^2}{2} c^{d=5} \equiv -m_D^T M_N^{-1} m_D = U_{\rm PMNS}^* m U_{\rm PMNS}^\dagger \,, \tag{1.43}$$

where $U_{\rm PMNS}$ is the unitary mixing matrix that diagonalizes the symmetric light neutrino mass matrix $\hat{m}$ generated by the Weinberg operator and which was introduced in Section 1.2.1. Thus, within the Seesaw mechanism the smallness of light neutrino masses naturally stem from the suppression of the new heavy scale M_N as can be seen in Eq. (1.43).

$d = 6$ operator: neutrino mixing

The unique [102] $d = 6$ effective operator that appears at tree level is

$$\delta\mathcal{L}^{d=6} = c_{\alpha\beta}^{d=6} \left(\overline{\ell_{\alpha L}}\tilde{\phi}\right) i\partial\!\!\!/ \left(\tilde{\phi}^\dagger \ell_{\beta_L}\right) \,, \tag{1.44}$$

where the $d = 6$ operator coefficient is given by the hermitian matrix [102, 103]

$$\eta \equiv \frac{v_{\rm EW}^2}{4} c^{d=6} = \frac{1}{2} m_D^\dagger M_N^{-2} m_D \,, \tag{1.45}$$

notice that since η is suppressed by two powers of the new heavy scale M_N, if the smallness of the light neutrinos (i.e. the smallness of the $d = 5$ Weinberg operator) comes only from the suppression of this scale, the $d = 6$ coefficient will be in principle even more suppressed.

When the Higgs acquires a vev, this $d = 6$ operator leads to corrections to the left-handed neutrino kinetic terms, which becomes non-diagonal in the flavor space. With the following transformation $\nu_{\alpha L} \to \nu'_{\alpha L} \equiv \left(\delta_{\alpha\beta} + 2\eta_{\alpha_\beta}\right)^{1/2} \nu_{L\beta}$, the neutrino kinetic terms are brought to a diagonal and canonical form [102]. As a result, the

leptonic NC and CC Lagrangians of Eq. (1.21) take the form[5]

$$\begin{aligned}
\mathcal{L}_{\rm NC} &\simeq \frac{g}{2c_{\rm W}}\left\{\overline{\nu_i}\left(U^{\dagger}_{\rm PMNS}\right)_{i\alpha}\left(\delta_{\alpha\beta}-\eta_{\alpha\beta}\right)\gamma^{\mu}P_L\left(\delta_{\beta\gamma}-\eta_{\beta\gamma}\right)\left(U_{\rm PMNS}\right)_{\gamma j}\nu_j\right. \\
&\quad \left.-\,\overline{\ell_{\alpha}}\gamma^{\mu}P_L\left(1-2s^2_{\rm W}\right)\ell_{\alpha}\right\}Z_{\mu} \\
&\equiv \frac{g}{2c_{\rm W}}\left\{\overline{\nu_i}\gamma^{\mu}P_L\left(N^{\dagger}N\right)_{ij}\nu_j-\overline{\ell_{\alpha}}\gamma^{\mu}P_L\left(1-2s^2_{\rm W}\right)\ell_{\alpha}\right\}Z_{\mu}\,, \\
\mathcal{L}_{\rm CC} &\simeq \frac{g}{\sqrt{2}}\overline{\ell_{\alpha}}\gamma^{\mu}P_L\left(\delta_{\alpha\beta}-\eta_{\alpha\beta}\right)\left(U_{\rm PMNS}\right)_{\beta i}\nu_i W^{-}_{\mu}+\text{h.c.} \\
&\equiv \frac{g}{\sqrt{2}}\overline{\ell_{\alpha}}\gamma^{\mu}P_L N_{\alpha i}\nu_i W^{-}_{\mu}+\text{h.c.}\,,
\end{aligned} \tag{1.46}$$

where the new leptonic mixing matrix N is not unitary anymore and is given by

$$N \equiv \left(I-\eta\right)U_{\rm PMNS}\,. \tag{1.47}$$

From the above relation, the coefficient of the $d = 6$ operator can be used to parametrized the deviation from unitarity of the leptonic mixing matrix $U_{\rm PMNS}$ that appears in the CC current interactions. This means that the inclusion of right-handed neutrinos to the SM particle content modifies the processes mediated by these two currents and thus, precision measurements of such observables can in principle set strong constraints on the parameters of the high-energy Seesaw model. This idea has been studied in detail in several works [66, 104–118].

[5]Primes will be omitted in the following.

Chapter 2

Global constraints on the Seesaw mixing

2.1 Parametrizations

Starting from the usual type-I Seesaw Lagrangian:

$$\mathscr{L} \;=\; \mathscr{L}_{\rm SM} - \frac{1}{2}\overline{N^i_{\rm R}}(M_N)_{ij}N^{cj}_{\rm R} - (Y_N)_{i\alpha}\overline{N^i_{\rm R}}\phi^\dagger \ell^\alpha_{\rm L} + \text{h.c.}\,, \tag{2.1}$$

where ϕ denotes the SM Higgs field, M_N the Majorana mass allowed for the right-handed neutrinos $N^i_{\rm R}$ and Y_N the Yukawa couplings between the neutrinos and the Higgs field. The vev of the Higgs $v_{\rm EW}$ will, in addition, induce Dirac masses $m_D = v_{\rm EW}Y_N/\sqrt{2}$. In the usual Seesaw limit, for $M_N \gg m_D$, the three light and mostly-active neutrinos observed in the neutrino oscillation phenomenon will be clearly separated from the heavy and mostly-sterile new states. Upon integrating out these heavy states, their low energy phenomenology will be encoded in a series of effective operators. The first such operator is the well-known $d = 5$ Weinberg operator [99] that, upon electroweak symmetry breaking, induces the Majorana masses for the light neutrinos:

$$\hat{m} \equiv m_D^t M_N^{-1} m_D = -U^*_{\rm PMNS} m U^\dagger_{\rm PMNS}, \tag{2.2}$$

where $U_{\rm PMNS} = U_{23}(\theta_{23})U_{13}(\theta_{13},\delta)U_{12}(\theta_{12})\text{diag}(e^{-i\alpha_1/2}, e^{-i\alpha_2/2}, 1)$ is the Unitary mixing matrix that diagonalizes the symmetric mass matrix $\hat{m}$ generated from the Weinberg operator. At tree level, the only $d = 6$ operator obtained upon integrating out the heavy neutrinos induces non-canonical neutrino kinetic terms for the three SM

active neutrinos when the Higgs develops its vev [102]. After diagonalizing and normalizing the kinetic terms, the mixing matrix appearing in charged current interactions will thus contain, not only the two Unitary rotations to diagonalize the $d = 5$ and $d = 6$ operators respectively, but also the necessary rescaling to bring the neutrino kinetic term to its canonical form. Thus, in all generality, the matrix describing the mixing between the light neutrino mass eigenstates and the SM charged leptons via W interactions will not be Unitary and to stress this feature we will dub it N. Since any general matrix can be parametrized as the product of an Hermitian and a Unitary matrix, these deviations from unitarity have been often parametrized as [103]:

$$N = (I - \eta)U_{\rm PMNS}, \tag{2.3}$$

where the small Hermitian matrix η (also called ϵ in other works) encodes the deviations from unitarity in neutrino mixing. This parametrization is very convenient from a phenomenological point of view. Indeed, since the particular neutrino mass eigenstate is never identified in physical observables, its index is always summed upon, while the flavour index labeling the charged leptons participating in the process is normally fixed. Thus, most observables depend on the combination:

$$\sum_i N_{\alpha i} N^\dagger_{i\beta} = \delta_{\alpha\beta} - 2\eta_{\alpha\beta} + \mathcal{O}\left(\eta^2_{\alpha\beta}\right) \tag{2.4}$$

and can thus be expressed only though the parameters contained in the Hermitian matrix η. Moreover, the physical interpretation of η is also very transparent in terms of the mixing between the extra heavy neutrinos and the SM flavours. Indeed, if the full mass matrix is diagonalized as:

$$U^T \begin{pmatrix} 0 & m_D^T \\ m_D & M_N \end{pmatrix} U = \begin{pmatrix} m & 0 \\ 0 & M \end{pmatrix}, \tag{2.5}$$

where m and M are diagonal matrices containing respectively the masses of the 3 light ν_i and heavy N_i mass eigenstates. The diagonalizing matrix U can be written as [119]:

$$U = \begin{pmatrix} c & s \\ -s^\dagger & \hat{c} \end{pmatrix} \begin{pmatrix} U_{\rm PMNS} & 0 \\ 0 & I \end{pmatrix}, \tag{2.6}$$

where

$$\begin{pmatrix} c & s \\ -s^\dagger & \hat{c} \end{pmatrix} \equiv \begin{pmatrix} \sum_{n=0}^{\infty} \frac{\left(-\Theta\Theta^\dagger\right)^n}{2n!} & \sum_{n=0}^{\infty} \frac{\left(-\Theta\Theta^\dagger\right)^n}{(2n+1)!}\Theta \\ -\sum_{n=0}^{\infty} \frac{\left(-\Theta^\dagger\Theta\right)^n}{(2n+1)!}\Theta^\dagger & \sum_{n=0}^{\infty} \frac{\left(-\Theta^\dagger\Theta\right)^n}{2n!} \end{pmatrix}, \tag{2.7}$$

and $\Theta \sim m_D^\dagger M_N^{-1}$ is the general matrix that describes the mixing between the heavy mass eigenstates and the active neutrino flavours. Thus, the non-unitary correction $I - \eta$ can be identified with the first term of the cosine expansion $1 - \Theta\Theta^\dagger/2$ such that:

$$\eta = \frac{\Theta\Theta^\dagger}{2}. \tag{2.8}$$

Furthermore, η is also (1/2 of) the coefficient of the $d = 6$ operator obtained upon integrating out the heavy neutrino fields:

$$\eta = \frac{m_D^\dagger M_N^{-2} m_D}{2}. \tag{2.9}$$

In all generality the $d = 6$ operator η is completely independent from the $d = 5$ $\hat{m}$ and thus from the measured neutrino masses and mixings in oscillation experiments [120, 121]. However, both $\hat{m}$ and η are ultimately built from m_D and M_N and thus, in particular cases, may not be fully independent. Apart from the completely general parametrization through η, here we will also investigate one such case. Namely, we will focus on the particular scenario in which:

- The SM is only extended through 3 right-handed neutrinos.
- The three extra neutrino mass eigenstates are heavier than the EW scale.
- Large, potentially observable, η is allowed despite the smallness of neutrino masses.
- The small neutrino masses are radiatively stable.

The only way to simultaneously satisfy these requirements is through an underlying L symmetry [122, 123] (see also Ref. [124, 125]) which leads to:

$$m_D = \frac{v_{\rm EW}}{\sqrt{2}} \begin{pmatrix} Y_{Ne} & Y_{N\mu} & Y_{N\tau} \\ \epsilon_1 Y'_{Ne} & \epsilon_1 Y'_{N\mu} & \epsilon_1 Y'_{N\tau} \\ \epsilon_2 Y''_{Ne} & \epsilon_2 Y''_{N\mu} & \epsilon_2 Y''_{N\tau} \end{pmatrix} \quad \text{and} \quad M_N = \begin{pmatrix} \mu_1 & \Lambda & \mu_3 \\ \Lambda & \mu_2 & \mu_4 \\ \mu_3 & \mu_4 & \Lambda' \end{pmatrix}, \tag{2.10}$$

with all ϵ_i and μ_j small lepton number violating parameters (see also Ref. [126] for a particular scenario where these small parameters arise naturally). By setting all $\epsilon_i = 0$ and $\mu_j = 0$, lepton number symmetry is indeed recovered with the following L assignments $L_e = L_\mu = L_\tau = L_1 = -L_2 = 1$ and $L_3 = 0$. Also $\hat{m} = 0$ (3 massless neutrinos in the L-conserving limit), $M_1 = M_2 = \Lambda$ (a heavy Dirac pair) and $M_3 = \Lambda'$ (a heavy decoupled Majorana singlet), but:

$$\eta = \frac{1}{2}\begin{pmatrix} |\theta_e|^2 & \theta_e\theta_\mu^* & \theta_e\theta_\tau^* \\ \theta_\mu\theta_e^* & |\theta_\mu|^2 & \theta_\mu\theta_\tau^* \\ \theta_\tau\theta_e^* & \theta_\tau\theta_\mu^* & |\theta_\tau|^2 \end{pmatrix} \quad \text{with} \quad \theta_\alpha \equiv \frac{Y_{N\alpha}v}{\sqrt{2}\Lambda}. \tag{2.11}$$

So that large η is possible even in the limit of massless neutrinos when L is conserved. Upon switching on the L-violating parameters in Eq. (2.10), neutrino masses and mixings $\hat{m}$ that can reproduce the observed neutrino oscillations are generated. However, these are not completely independent from η and the following relationship between the θ_α in Eq. (2.11) and $\hat{m}$ follows [78]:

$$\begin{aligned} \theta_\tau \simeq \frac{1}{\hat{m}_{e\mu}^2 - \hat{m}_{ee}\hat{m}_{\mu\mu}} \Big(&\theta_e \left(\hat{m}_{e\mu}\hat{m}_{\mu\tau} - \hat{m}_{e\tau}\hat{m}_{\mu\mu}\right) + \\ &\theta_\mu \left(\hat{m}_{e\mu}\hat{m}_{e\tau} - \hat{m}_{ee}\hat{m}_{\mu\tau}\right) \pm \sqrt{\theta_e^2\hat{m}_{\mu\mu} - 2\theta_e\theta_\mu\hat{m}_{e\mu} + \theta_\mu^2\hat{m}_{ee}}\times \\ &\times\sqrt{\hat{m}_{e\tau}^2\hat{m}_{\mu\mu} - 2\hat{m}_{e\mu}\hat{m}_{e\tau}\hat{m}_{\mu\tau} + \hat{m}_{ee}\hat{m}_{\mu\tau}^2 + \hat{m}_{e\mu}^2\hat{m}_{\tau\tau} - \hat{m}_{ee}\hat{m}_{\mu\mu}\hat{m}_{\tau\tau}}\Big) . \end{aligned} \tag{2.12}$$

Thus, this extra constraint will lead to correlations among the heavy-active mixing parameters θ_α and therefore also $\eta_{\alpha\beta}$ through Eq. (2.11), not present in the completely general scenario with more than 3 heavy neutrinos. From now on we will refer to the unrestricted scenario as **G-SS** (*general Seesaw*) and to the particular case with 3 extra heavy neutrinos as **3N-SS**. The parameters characterizing the heavy neutrino mixing and the correlations between them in each case are summarized in Table 2.1. In particular, the constraints on η for the G-SS come from the fact that η is positive definite (see Eq. (2.8)).Regarding θ_τ in the 3N-SS case, its value is fixed by θ_e and θ_μ through Eq. (2.12) once the SM neutrino masses and mixings encoded in the $d = 5$ operator $\hat{m}$ are specified. In our analysis we will thus scan the allowed parameter space of the 3N-SS by leaving θ_e and θ_μ free in the fit, together with the remaining unknown values characterizing $\hat{m}$: the Dirac phase δ, the Majorana phases α_1 and α_2, the absolute neutrino mass and the mass hierarchy (normal or inverted). Regarding

	η_{ee}	$\eta_{\mu\mu}$	$\eta_{\tau\tau}$	$\eta_{e\mu}$	$\eta_{e\tau}$	$\eta_{\mu\tau}$
G-SS	$\eta_{ee} > 0$ free	$\eta_{\mu\mu} > 0$ free	$\eta_{\tau\tau} > 0$ free	$\lvert\eta_{e\mu}\rvert \leq \sqrt{\eta_{ee}\eta_{\mu\mu}}$ free	$\lvert\eta_{e\tau}\rvert \leq \sqrt{\eta_{ee}\eta_{\tau\tau}}$ free	$\lvert\eta_{\mu\tau}\rvert \leq \sqrt{\eta_{\mu\mu}\eta_{\tau\tau}}$ free
3N-SS	$\eta_{ee} = \frac{\lvert\theta_e\rvert^2}{2}$ free	$\eta_{\mu\mu} = \frac{\lvert\theta_\mu\rvert^2}{2}$ free	$\eta_{\tau\tau} = \frac{\lvert\theta_\tau\rvert^2}{2}$ fixed by Eq. (2.12)	$\eta_{e\mu} = \frac{\theta_e\theta_\mu^*}{2}$ fixed by θ_e, θ_μ	$\eta_{e\tau} = \frac{\theta_e\theta_\tau^*}{2}$ fixed by θ_e, θ_τ	$\eta_{\mu\tau} = \frac{\theta_\mu\theta_\tau^*}{2}$ fixed by θ_μ, θ_τ

Table 2.1: Summary of the parameters characterizing the mixing between flavour eigenstates and the extra heavy neutrinos for a completely general Seesaw scenario (G-SS) and the particular case of 3 extra heavy neutrinos (3N-SS). The constraints and correlations between parameters in each model are also summarized in the table. The value of θ_τ for the 3N-SS case is computed through Eq. (2.12) as a function of θ_e, θ_μ, δ, α_1, α_2, the absolute neutrino mass scale and the mass hierarchy. The rest of the oscillation parameters are fixed to their best fits from Ref. [127].

the absolute neutrino mass scale we will add the constraint from Planck on the sum of the light neutrino masses $\sum m_i < 0.23$ eV at a 95% CL [12]. The rest of the oscillation parameters are fixed to their best fits from Ref. [127] since they are well-constrained by present neutrino oscillation data.

When presenting the results of the global fit in Section 3.3 we will derive constraints on the mixing of the heavy neutrinos with the SM active flavours θ_α in Eq. (2.11) for the 3N-SS. Regarding the G-SS, we do not specify the number of heavy neutrinos with which the SM is extended since all the observable effects are simply encoded in the matrix η. Thus, each heavy neutrino can have a different mixing $\Theta_{\alpha i}$ and, to ease the comparison with the results from the 3N-SS, we will use the combination $\sqrt{2\eta_{\alpha\alpha}}$ which represents the total mixing from all the additional heavy neutrinos with the flavour α and an upper bound on the individual mixings $\Theta_{\alpha i}$:

$$\Theta_{\alpha i} = \left(m_D^\dagger M^{-1}\right)_{\alpha i} \quad \text{and} \quad 2\eta_{\alpha\alpha} = \sum_i |\Theta_{\alpha i}|^2. \tag{2.13}$$

2.2 Observables

Global constraints on the mixing between the heavy and active neutrinos will be derived through a fit to the following 28 observables:

- The W boson mass M_W

- The effective weak mixing angle $\theta_{\rm W}$: $s^{2\ \rm lep}_{\rm W\ eff}$ and $s^{2\ \rm had}_{\rm W\ eff}$
- Four ratios of Z fermionic decays: R_l, R_c, R_b and $\sigma^0_{\rm had}$
- The invisible width of the Z $\Gamma_{\rm inv}$
- Ratios of weak decays constraining EW universality: $R^\pi_{\mu e}$, $R^\pi_{\tau\mu}$, $R^W_{\mu e}$, $R^W_{\tau\mu}$, $R^K_{\mu e}$, $R^K_{\tau\mu}$, $R^l_{\mu e}$ and $R^l_{\tau\mu}$
- 9 weak decays constraining the CKM unitarity
- 3 radiative LFV decays: $\mu \to e\gamma$, $\tau \to \mu\gamma$ and $\tau \to e\gamma$

The dependence of each observable on the non-unitarity mixing matrix $N_{\alpha i}$ and the parameters $\eta_{\alpha\beta}$ will be presented and discussed in this section. In Ref. [78] it was recently shown that loop level corrections involving the new degrees of freedom can be safely neglected. However, many SM-mediated loop corrections are relevant for these precision observables and will therefore be accounted for [128]. Notice that, in principle, these SM loop corrections also contain an indirect dependence on the non-unitarity parameters, notably through their dependence on G_F as determined in muon decay. This subleading dependence of the observables will be neglected and only the corrections from non-unitarity affecting the tree level relations will be discussed in the following expressions. The numerical analysis, however, contains all relevant SM loop corrections when comparing with the corresponding observables. The loop-corrected SM expectation, together with the leading non-unitarity correction and the experimental measurements that will be the inputs of our global fit are all summarized in Tab.(2.2).

2.2.1 Constraints from μ decay: G_F, M_Z, M_W and $\theta_{\rm W}$

As usual, all SM predictions will be made in terms of the very accurate measurements of α, M_Z and G_F as measured in μ decay, G_μ [128]:

$$\begin{aligned} \alpha &= (7.2973525698 \pm 0.0000000024) \cdot 10^{-3}, \\ M_Z &= (91.1876 \pm 0.0021)\ \text{GeV}, \\ G_\mu &= (1.1663787 \pm 0.0000006) \cdot 10^{-5}\ \text{GeV}^{-2}. \end{aligned} \tag{2.14}$$

However, a non-unitary mixing matrix $N_{\alpha i}$ would modify the expected decay rate of $\mu \to e\nu\bar{\nu}$. Indeed, since the final state neutrinos are not determined, their index must be summed upon obtaining:

Observable	SM prediction	Experimental value
$M_W \simeq M_W^{\rm SM}\,(1+0.20\,(\eta_{ee}+\eta_{\mu\mu}))$	(80.363 ± 0.006) GeV	(80.385 ± 0.015) GeV
$s^{2\ \rm lep}_{\rm W\ eff} \simeq s^{2\ \rm lep\ SM}_{\rm W\ eff}\,(1-1.30\,(\eta_{ee}+\eta_{\mu\mu}))$	0.23152 ± 0.00010	0.23113 ± 0.00021
$s^{2\ \rm had}_{\rm W\ eff} \simeq s^{2\ \rm had\ SM}_{\rm W\ eff}\,(1-1.30\,(\eta_{ee}+\eta_{\mu\mu}))$	0.23152 ± 0.00010	0.23222 ± 0.00027
$R_l \simeq R_l^{\rm SM}\,(1+0.18\,(\eta_{ee}+\eta_{\mu\mu}))$	20.740 ± 0.010	20.804 ± 0.050
$R_c \simeq R_c^{\rm SM}\,(1+0.11\,(\eta_{ee}+\eta_{\mu\mu}))$	0.17226 ± 0.00003	0.1721 ± 0.0030
$R_b \simeq R_b^{\rm SM}\,(1-0.06\,(\eta_{ee}+\eta_{\mu\mu}))$	0.21576 ± 0.00003	0.21629 ± 0.00066
$\sigma^0_{\rm had} \simeq \sigma^{0\ \rm SM}_{\rm had}\,(1+0.55\,(\eta_{ee}+\eta_{\mu\mu})+0.53\eta_{\tau\tau})$	(41.479 ± 0.008) nb	(41.541 ± 0.037) nb
$\Gamma_{\rm inv} \simeq \Gamma_{\rm inv}^{\rm SM}\,(1-0.33\,(\eta_{ee}+\eta_{\mu\mu})-1.32\eta_{\tau\tau})$	(0.50166 ± 0.00005) GeV	(0.4990 ± 0.0015) GeV
$R^{\pi}_{\mu e} \simeq (1-(\eta_{\mu\mu}-\eta_{ee}))$	1	1.0042 ± 0.0022
$R^{\pi}_{\tau\mu} \simeq (1-(\eta_{\tau\tau}-\eta_{\mu\mu}))$	1	0.9941 ± 0.0059
$R^{W}_{\mu e} \simeq (1-(\eta_{\mu\mu}-\eta_{ee}))$	1	0.992 ± 0.020
$R^{W}_{\tau\mu} \simeq (1-(\eta_{\tau\tau}-\eta_{\mu\mu}))$	1	1.071 ± 0.025
$R^{K}_{\mu e} \simeq (1-(\eta_{\mu\mu}-\eta_{ee}))$	1	0.9956 ± 0.0040
$R^{K}_{\tau\mu} \simeq (1-(\eta_{\tau\tau}-\eta_{\mu\mu}))$	1	0.978 ± 0.014
$R^{l}_{\mu e} \simeq (1-(\eta_{\mu\mu}-\eta_{ee}))$	1	1.0040 ± 0.0032
$R^{l}_{\tau\mu} \simeq (1-(\eta_{\tau\tau}-\eta_{\mu\mu}))$	1	1.0029 ± 0.0029
$\left\lvert V^{\beta}_{ud}\right\rvert \simeq \sqrt{1-\lvert V_{us}\rvert^2}(1+\eta_{\mu\mu})$	$\sqrt{1-\lvert V_{us}\rvert^2}$	0.97417 ± 0.00021
$\left\lvert V^{\tau\to K\nu_\tau}_{us}\right\rvert \simeq \lvert V_{us}\rvert\,(1+\eta_{ee}+\eta_{\mu\mu}-\eta_{\tau\tau})$	$\lvert V_{us}\rvert$	0.2212 ± 0.0020
$\left\lvert V^{\tau\to K,\pi}_{us}\right\rvert \simeq \lvert V_{us}\rvert\,(1+\eta_{\mu\mu})$	$\lvert V_{us}\rvert$	0.2232 ± 0.0019
$\left\lvert V^{K_L\to\pi e\overline{\nu}_e}_{us}\right\rvert \simeq \lvert V_{us}\rvert\,(1+\eta_{\mu\mu})$	$\lvert V_{us}\rvert$	0.2237 ± 0.0011
$\left\lvert V^{K_L\to\pi\mu\overline{\nu}_\mu}_{us}\right\rvert \simeq \lvert V_{us}\rvert\,(1+\eta_{ee})$	$\lvert V_{us}\rvert$	0.2240 ± 0.0011
$\left\lvert V^{K_S\to\pi e\overline{\nu}_e}_{us}\right\rvert \simeq \lvert V_{us}\rvert\,(1+\eta_{\mu\mu})$	$\lvert V_{us}\rvert$	0.2229 ± 0.0016
$\left\lvert V^{K^\pm\to\pi e\overline{\nu}_e}_{us}\right\rvert \simeq \lvert V_{us}\rvert\,(1+\eta_{\mu\mu})$	$\lvert V_{us}\rvert$	0.2247 ± 0.0012
$\left\lvert V^{K^\pm\to\pi\mu\overline{\nu}_\mu}_{us}\right\rvert \simeq \lvert V_{us}\rvert\,(1+\eta_{ee})$	$\lvert V_{us}\rvert$	0.2245 ± 0.0014
$\left\lvert V^{K,\pi\to\mu\nu}_{us}\right\rvert \simeq \lvert V_{us}\rvert\,(1+\eta_{\mu\mu})$	$\lvert V_{us}\rvert$	0.2315 ± 0.0010

Table 2.2: List of observables input to the global fit. The first column contains the leading dependence on the non-unitarity parameters η, the second column contains the loop-corrected SM expectation, and the third column the experimental measurement used in the fit.

$$\Gamma_\mu = \frac{m_\mu^5 G_F^2}{192\pi^3} \sum_i |N_{\mu i}|^2 \sum_j |N_{ej}|^2 \simeq \frac{m_\mu^5 G_F^2}{192\pi^3} \left(1 - 2\eta_{ee} - 2\eta_{\mu\mu}\right) \equiv \frac{m_\mu^5 G_\mu^2}{192\pi^3}. \tag{2.15}$$

Thus, G_F as determined through muon decay (G_μ) acquires a non-unitary correction that will propagate to most observables:

$$G_F = G_\mu \left(1 + \eta_{ee} + \eta_{\mu\mu}\right). \tag{2.16}$$

In particular, the relation between G_μ and M_W allows to constrain η_{ee} and $\eta_{\mu\mu}$ through kinematic measurements of M_W:

$$G_\mu = \frac{\alpha\pi M_Z^2 \left(1 + \eta_{ee} + \eta_{\mu\mu}\right)}{\sqrt{2} M_W^2 \left(M_Z^2 - M_W^2\right)}. \tag{2.17}$$

Similarly, the weak mixing angle $s_{\rm W}^2$ will be modified and independent determinations of $s_{\rm W}^2$ will be used to further constrain η_{ee} and $\eta_{\mu\mu}$:

$$s_W^2 = \frac{1}{2}\left(1 - \sqrt{1 - \frac{2\sqrt{2}\alpha\pi}{G_\mu M_Z^2}\left(1 - \eta_{ee} - \eta_{\mu\mu}\right)}\right), \tag{2.18}$$

Regarding different measurements of $s_{\rm W}^2$ it is important to note that in some low energy determinations, such as from the *weak charge of the proton* or *Møller scattering*, the dependence on this parameter appears through the following combination $-1/2 + 2s_{\rm W}^2$. Since the value of $s_{\rm W}^2$ is close to $1/4$, there is a partial cancellation in this observables that, in the SM, allows for a very accurate determination of $s_{\rm W}^2$, since small changes in its value significantly affect the degree of the cancellation and hence the size of the observable. For the same reason, we find that these observables are also very sensitive to corrections of the order of SM loop corrections times the non-unitary parameters η. Indeed, including some of these corrections we find that the corresponding coefficients in front of the η parameters in Tab.(2.2) would vary up to a factor 2, indicating that our approximation of neglecting these terms is not good enough for these precision observables. Since the inclusion of these corrections is beyond the scope of this work, we choose not to include these particular determinations of $s_{\rm W}^2$ in the list of observables for our global fit.

2.2.2 Constraints from Z decays

Z decays into charged fermions

The Z decays into charged fermions are not directly modified in presence of heavy neutrinos or a non-unitary lepton mixing matrix at tree level. However, these measurements depend on G_F and s_W and, as such, an indirect dependence on the non-unitarity parameters appears through its determination via muon decay, as described above. In particular:

$$\Gamma\left(Z \to f\bar{f}\right) \equiv \Gamma_f = \frac{G_\mu M_Z^3 \left(g_V^{f2} + g_A^{f2}\right)}{6\sqrt{2}\pi} \left(1 + \eta_{ee} + \eta_{\mu\mu}\right) \tag{2.19}$$

where the vector and axial-vector form factors are given by:

$$\begin{aligned} g_V^f &= N_C \left(T_f - 2Q_f s_{\rm W}^2\right) \\ g_A^f &= N_C T_f \end{aligned} \tag{2.20}$$

with N_C the color factor, $N_C = 3$ (1) for quarks (leptons) and where Q_f and T_f are the electric charge and third component of the weak isospin of the fermion f. Notice that an additional dependence on η_{ee} and $\eta_{\mu\mu}$ will be present in g_V through $s_{\rm W}^2$ and Eq. (2.18).

The usual combinations of decay rates will be used as observables for the global fit:

$$R_q = \frac{\Gamma_q}{\Gamma_{\rm had}}, \quad R_l = \frac{\Gamma_{\rm had}}{\Gamma_l} \quad \text{and} \quad \sigma^0_{\rm had} = \frac{12\pi\Gamma_{ee}\Gamma_{\rm had}}{M_Z^2\Gamma_Z^2}\,; \tag{2.21}$$

where $\Gamma_{\rm had} \equiv \sum_{q\neq t} \Gamma_q$.

Invisible Z width

In presence of a non-unitary lepton mixing matrix $N_{\alpha i}$, the Z coupling to neutrinos is directly affected and becomes non diagonal since $(N^\dagger N)_{ij} \neq \delta_{ij}$. Thus, apart from its indirect dependence through G_F, the invisible width of the Z, from which the number of active neutrinos can be determined, is directly sensitive to the mixing of heavy neutrinos:

$$\Gamma_{\rm inv} = \frac{G_F M_Z^3 \sum_{ij} |(N^\dagger N)_{ij}|^2}{12\sqrt{2}\pi} \simeq \frac{G_\mu M_Z^3}{12\sqrt{2}\pi}\big(3 - (4\,\eta_{\tau\tau} + \eta_{ee} + \eta_{\mu\mu})\big) \equiv \frac{G_\mu M_Z^3 N_\nu}{12\sqrt{2}\pi} \tag{2.22}$$

Notice that, since $\eta_{\alpha\beta}$ is positive definite from Eq. (2.8), the number of active neutrinos as measured through the invisible Z width will be smaller than 3 in presence of mixing with heavy neutrinos, to be compared with the present determination of $N_\nu = 2.990 \pm 0.007$ from LEP [129].

2.2.3 Constraints from weak interaction universality tests

The lepton flavour universality of weak interactions is strongly constrained through ratios of lepton and meson decays differing in the charged lepton generation involved, such as $\pi \to \mu\nu_i$ vs $\pi \to e\nu_i$. Since the final state neutrino cannot be determined, these processes are proportional to $\sum_i |N_{\alpha i}|^2 \approx 1 - 2\eta_{\alpha\alpha}$, where α is the flavour of the charged lepton. Thus, a flavour dependence is induced in presence on non-unitary mixing and the weak interaction universality constraints become powerful probes of heavy neutrino mixing:

$$\frac{\Gamma_\alpha}{\Gamma_\beta} \equiv \frac{\Gamma_\alpha^{\rm SM}}{\Gamma_\beta^{\rm SM}} R_{\alpha\beta}^2 = \frac{\Gamma_\alpha^{\rm SM}}{\Gamma_\beta^{\rm SM}} \frac{\sum_i |N_{\alpha i}|^2}{\sum_i |N_{\beta i}|^2} \simeq \frac{\Gamma_\alpha^{\rm SM}}{\Gamma_\beta^{\rm SM}} \left(1 - 2\eta_{\alpha\alpha} + 2\eta_{\beta\beta}\right), \tag{2.23}$$

where the ratio of the SM expectations for the decay widths $\Gamma_\alpha^{\rm SM}$ will be given by a function of the charged lepton masses involved containing the corresponding phase space and chirality flip factors as well as the different loop corrections. Thus, at tree level and for the particular case of π decays:

$$\frac{\Gamma_\alpha^{\pi{\rm SM}}}{\Gamma_\beta^{\rm SM}} = \left(\frac{m_\alpha\,(m_\pi^2 - m_\alpha^2)}{m_\beta^2\,(m_\pi^2 - m_\beta^2)}\right)^2 . \tag{2.24}$$

Constraints on the values of the ratios of weak coupling constants $R_{\alpha\beta}$ as defined in Eq. (2.23) have been derived through ratios of different decays [130] and are summarized in Tab. (2.2).

2.2.4 Unitarity of the CKM matrix

The presence of extra heavy neutrinos leads to unitarity violations of the lepton PMNS mixing matrix leaving the CKM quark mixing unaffected. However, the

processes through which the elements of the CKM matrix V are determined are affected both directly (for processes involving leptons) and indirectly (through the determination of G_F in muon decays). In particular, the unitarity relation among the elements of the first row of the CKM matrix is very strongly constrained and reads:

$$|V_{ud}|^2 + |V_{us}|^2 + |V_{ub}|^2 = 1 \tag{2.25}$$

For the present accuracy on V_{us}, the value of $V_{ub} = (4.13 \pm 0.49) \times 10^{-3}$ [128] can be safely neglected in Eq. (2.25). This relation, together with the measurements from the different processes used to constrain V_{ud} and V_{us} will thus also present indirect sensitivities to $\eta_{\alpha\beta}$. In particular we will rewrite through Eq. (2.25):

$$|V_{ud}| = \sqrt{1 - |V_{us}|^2} \tag{2.26}$$

and use the following experimental constraints to fit for V_{us} and the $\eta_{\alpha\beta}$ parameters on which they depend. In our final constraints on $\eta_{\alpha\beta}$ the dependence on V_{us} has been treated as a nuisance parameter and the χ^2 has been minimized with respect to it.

Superallowed β decay

Superallowed β decays provide the best determination of $|V_{ud}|$. However, in presence of a non-unitary PMNS matrix it will receive a direct correction with $(1 - 2\eta_{ee})$ from the electron and neutrino coupling, as well as the indirect correction from G_F in Eq. (2.16). All in all the value of V_{ud} extracted from this process corresponds to:

$$\left|V_{ud}^{\beta}\right| = (1 + \eta_{\mu\mu}) \, |V_{ud}| \, . \tag{2.27}$$

The most recent update on $\left|V_{ud}^{\beta}\right|$ based on 20 different superallowed β transitions [131] is listed in Tab. (2.2) and will be an input for our fit.

$|V_{us}|$

$|V_{us}|$ can be determined through τ decays and semileptonic or leptonic K decays. The values of $f_+(0)$ and f_K/f_π involved in these observables have been taken from [132].

- K decays

Kaon decays offer a direct way to determine $|V_{us}|$. Apart from their sensitivity to this parameter, decays with μ (e) final states also have a direct dependence on $\eta_{\mu\mu}$ (η_{ee}) which cancels against the indirect dependence through G_μ leading to:

$$\left|V_{us}^{K\to\pi e\overline{\nu}_e}\right| = (1+\eta_{\mu\mu})\,|V_{us}|\,, \tag{2.28}$$

$$\left|V_{us}^{K\to\pi\mu\overline{\nu}_\mu}\right| = (1+\eta_{ee})\,|V_{us}|\,. \tag{2.29}$$

The present determinations of $\left|V_{us}^{K\to\pi e\overline{\nu}_e}\right|$ and $\left|V_{us}^{K\to\pi\mu\overline{\nu}_\mu}\right|$ are listed in Tab.(2.2) and have been obtained from [133,134] together with $f_+(0)$ from [132], the correlation matrix among observables from [133] has also been taken into account.

An alternative determination of $|V_{us}|$ stems from the ratio of the branching fractions $\mathcal{B}(K\to\mu\nu)/\mathcal{B}(\pi\to\mu\nu)$. Notice that in this ratio any direct or indirect dependence on leptonic non-unitarity cancels allowing to constrain the ratio $|V_{us}|/|V_{ud}|$ as in the SM. Since this measurement is latter combined with $\left|V_{ud}^{\beta}\right|$ from Eq. (2.27) to obtain $\left|V_{us}^{K,\pi\to\mu\nu}\right|$ the same $(1+\eta_{\mu\mu})$ correction as for $\left|V_{ud}^{\beta}\right|$ is finally present:

$$\left|V_{us}^{K,\pi\to\mu\nu}\right| = (1+\eta_{\mu\mu})\,|V_{us}|\,. \tag{2.30}$$

- τ decays

  An alternative constraint on $|V_{us}|$ can be obtained from the $\tau\to K\nu_\tau$ decay rate. In presence of non-unitary leptonic mixing, a direct correction by $(1-2\eta_{\tau\tau})$ will be present from the τ coupling as well as the indirect correction from G_F leading to the following dependence:

  $$\left|V_{us}^{\tau\to K\nu_\tau}\right| = (1+\eta_{ee}+\eta_{\mu\mu}-\eta_{\tau\tau})\,|V_{us}|\,. \tag{2.31}$$

  The value of $\left|V_{us}^{\tau\to K\nu_\tau}\right|$ is given in Tab. (2.2) [135].

Another possibility is to constrain $|V_{us}|$ from the ratio $\mathcal{B}(\tau\to K\nu_\tau)/\mathcal{B}(\tau\to\pi\nu_\tau)$. In complete analogy to Eq. (2.30), the sensitivity to the non-unitarity parameters takes the form:

$$\left|V_{us}^{\tau\to K,\pi}\right| = (1+\eta_{\mu\mu})\,|V_{us}|\,. \tag{2.32}$$

All these observables with the values listed in Tab. (2.2) will be used to fit for η_{ee}, $\eta_{\mu\mu}$ and $\eta_{\tau\tau}$. Regarding $|V_{us}|$, its value will be free to vary in the fit and will

be treated as a nuisance parameter, choosing the value of $|V_{us}|$ that minimizes the χ^2 for each value of η_{ee}, $\eta_{\mu\mu}$ and $\eta_{\tau\tau}$.

2.2.5 Lepton flavor violating observables

Flavour transitions $\alpha \to \beta$ in presence of non-unitary mixing such that $(N^\dagger N)_{\alpha\beta} = -2\eta_{\alpha\beta} \neq 0$ are no longer protected by the GIM [136] mechanism. Thus, the stringent constraints that exist on lepton flavour violating (LFV) processes translate into strong probes of the PMNS unitarity, in particular on the off-diagonal elements $\eta_{\alpha\beta}$. Notice that from Eq. (2.8) η is a positive-definite matrix and its off diagonal elements subject to the Schwarz inequality:

$$|\eta_{\alpha\beta}| \leq \sqrt{\eta_{\alpha\alpha}\eta_{\beta\beta}}, \tag{2.33}$$

as summarized in Table 2.1. Thus, the direct constraints on the diagonal elements of η stemming from the processes discussed above also constrain indirectly the size of the off-diagonal entries. Moreover, for the 3N-SS, Eq. (2.11) implies that the Schwarz inequality is saturated to an equality. Therefore, in the G-SS a global fit to constrain the diagonal elements of η with the list of observables described above will be performed. Then, constraints on the off-diagonal entries will be derived indirectly through the Schwarz inequality and compared with the direct bounds from LFV processes. For the 3N-SS, the LFV observables will be added directly to the global fit since they also constrain the diagonal elements through the saturation of the inequality.

Below we list and describe the set of LFV transitions that would take place through non-unitary leptonic mixing. The present experimental bounds and future sensitivities are summarized in Table. 2.3. A comparison summarizing the present relative importance of these observables constraining the off-diagonal elements of η (solid lines) is presented in Fig. 2.1. Since the LFV observables typically depend on the value of the heavy masses, we have performed the comparison for the 3N-SS, since there is only a common scale that simplifies the comparison. As can be seen, radiative decays $l_\alpha \to l_\beta\gamma$ presently dominate the existing bounds and will thus be added to the global fit in the 3N-SS. However, regarding future expectations (dotted lines), the constraints on $|\eta_{e\mu}|$ will be dominated by $\mu \to eee$ or $\mu - e$ transitions in nuclei rather than by $\mu \to e\gamma$. On the other hand, the present and future sensitivity to $|\eta_{e\tau}|$ and $|\eta_{\mu\tau}|$ is completely dominated by the radiative decays $l_\alpha \to l_\beta\gamma$. In

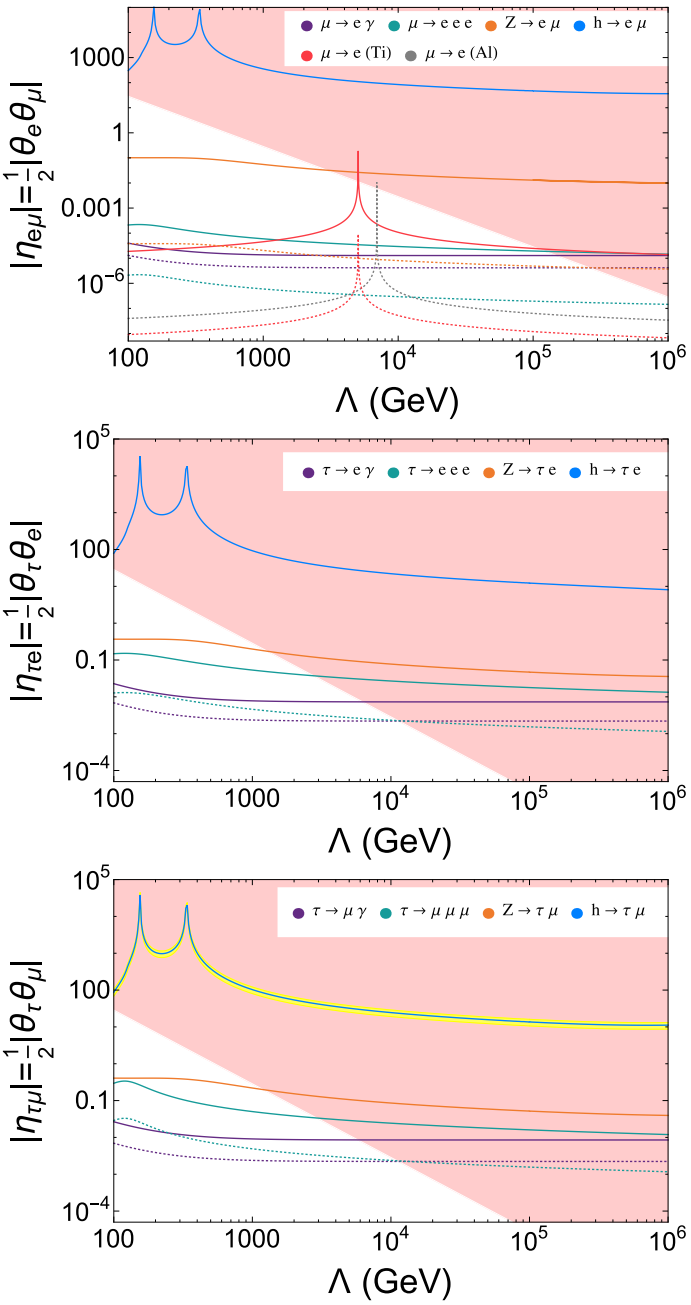

Figure 2.1: 90% CL constraints on $\eta_{\alpha\beta}$ from LFV observables in the 3N-SS. Solid lines represent current experimental bounds while dotted lines represent future sensitivities as listed in Table. 2.3. The red-shadowed region represents the non-perturbative region with $|Y_N|^2 > 6\pi$. In the bottom panel, given the preference for non-zero $h \to \tau\mu$ [137, 138] we show the preferred value in blue and the the 1σ region in yellow.

particular, the constraints on $|\eta_{\alpha\beta}|$ from the LFV decays of the Z and Higgs bosons, $Z \to l_\alpha l_\beta$ and $h \to l_\alpha l_\beta$, are at least one or three orders of magnitude weaker than the bounds from radiative decays respectively. Unfortunately this precludes the explanation of the present mild preference for non-zero $h \to \mu\tau$ [137, 138] through heavy neutrino mixing (see yellow band in the lower panel of Fig. 2.1). Indeed, the values of the Yukawas required to explain these events are, not only excluded by the other observables depicted in the third panel of Fig. 2.1, but also fall into the non-perturbative region, shaded red in the figure.

Observable	Experimental bound	Future sensitivity
$\mu \to e\gamma$	$< 4.2 \cdot 10^{-13}$ [128]	$< 6 \cdot 10^{-14}$ [139]
$\tau \to \mu\gamma$	$< 3.3 \cdot 10^{-8}$ [128]	$< 3 \cdot 10^{-9}$ [140]
$\tau \to e\gamma$	$< 4.4 \cdot 10^{-8}$ [128]	$< 3 \cdot 10^{-9}$ [140]
$Z \to e\mu$	$< 7.1 \cdot 10^{-7}$ [141]	$< 10^{-13}$ [142]
$Z \to \tau e$	$< 9.3 \cdot 10^{-6}$ [143, 144]	–
$Z \to \tau\mu$	$< 1.1 \cdot 10^{-5}$ [144, 145]	–
$h \to e\mu$	$< 3.4 \cdot 10^{-4}$ [146]	–
$h \to \tau e$	$< 6.6 \cdot 10^{-3}$ [146]	–
$h \to \tau\mu$	$(8.2 \pm 3.2) \cdot 10^{-3}$ [137, 138]	–
$\mu \to eee$	$< 10^{-12}$ [147]	$< 10^{-16}$ [148]
$\tau \to eee$	$< 2.7 \cdot 10^{-8}$ [149]	$< 2 \cdot 10^{-10}$ [140]
$\tau \to \mu\mu\mu$	$< 2.1 \cdot 10^{-8}$ [149]	$< 2 \cdot 10^{-10}$ [140]
$\mu \to e$ (Al)	–	$< 10^{-17}$ [150]
$\mu \to e$ (Ti)	$< 4.3 \cdot 10^{-12}$ [151]	$< 10^{-18}$ [152]

Table 2.3: Summary of the present constraints and expected future sensitivities for the different LFV observables considered.

LFV Z decays

For the 3N-SS, the $Z \to l_\alpha^\mp l_\beta^\pm$ decay branching ratio is simplified to [153]

$$\mathcal{B}\left(Z \to l_\alpha^\mp l_\beta^\pm\right) = \frac{\alpha^2 M_Z^3 G_\mu}{24\sqrt{2}\pi^3 s_w \Gamma_Z} |\eta_{\alpha\beta}|^2 \left|F(\lambda) - F(0) + G(\lambda,0) + G(0,\lambda) - 2G(0,0)\right|^2, \tag{2.34}$$

where

$$\begin{aligned} G(\lambda_i,\lambda_j) &= 2C_{24} - 1 - \lambda_Q\left(C_0 + C_{11} + C_{12} + C_{23}\right) - \frac{\lambda_i\lambda_j}{2} C_0, \\ F(\lambda) &= 2c_w^2\left[\lambda_Q\left(\bar{C}_{11} + \bar{C}_{12} + \bar{C}_{23}\right) - 6\bar{C}_{24} + 1\right] - \lambda(1-2s_w^2)\bar{C}_{24} \\ &- 2s_w^2\lambda\bar{C}_0 + \frac{1-2c_w^2}{2}\left[(1+\lambda)B_1 + 1\right], \end{aligned} \tag{2.35}$$

and $\lambda = \Lambda^2/M_W^2$, $\lambda_Q = (p_\alpha - p_\beta)^2/M_W^2 = M_Z^2/M_W^2 + \mathcal{O}(m_l^2/M_W^2)$ and $C_{\{0,11,12,23\}}$, $C_{\{0,11,12,23,24\}}$ and B_1 defined in Appendix C of [153].

As shown in Fig. 2.1, at present $l_\alpha \to l_\beta\gamma$ is able to set bounds much stronger than through this process.

LFV h decays

In the case of the LFV Higgs decay the expression at $\mathcal{O}\left(\eta_{\alpha\beta}^2\right)$ for the branching ratio is much more involved than in the $Z \to l_\alpha^\mp l_\beta^\pm$ case. In Fig. 2.1 we have used the complete computation presented in [154–156]. Nevertheless, we instead present here an approximate expression which can be useful in order to understand the dependence on the parameters in the 3N-SS.

$$\mathcal{B}\left(h \to l_\alpha^\mp l_\beta^\pm\right) \approx \frac{\alpha^3}{64\,\pi^2 s_w^6 \Gamma_h}\left(\frac{\Lambda}{M_W}\right)^4 M_h\,|\eta_{\alpha\beta}|^2\left(\frac{m_\alpha^2}{M_W^2}\,|f_L|^2 + \frac{m_\beta^2}{M_W^2}\,|f_R|^2\right), \tag{2.36}$$

where

$$\begin{aligned} f_L &= \frac{M_h^2}{2}\left(C_0 + C_{11} - C_{12}\right), \\ f_R &= \frac{M_h^2}{2}\left(C_0 + C_{12}\right), \end{aligned} \tag{2.37}$$

and $C_{\{0,11,12\}} = C_{\{0,11,12\}}(m_\alpha^2, M_h^2, \Lambda^2, M_W^2, M_W^2)$. This approximate result is reasonably accurate for scales above few TeV and works very well for $\Lambda \gtrsim 10$ TeV. However,

since here we are neglecting $\mathcal{O}\left(M_W^2/\Lambda^2\right)$ contributions, it fails for $\Lambda \lesssim 1$ TeV. In any case, the full calculation shows that the constraints on $|\eta_{\alpha\beta}|$ are still very far from the present radiative bounds, falling indeed in the non perturbative region.

$l_\alpha \to l_\beta l_\beta l_\beta$ decay

Another LFV observable that would be induced by heavy neutrino mixing is the $l_\alpha \to l_\beta l_\beta l_\beta$. Its branching ratio, for the 3N-SS, is given by [157]

$$\begin{aligned}\mathcal{B}\left(l_\alpha \to l_\beta l_\beta l_\beta\right) &= \frac{G_\mu^4 M_W^4 m_\alpha^5 \left|\eta_{\alpha\beta}\right|^2}{18432\pi^7\Gamma_\alpha}\left\{54 - 1188 s_{\rm W}^2 + s_{\rm W}^4\left(1105 + 96\log\left(\frac{m_\alpha^2}{m_\beta^2}\right)\right)\right. \\ &+ \left. 2\log^2\frac{\Lambda^2}{M_W^2}\left(27 - 96 s_{\rm W}^2 + 128 s_{\rm W}^4\right) - 4\log\frac{\Lambda^2}{M_W^2}\left(27 - 219 s_{\rm W}^2 + 296 s_{\rm W}^4\right)\right\}. \end{aligned} \tag{2.38}$$

Notice that, while additional non-unitarity corrections from G_μ and $s_{\rm W}^2$ (also through Γ_α when $\alpha \neq \mu$) would be present, these are higher order in η and therefore subleading since the whole process is already proportional to $|\eta_{\alpha\beta}|^2$.

Fig. 2.1 shows that the present $\mu \to eee$ decay bound on $|\eta_{e\mu}|$ is quite competitive with the one coming from $\mu \to e\gamma$. The constraint is presently dominated by $\mu \to e\gamma$, but it is expected to be overcome by $\mu \to eee$ in the future. On the other hand, the present and future sensitivity to $|\eta_{e\tau}|$ and $|\eta_{\mu\tau}|$ is dominated by the radiative decays.

$\mu \to e$ conversion

In the 3N-SS, the ratio between $\mu \to e$ conversion rate over the capture rate Γ_{capt} in light nuclei is given by [114]

$$R_{\mu\to e} \simeq \frac{G_\mu^2\alpha^5 m_\mu^5}{2 s_w^4 \pi^4 \Gamma_{\rm capt}}\frac{Z_{\rm eff}^4}{Z}|\eta_{e\mu}|^2 F_p^2\Big[\left(A+Z\right)F_u + \left(2A - Z\right)F_d\Big]^2 \quad . \tag{2.39}$$

where A corresponds to the mass number, Z ($Z_{\rm eff}$) stands for the (effective) atomic number, F_p is a nuclear form factor and

$$\begin{aligned} F_u &= \frac{2}{3}s_W^2\frac{16\log\left(\frac{\Lambda^2}{M_W^2}\right)-31}{12}-\frac{3+3\log\left(\frac{\Lambda^2}{M_W^2}\right)}{8}, \\ F_d &= -\frac{1}{3}s_W^2\frac{16\log\left(\frac{\Lambda^2}{M_W^2}\right)-31}{12}-\frac{3-3\log\left(\frac{\Lambda^2}{M_W^2}\right)}{8}, \end{aligned}$$

The bounds shown in Fig. 2.1 have been obtained from $\mu \to e$ conversion transitions in $^{27}_{13}$Al and $^{48}_{22}$Ti. The input values for the nuclear parameters F_p, $Z_{\rm eff}$ and $\Gamma_{\rm capt}$ have been extracted from [158, 159] and are summarized in Table 1 of [114].

According to the forecasted performances the future sensitivity to $|\eta_{e\mu}|$ will be dominated by this observable. Remarkably, future $\mu \to e$ searches [152] could improve the present bound by three orders of magnitude making it a very promising channel to probe for new physics signal in LFV decays.

Radiative decays

In the G-SS, the branching ratio for the radiative decays $l_\alpha \to l_\beta\gamma$ is given by:

$$\frac{\Gamma\left(l_\alpha \to l_\beta\gamma\right)}{\Gamma\left(l_\alpha \to l_\beta\nu_\alpha\overline{\nu}_\beta\right)} = \frac{3\alpha}{32\pi}\frac{\left|\sum_{k=1}^{n} U_{\alpha k}U_{k\beta}^{\dagger}F\left(x_k\right)\right|^2}{\left(UU^\dagger\right)_{\alpha\alpha}\left(UU^\dagger\right)_{\beta\beta}}, \tag{2.40}$$

where $x_k \equiv \frac{M_k^2}{M_W^2}$, and

$$F(x_k) \equiv \frac{10-43x_k+78x_k^2-49x_k^3+4x_k^4+18x_k^3\ln x_k}{3(x_k-1)^4}. \tag{2.41}$$

For $M_k \gg M_W$ the limit can be simplified to:

$$\frac{\Gamma\left(l_\alpha \to l_\beta\gamma\right)}{\Gamma\left(l_\alpha \to l_\beta\nu_\alpha\overline{\nu}_\beta\right)} \simeq \frac{3\alpha}{8\pi}\left|\eta_{\alpha\beta}\right|^2\left(F\left(\infty\right)-F\left(0\right)\right)^2 = \frac{3\alpha}{2\pi}\left|\eta_{\alpha\beta}\right|^2. \tag{2.42}$$

This expression shows how the non-unitarity induced in the PMNS by the heavy neutrinos and the separation of the two scales prevents the GIM cancellation. Indeed, the cancellation is recovered in the limit $x_k \ll 1$.

These radiative decays are the observables dominating the present constraints on $\eta_{\alpha\beta}$ as shown in Fig. 2.1 and will thus be the ones introduced in the fit through Eq. (2.42) for the 3N-SS. In the G-SS, these constraints will be compared with the bounds stemming from the Schwarz inequality Eq. (2.33) from the outcome of the global fit to the diagonal entries.

2.3 Results

With the list of observables described in the previous section and under a Gaussian approximation we construct a χ^2 function to scan the parameter spaces of the G-SS and the 3N-SS. For the G-SS the free parameters of the fit are directly η_{ee}, $\eta_{\mu\mu}$ and $\eta_{\tau\tau}$ without further constraints and all the observables listed in Section 2.2 except for the LFV transitions will be used to constrain them. The LFV radiative decays rather constrain the off-diagonal elements of the matrix η. Therefore, to obtain the global constraints on the off-diagonal elements, the LFV radiative decays will be combined and compared with the indirect bounds implied by the Schwarz inequality Eq. (2.33) from the lepton flavour conserving observables.

Regarding the 3N-SS, the free parameters for the fit are θ_e and θ_μ (modulus and phase) while θ_τ is given by Eq. (2.12) once the light neutrino masses and mixings are specified through the $d = 5$ operator $\hat{m}$. Thus, we also take as free parameters of the fit the values of the unknown phases of the PMNS matrix Dirac (δ) and Majorana (α_1 and α_2) as well as the mass of the lightest neutrino mass eigenstate for both a normal and an inverted neutrino mass ordering. The rest of the oscillation parameters are fixed to their best fits from Ref. [127] since they are well-constrained by present neutrino oscillation data. Notice that, a priori, the number of free parameters we fit for in the 3N-SS case is larger than in the G-SS. However, this larger number of parameters is only included to take into account the constraints affecting θ_τ (and therefore $\eta_{\tau\tau}$) via Eq. (2.12) that are absent in the G-SS. Indeed, as we will see from the results of the fit, these constraints imply extra correlations between the parameters of the 3N-SS and there is in fact less freedom in the relevant parameters η_{ee}, $\eta_{\mu\mu}$ and $\eta_{\tau\tau}$ to fit for the observables. Since for the 3N-SS the Schwarz inequality Eq. (2.33) is saturated $|\eta_{\alpha\beta}| = \sqrt{\eta_{\alpha\alpha}\eta_{\beta\beta}}$, the LVF radiative decays also imply non-trivial constraints on the values of θ_α and the diagonal elements $\eta_{\alpha\alpha}$ and will hence be included in the list of observables of the global fit. Notice that, under the approximation of Eq. (2.42), the LFV radiative decays do not depend on the Majorana

mass scale. Therefore, since none of the observables for the G-SS or 3N-SS cases depend directly on the Majorana masses, the bounds on the mixing derived apply for any choice of the heavy neutrino masses above the electroweak scale.

In Fig. 2.2 we present our results from the global fit, performed by scanning the relevant parameter spaces through a Markov chain Monte Carlo algorithm. The results presented here correspond to the frequentist confidence intervals for 1σ, 90% and 2σ significance. We present the results directly in the heavy-active neutrino mixing θ_α for the 3N-SS under the assumption of a normal neutrino ordering (middle panels) and inverted neutrino ordering (lower panels). To ease the comparison of the constraints, we present the results for the G-SS (upper panels) in the variable $\sqrt{2\eta_{\alpha\alpha}}$, which can be identified with the total effective mixing of the different heavy mass eigenstates with the flavour α, see Eq. (2.13), and an upper bound on the individual mixing $\Theta_{\alpha i}$ of any additional heavy neutrino N_i. As can be seen, while the bounds on the individual parameters are comparable in strength for the two scenarios, the constraints imposed by Eqs. (2.11) and (2.12) for the 3N-SS reflect in strong correlations for their allowed regions. In particular, $\mu \to e\gamma$ imposes a very stringent constraint in the product $\theta_e\theta_\mu$ leading to the hyperbolic constraints in the middle-left and bottom-left panels of the figure and absent in the upper for the G-SS. On the other hand, in the middle and bottom-right panels of the figure non-trivial correlations between θ_e and θ_τ, absent in the upper-right panel for the G-SS, can be observed. This stems from the fact that θ_τ is not free to take any value preferred by the observables, but constrained by θ_e, θ_μ and the neutrino masses and mixings through Eq. (2.12).

To summarize the results of the global fit we present in Fig. 2.3 the profiles of the $\Delta\chi^2$ obtained as a function of the individual θ_α and minimized over all the other parameters. The 1 and 2σ regions are colored in red and blue respectively. As can be seen, the observables considered (notably the invisible width of the Z and M_W) overall show a mild (between 1 and 2σ) preference for some degree of non-unitarity $\theta \sim 0.03-0.04$. The constraints on the universality of the weak interactions, particularly from ratios of pion and lepton decays, prefer these unitarity deviations with non-vanishing mixing with the heavy neutrinos to take place in the electron and tau sectors. This preference is clear in the upper panels of Fig. (2.3), which show the constraints for the unbounded G-SS. But, even in the more constraint case of a 3N-SS (middle panels for normal hierarchy and lower panels for inverted), there is enough freedom to accommodate this general preference shown by the datasets considered. The more characteristic feature that distinguishes the 3N-SS from the G-SS in Fig. 2.3

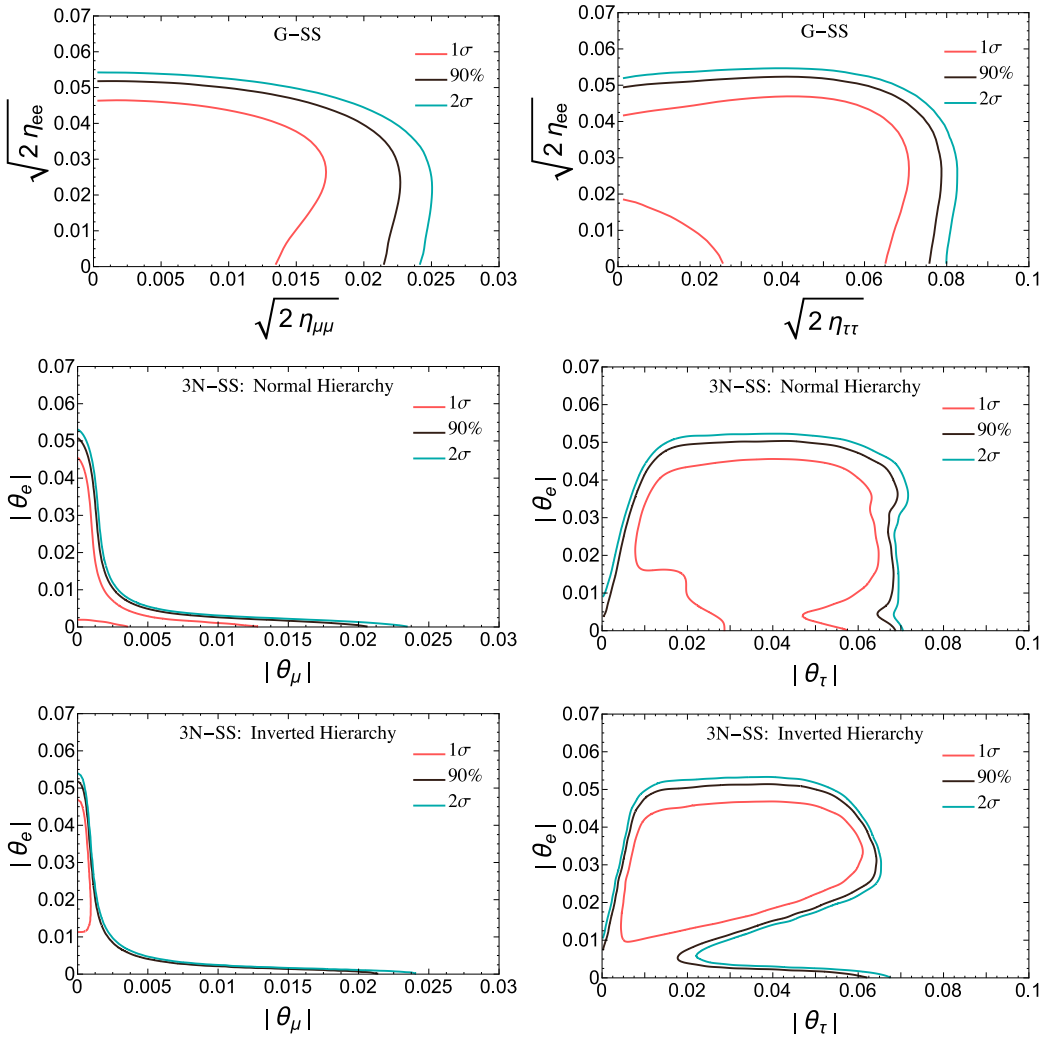

Figure 2.2: Frequentist confidence intervals at 1σ, 90% and 2σ on the parameter space of the G-SS (upper panels) and the 3N-SS for normal hierarchy (middle panels) and inverted hierarchy (bottom panels).

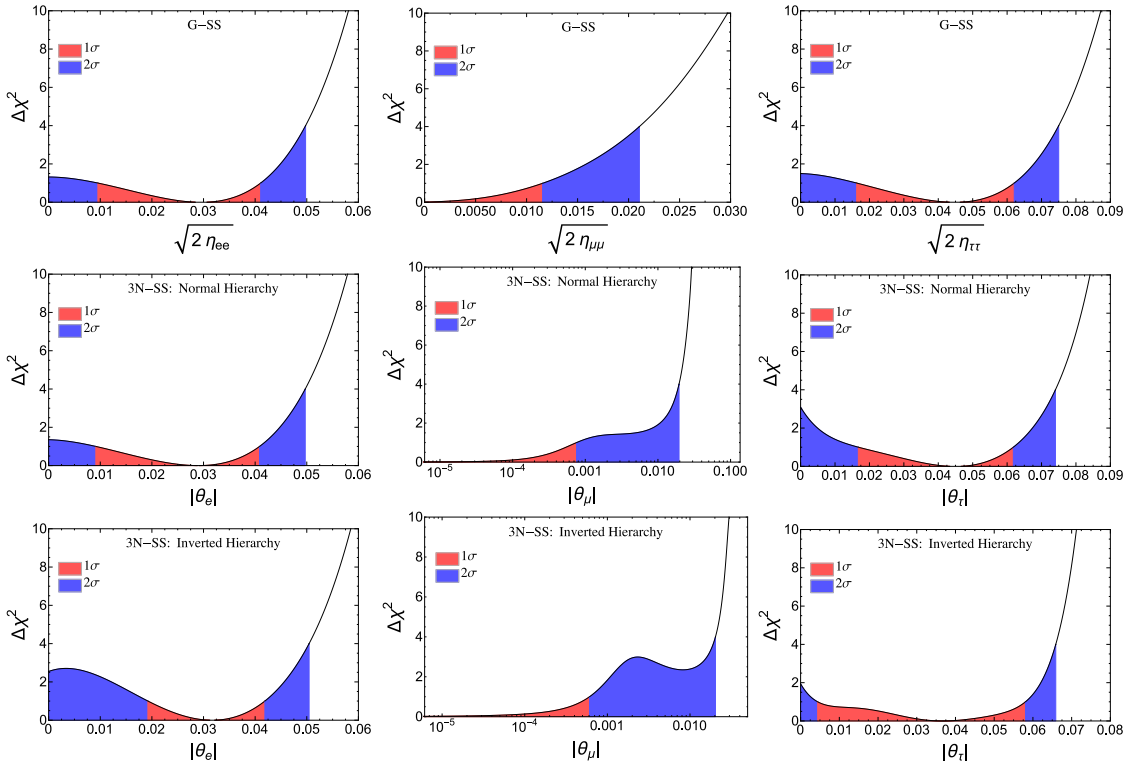

Figure 2.3: $\Delta\chi^2$ profile minimized over all fit variables except for one θ_α (or $\sqrt{2\eta_{\alpha\alpha}}$) in the case of the G-SS) at a time. The upper panels are for the G-SS, and the middle and lower panels for the 3N-SS for a normal and inverted hierarchy respectively.

is the constraint in θ_μ which, for the 3N-SS shows a very non-Gaussian behavior with a very stringent 1σ limit and a much milder 2σ bound comparable to the one found for the G-SS. The reason for the comparatively much stronger 1σ constraint stems from the very stringent constraint from $\mu \to e\gamma$, which for the 3N-SS imply either a very small θ_e or θ_μ. Together with the 1σ preference for non-vanishing θ_e, this implies a very strong 1σ upper bound for θ_μ. On the other hand, at the 2σ level θ_e can be arbitrarily small and thus the bound on θ_μ from $\mu \to e\gamma$ is evaded. Regarding the G-SS, $\mu \to e\gamma$ only constrains the element $\eta_{e\mu}$ and not η_{ee} or $\eta_{\mu\mu}$ since, contrary to the 3N-SS, the Schwarz inequality Eq. (2.33) is not saturated. Regarding θ_e and θ_τ, the limits for the 3N-SS and the G-SS are much more similar between them. Indeed, despite the constraint from Eq. (2.12) on θ_τ, the preferred value for this parameter in the 3N-SS does not show significant deviations with respect to the G-SS. However, non-trivial correlations among the Majorana phases α_1 and α_2 as well as among the phases of θ_e and θ_τ: α_e and α_τ when a normal neutrino mass ordering is assumed are required to satisfy Eq. (2.12). These phase correlations are shown in Fig. 2.4. Two

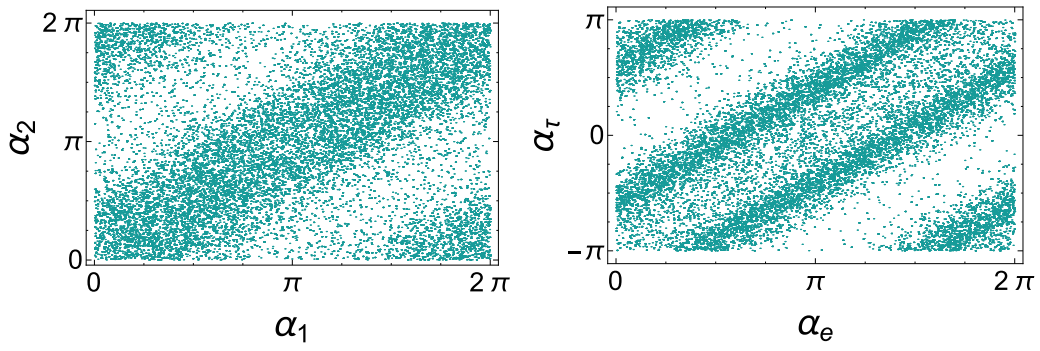

Figure 2.4: Points scanned by the MCMC algorithm with a $\Delta\chi^2 < 1$ showing the mild preferred correlation between the two Majorana phases of the PMNS matrix α_1 and α_2 (left panel) and between the phases of θ_e and θ_τ: α_e and α_τ (right panel) for the 3N-SS and under a normal hierarchy assumption.

interesting features can be observed: (i) The values of the PMNS Majorana phases such that $\alpha_1 - \alpha_2 \sim 2n\pi$ are favoured (left plot); (ii) The data prefers values for the phases of θ_τ and θ_e which satisfy $\alpha_\tau - \alpha_e \sim (2n+1)\,\pi$ (right plot). In the IH case, we have not found any significant correlation among the phases.

Regarding the off-diagonal elements $|\eta_{\alpha\beta}|$, we present in Fig. 2.5 the limits obtained from the combination of all observables as a function of $\sqrt{2|\eta_{\alpha\beta}|}$ and marginal-

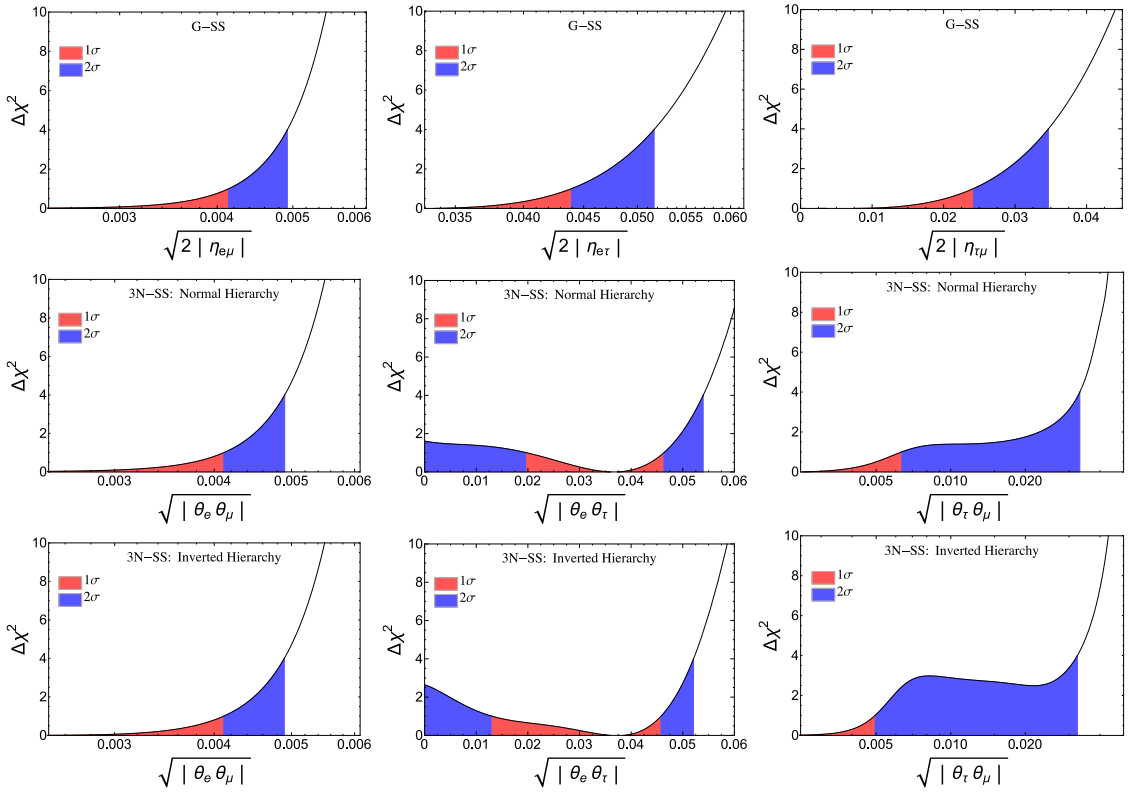

Figure 2.5: Bounds on the off-diagonal entries of $\eta_{\alpha\beta}$ ($|\theta_\alpha\theta_\beta|$ for the 3N-SS). The upper panels are for the G-SS, and the middle and lower panels for the 3N-SS for a normal and inverted hierarchy respectively. For the G-SS the strongest limit between the direct bound from radiative LFV decays and the indirect limit from the diagonal entries through the Schwarz inequality is shown for each element.

ized over all the other parameters for the G-SS (upper panels) and the 3N-SS for NH (middle panels) and IH (lower panels). As in Fig. 2.3, the 1 and 2σ regions are colored in red and blue respectively. For the G-SS the strongest limit between the direct bound from radiative LFV decays and the indirect limit from the diagonal entries through the Schwarz inequality is shown. For $|\eta_{e\mu}|$ the constraint from $\mu \to e\gamma$ gives the most stringent bound while for $|\eta_{e\tau}|$ and $|\eta_{\mu\tau}|$ the indirect constraints from the lepton flavor conserving (LFC) processes included in the global fit together with the Schwarz inequality Eq. (2.33) rather dominate. Moreover, the bound on the product $|\theta_e\theta_\tau|$ for the 3N-SS shows a 1σ preference for a non-zero value. This mild hint can be translated into a prediction for LFV $\tau - e$ transitions, in particular, to a branching ratio of $\tau \to e\gamma$ of $\sim 2.5\cdot 10^{-10}$ for $|\eta_{e\tau}| \sim 6\cdot 10^{-4}$. This is rather challenging to probe but not very far from the future sensitivities expected at Super-B factories.

2.4 Discussion and conclusions

A global fit to lepton flavor and electroweak precision data has been performed to constrain the size presently allowed for the mixing of the extra heavy Seesaw neutrinos with the SM leptons. The analysis has been performed both in a completely general Seesaw (G-SS) with the effects of the extra neutrinos encoded in effective operators with no assumed correlations and for the particular case where only three heavy neutrinos are considered (3N-SS). The results of the fit are summarized in Table 2.4.

For the G-SS with an arbitrary number of extra heavy neutrinos the bounds are expressed in the quantity $\sqrt{2|\eta_{\alpha\beta}|} = \sum_i \sqrt{\Theta_{\alpha i}\Theta^*_{\beta i}}$ (see Eq. (2.13)). Thus, the diagonal elements $\sqrt{2\eta_{\alpha\alpha}}$ correspond to the sum (in quadrature) of all mixings $\Theta_{\alpha i}$ of the individual extra heavy neutrinos N_i to a given SM flavor α and represent an upper bound on each individual mixing. The off-diagonal entries, on the other hand, are the combinations that can mediate LFV transitions and even provide extra sources of CP-violation. Notice that, from this definition, η is a positive definite matrix and its off-diagonal elements subject to the Schwarz inequality $|\eta_{\alpha\beta}| \leq \sqrt{\eta_{\alpha\alpha}\eta_{\beta\beta}}$.

In the case of the 3N-SS, only one mixing parameter θ_α per SM flavor α can be large enough to saturate the bounds derived here, so as to comply with our present constraints on light neutrino masses and mixings from neutrino oscillation data (see discussion in Section 2.1). Thus, the Schwarz inequality is saturated to an equality for the 3N-SS. Furthermore, some non-trivial correlations between the parameters

		G-SS		3N-SS	
		LFC	LFV	NH	IH
$\sqrt{2\eta_{ee}}$, $\lvert\theta_e\rvert$	1σ	$\mathbf{0.031^{+0.010}_{-0.020}}$	–	$0.029^{+0.012}_{-0.020}$	$\mathbf{0.031^{+0.010}_{-0.012}}$
	2σ	$< \mathbf{0.050}$	–	< 0.050	$< \mathbf{0.050}$
$\sqrt{2\eta_{\mu\mu}}$, $\lvert\theta_\mu\rvert$	1σ	$< \mathbf{0.011}$	–	$< \mathbf{7.6 \cdot 10^{-4}}$	$< 6.9 \cdot 10^{-4}$
	2σ	$< \mathbf{0.021}$	–	< 0.020	$< \mathbf{0.023}$
$\sqrt{2\eta_{\tau\tau}}$, $\lvert\theta_\tau\rvert$	1σ	$\mathbf{0.044^{+0.019}_{-0.027}}$	–	$\mathbf{0.043^{+0.018}_{-0.027}}$	$0.037^{+0.021}_{-0.032}$
	2σ	$< \mathbf{0.075}$	–	$< \mathbf{0.074}$	< 0.066
$\sqrt{2\eta_{e\mu}}$, $\sqrt{\lvert\theta_e\theta_\mu\rvert}$	1σ	< 0.018	$< \mathbf{4.1 \cdot 10^{-3}}$	$< \mathbf{4.1 \cdot 10^{-3}}$	$< 4.1 \cdot 10^{-3}$
	2σ	< 0.026	$< \mathbf{4.9 \cdot 10^{-3}}$	$< \mathbf{4.9 \cdot 10^{-3}}$	$< 4.9 \cdot 10^{-3}$
$\sqrt{2\eta_{e\tau}}$, $\sqrt{\lvert\theta_e\theta_\tau\rvert}$	1σ	$< \mathbf{0.045}$	< 0.107	$\mathbf{0.036^{+0.010}_{-0.016}}$	$0.036^{+0.010}_{-0.023}$
	2σ	$< \mathbf{0.052}$	< 0.127	$< \mathbf{0.054}$	0.052
$\sqrt{2\eta_{\mu\tau}}$, $\sqrt{\lvert\theta_\mu\theta_\tau\rvert}$	1σ	$< \mathbf{0.024}$	< 0.115	$< \mathbf{0.007}$	0.005
	2σ	$< \mathbf{0.035}$	< 0.137	$< \mathbf{0.033}$	0.032

Table 2.4: Comparison of all 1 and 2σ constraints on the heavy-active neutrino mixing. For the G-SS the bounds are expressed for $\sqrt{2\eta_{\alpha\beta}}$ (see Eq. (2.13)). For the off-diagonal entries the indirect bounds from the LFC observables via the Schwarz inequality Eq. (2.33) are compared with the direct LFV bounds and the dominant bound is highlighted in bold face. For the 3N-SS the bounds are shown for θ_α for assumptions of a normal (NH) and inverted hierarchy (IH), the less stringent bound is highlighted in bold face as an overall bound on the 3N-SS case.

θ_α are also present (see Eq. (2.12)).

As shown in Table 2.4 the data show a mild, between 1 and 2σ preference, for non-zero heavy-active mixing of order $\sim 0.03 - 0.04$ in the e and τ sectors. At the 2σ level, upper bounds in all mixing parameters are found. The most stringent one ~ 0.02 is found for the mixing with muons, followed by ~ 0.05 for electrons and ~ 0.07 for taus. Regarding the off diagonal entries, for the G-SS the indirect bounds from

LFC processes can be compared with the direct constraints from LFV observables. Interestingly, the constraint from $\mu \to e\gamma$ strongly dominates over all others leading to a bound one order of magnitude better ~ 0.005 in the $e-\mu$ entry, while the $e-\tau$ and $\mu-\tau$ values are rather dominated by the indirect constraints from the Schwarz inequality (comparison between the LFC and LFV columns). Regarding the 3N-SS, even though the necessity of correctly reproducing the observed neutrino mass and mixing pattern introduces non-trivial correlations among the θ_α and the neutrino masses and mixings (dependence on normal or inverted hierarchy assumptions shown in the comparison of the third and fourth columns), there is still enough freedom to obtain very similar bounds to those found for the G-SS. This however implies some non-trivial correlations preferred at 1σ notably among the PMNS matrix Majorana phases as well as among the phases of θ_e and θ_τ as shown in Fig. 2.4.

The bounds derived here represent the most updated set of constraints and compare well with previous studies. Notably, it is interesting to compare with another recent global fit presented in Ref. [116] were bounds to the G-SS were also studied. We find that the agreement between the two sets of constraints is generally good. The same preference for non-zero mixing in the electron and tau sectors was found but in their case the preferred value is slightly ($\sim 20-30\%$) larger. Similarly the upper bound on muon mixing is weaker in Ref. [116]. Conversely the limits on the off-diagonal elements are slightly ($\sim 20-40\%$) stronger in Ref. [116] for the $e-\tau$ and $\mu-\tau$ sectors. The only very noticeable difference is in the $e-\mu$ sector where the limit from $\mu \to e\gamma$ is almost a factor 3 stronger than the one presented here (despite not being yet updated to the final MEG result). This difference can be attributed to not considering the propagation of the heavy neutrinos in the loop for the process which tends to restore the GIM cancellation (given the Unitarity of the full mixing matrix) and to therefore slightly weaken by the corresponding factor the bound stemming from the process. This extra contribution was not taken into account in Ref. [116] since a more agnostic source of the non-unitarity of the PMNS matrix was adopted while here we concentrate in constraining heavy neutrino mixings. The rest of the discrepancies can stem from small differences in our analyses. For example our observables for weak lepton universality and CKM unitarity are more updated and our bounds correspond to frequentist confidence regions while Ref. [116] rather presented Bayesian credible intervals. Regarding the 3N-SS, the closest study of a similar setup in the literature is that of Ref. [125]. This work is rather complementary to our results focusing instead in the region between 10 to 250 GeV, where more stringent constraints are derived since the extra neutrinos would be kinematically

accessible.

It is also interesting to translate the bounds derived here to other common parametrizations, useful in particular for the analysis of neutrino non-standard interactions (see e.g. Ref. [160]). Indeed, the non-unitary PMNS matrix induced by the mixing with the extra heavy neutrinos modifies the neutrino production and detection processes, which can be encoded in production/detection NSI [103, 112]. In particular:

$$|\varepsilon^{p,d}_{\alpha\beta}| = |\eta_{\alpha\beta}| \leq \begin{pmatrix} 1.3 \cdot 10^{-3} & 1.2 \cdot 10^{-5} & 1.4 \cdot 10^{-3} \\ 1.2 \cdot 10^{-5} & 2.2 \cdot 10^{-4} & 6.0 \cdot 10^{-4} \\ 1.4 \cdot 10^{-3} & 6.0 \cdot 10^{-4} & 2.8 \cdot 10^{-3} \end{pmatrix} . \tag{2.43}$$

Furthermore, neutrino interactions with matter are also affected and these effects can also be described by matter NSI [112]:

$$\varepsilon^{m}_{\alpha\beta} = 2\eta_{\alpha e}\delta_{\beta e} + 2\eta_{e\beta}\delta_{e\alpha} - \frac{n_n}{n_e}\, 2\eta_{\alpha\beta}, \tag{2.44}$$

where n_e and n_n are the electron and neutron densities of the matter traversed by the neutrinos.

Finally, an alternative parametrization of the non-unitarity of the PMNS matrix of the form $N = TU$ with T a lower triangular matrix [161–163]:

$$T = \begin{pmatrix} \alpha_{ee} & 0 & 0 \\ \alpha_{\mu e} & \alpha_{\mu\mu} & 0 \\ \alpha_{\tau e} & \alpha_{\tau\mu} & \alpha_{\tau\tau} \end{pmatrix} \tag{2.45}$$

is also considered appropriate to study the effects of non-unitary PMNS mixing in neutrino oscillation searches [103, 164–167]. Comparing Eqs. (2.3) and (2.45) it is easy to see that $\alpha_{\beta\beta} \approx 1 - \eta_{\beta\beta}$, while $|\alpha_{\beta\gamma}| \approx 2|\eta_{\beta\gamma}| = |\epsilon_{\beta\gamma}|$ so that the bounds derived here can be trivially translated to this parametrization too. All in all this level of non-unitarity (or equivalently NSI as in Eq. (2.43)) is extremely tough to probe at present or near-future neutrino oscillations facilities and its effects would be negligible. However, prospective very precise neutrino oscillation facilities such as the Neutrino factory [168, 169] could probe beyond this very stringent present limits for some elements [103, 164].

Notice that the bounds derived here apply for any heavy neutrino mass above the electroweak scale. For lighter heavy neutrino masses, the LFV radiative decays start to be suppressed by the restoration of the GIM mechanism (see Eq. (2.42)) and therefore the constraints shown in the LFV column of Table 2.4 are not valid. The rest of the bounds summarized in the LFC column of Table 2.4 do apply down to $\mathcal{O}(500\ \text{MeV})$ with the only exception of the invisible width of the Z, since for masses below $\sim M_Z/2$ the heavy neutrinos can be kinematically produced and unitarity is restored. Therefore, in the region between the Kaon mass and the EW scale we do not expect any significant change in the G-SS bounds shown in the LFC column of Table 2.4. Nevertheless, at these lower energies were the extra neutrinos can be directly produced, more stringent constraints than the ones derived here, from direct searches [165, 170–174] and cosmology [175–187] apply.

In summary, we have combined present probes on weak lepton universality, searches for LFV processes and precision electroweak observables to derive updated and global constraints on the allowed mixing of heavy Seesaw neutrinos with the SM fermions. These bounds apply for any value of the Majorana scale larger than the electroweak scale and have been computed both for a completely general scenario as well as for the case in which only 3 extra heavy neutrinos are considered. At the 1σ level a mild preference for non-zero mixing in the electron and tau sectors around $0.03-0.04$ was found, which could be probed for by improving the LFC searches that currently lead to that preference, as well as through $\tau-e$ LFV transitions. At the 2σ level, upper bounds between 10^{-1} and 10^{-2} for all elements were derived with a most stringent constraint on the mixing in the $e-\mu$ sector an order of magnitude better from the $\mu \to e\gamma$ process. While this is by far the present dominant bound, it will be superseded in the future by $\mu \to eee$ and/or $\mu - e$ conversion in nuclei searches. Apart from this and other improvements in the datasets considered, this level of mixing is challenging but still plausible to probe at future collider [125, 142, 188, 189] and dedicated neutrino oscillation searches [103, 164].

Chapter 3

One-loop global constraints on the 3N-SS

3.1 Parametrization

In this work we explore the constraints that can be derived through various EW observables on the extra neutrino mass eigenstates mixing with charged leptons in a Seesaw scenario:

$$\mathscr{L} \;=\; \mathscr{L}_{\rm SM} - \frac{1}{2}\overline{N_{\rm R}^{i}}(M_N)_{ij}N_{\rm R}^{cj} - (Y_N)_{i\alpha}\overline{N_{\rm R}^{i}}\phi^{\dagger}\ell_{\rm L}^{\alpha} + \text{h.c.}\,. \tag{3.1}$$

Here, ϕ denotes the SM Higgs field, which breaks the EW symmetry after acquiring its vev $v_{\rm EW}$. We have also introduced the Majorana mass M_N allowed for the right-handed neutrinos $N_{\rm R}^{i}$ as well as the Yukawa couplings between the neutrinos and the Higgs field. We will restrict our study to the extension of the SM by 3 right-handed neutrino fields. The vev of the Higgs will induce Dirac masses $m_D = v_{\rm EW}Y_N/\sqrt{2}$. Thus, the full 6×6 mixing matrix U is the unitary matrix that diagonalizes the extended neutrino mass matrix:

$$U^{T}\begin{pmatrix} 0 & m_D^{T} \\ m_D & M_N \end{pmatrix}U = \begin{pmatrix} m & 0 \\ 0 & M \end{pmatrix}, \tag{3.2}$$

where m and M are diagonal matrices containing respectively the masses of the 3 light ν_i and 3 heavy N_i mass eigenstates. The diagonalizing matrix U can be written

as [119]:

$$U = \begin{pmatrix} c & s \\ -s^\dagger & \hat{c} \end{pmatrix} \begin{pmatrix} U_{\rm PMNS} & 0 \\ 0 & I \end{pmatrix}, \tag{3.3}$$

where

$$\begin{pmatrix} c & s \\ -s^\dagger & \hat{c} \end{pmatrix} \equiv \begin{pmatrix} \sum_{n=0}^{\infty} \frac{\left(-\Theta\Theta^\dagger\right)^n}{(2n)!} & \sum_{n=0}^{\infty} \frac{\left(-\Theta\Theta^\dagger\right)^n}{(2n+1)!}\Theta \\ -\sum_{n=0}^{\infty} \frac{\left(-\Theta^\dagger\Theta\right)^n}{(2n+1)!}\Theta^\dagger & \sum_{n=0}^{\infty} \frac{\left(-\Theta^\dagger\Theta\right)^n}{2n!} \end{pmatrix} \tag{3.4}$$

and $U_{\rm PMNS}$ is, *approximately*, the PMNS matrix measured in neutrino oscillation experiments up to the non-Unitary (Hermitian) corrections from c. For alternative parametrizations of the full mixing matrix see Refs [66,162,163,190,191]. Indeed, due to this Hermitian correction, the actual PMNS matrix appearing in charge current interactions mixing the light neutrinos and charged leptons will, in general, not be Unitary and we will refer to it as N:

$$N = c\, U_{\rm PMNS} \tag{3.5}$$

The general matrix Θ, representing the mixing between active (ν_e, ν_μ and ν_τ) and heavy (N_1, N_2 and N_3) neutrino states, and the mass eigenstates m and M are determined from Eq. (3.2) which leads to:

$$c^* U^*_{\rm PMNS} m U^\dagger_{\rm PMNS} c = -s^* M s^\dagger. \tag{3.6}$$

In the Seesaw limit, that is $M_N \gg m_D$, these conditions reduce to the well-known results:

$$\begin{aligned} \Theta &\simeq m_D^\dagger M_N^{-1} \\ U^*_{\rm PMNS} m U^\dagger_{\rm PMNS} &\simeq -m_D^t M_N^{-1} m_D \equiv -\hat{m} \\ M &\simeq M_N. \end{aligned} \tag{3.7}$$

Notice that, naively, the mixing between the active and heavy neutrinos $\Theta\Theta^\dagger \sim m/M$ and, given the smallness of neutrino masses m, the mixing effects we will study here would be unobservably small. However, in the context of Seesaw mechanisms with an approximate conservation of $B - L$ such as the inverse [192, 193] or the linear [194] Seesaws, this symmetry suppresses the neutrino mass m while allowing a sizable mixing. This approximate symmetry not only ensures an equally approximate

cancellation in the combination $m_D^t M_N^{-1} m_D$ leading to the observed neutrino masses while allowing large -potentially observable- $\Theta\Theta^\dagger = m_D^\dagger M_N^{-2} m_D$, but also ensures the radiative stability and technical naturalness of the scheme [122].

When extending the SM Lagrangian by only 3 new singlet (right-handed neutrino) fields essentially the only neutrino mass matrix with an underlying L symmetry that leads to 3 heavy massive neutrinos is [123] (see also Ref. [124]):

$$m_D = \frac{v_{\rm EW}}{\sqrt{2}} \begin{pmatrix} Y_e & Y_\mu & Y_\tau \\ \epsilon_1 Y'_e & \epsilon_1 Y'_\mu & \epsilon_1 Y'_\tau \\ \epsilon_2 Y''_e & \epsilon_2 Y''_\mu & \epsilon_2 Y''_\tau \end{pmatrix} \quad \text{and} \quad M_N = \begin{pmatrix} \mu_1 & \Lambda & \mu_3 \\ \Lambda & \mu_2 & \mu_4 \\ \mu_3 & \mu_4 & \Lambda' \end{pmatrix}, \tag{3.8}$$

with all ϵ_i and μ_j small lepton number violating parameters (see also Ref. [126] for a particular scenario where these small parameters arise naturally). Indeed, setting all $\epsilon_i = 0$ and $\mu_j = 0$, lepton number symmetry is recovered with the following L assignments $L_e = L_\mu = L_\tau = L_1 = -L_2 = 1$ and $L_3 = 0$. In Eq. (3.7) this leads to: $\hat{m} = 0$ (3 massless neutrinos in the L-conserving limit), $M_1 = M_2 = \Lambda$ (a heavy Dirac pair) and $M_3 = \Lambda'$ (a heavy decoupled Majorana singlet), but:

$$\Theta = \frac{v_{\rm EW}}{2\Lambda} \begin{pmatrix} -iY_e^* & Y_e^* & 0 \\ -iY_\mu^* & Y_\mu^* & 0 \\ -iY_\tau^* & Y_\tau^* & 0 \end{pmatrix} \equiv \frac{1}{\sqrt{2}} \begin{pmatrix} -i\theta_e & \theta_e & 0 \\ -i\theta_\mu & \theta_\mu & 0 \\ -i\theta_\tau & \theta_\tau & 0 \end{pmatrix} \text{ and } \Theta\Theta^\dagger = \begin{pmatrix} |\theta_e|^2 & \theta_e\theta_\mu^* & \theta_e\theta_\tau^* \\ \theta_\mu\theta_e^* & |\theta_\mu|^2 & \theta_\mu\theta_\tau^* \\ \theta_\tau\theta_e^* & \theta_\tau\theta_\mu^* & |\theta_\tau|^2 \end{pmatrix}. \tag{3.9}$$

Thus, vanishing light neutrino masses can still be associated with arbitrarily large mixing between the heavy Dirac pair and active neutrinos and, for these kind of Seesaw scenarios, the bounds on the mixing we will explore are complementary and independent to the stringent constraints on the absolute light neutrino mass scale.

The small L-violating parameters ϵ_i and μ_j will induce small non-zero neutrino masses and mixing among these light mass eigenstates but will only translate in negligible perturbations to the matrix Θ. With the simple form in Eq. (3.9) for the heavy-active mixing, the series expansions in Eq. (3.4) can be added exactly obtaining:

$$s = \frac{\sin\theta}{\theta}\Theta \quad \text{and} \quad c = I - \frac{1-\cos\theta}{\theta^2}\Theta\Theta^\dagger, \tag{3.10}$$

with

$$\theta = \sqrt{|\theta_e|^2 + |\theta_\mu|^2 + |\theta_\tau|^2}. \tag{3.11}$$

Regarding the role of the ϵ_i and μ_j parameters in the generation of the light neutrino masses and mixings observed in neutrino oscillations, all of them except μ_1 and μ_3 will lead to $\hat{m} \neq 0$ through Eq. (3.7) when switched on:

$$\begin{aligned} \hat{m} &= \left(\mu_2 + \frac{\mu_4^2}{\Lambda'}\right) \mathbf{m_D^t} \Lambda^{-2} \mathbf{m_D} - \epsilon_1 \mathbf{m_D'^t} \Lambda^{-1} \mathbf{m_D} - \epsilon_1 \mathbf{m_D^t} \Lambda^{-1} \mathbf{m_D'} + \epsilon_2^2 \mathbf{m_D''^t} \Lambda'^{-1} \mathbf{m_D''} \\ &+ \epsilon_2 \frac{\mu_4}{\Lambda'} \left(\mathbf{m_D^t} \Lambda^{-1} \mathbf{m_D''} + \mathbf{m_D''^t} \Lambda'^{-1} \mathbf{m_D}\right), \end{aligned} \tag{3.12}$$

with

$$\mathbf{m_D} \equiv \frac{v_{\rm EW}}{\sqrt{2}}(Y_e, Y_\mu, Y_\tau), \quad \mathbf{m_D'} \equiv \frac{v_{\rm EW}}{\sqrt{2}}(Y_e', Y_\mu', Y_\tau') \quad \text{and} \quad \mathbf{m_D''} \equiv \frac{v_{\rm EW}}{\sqrt{2}}(Y_e'', Y_\mu'', Y_\tau'')\,. \tag{3.13}$$

Indeed, even though μ_1 and μ_3 do violate L, upon their inclusion the mass matrix in Eq. (3.2) does not increase its rank, which, in absence of the other ϵ_i and μ_j, is only 3 and thus 3 massless eigenstates are still recovered[1]. The parameters μ_2 and μ_4 do contribute at tree level to generate light neutrino masses, however, their effect can be absorbed in a redefinition of the vectors $\mathbf{m_D'}$ and $\mathbf{m_D''}$ as follows:

$$\epsilon_1 \mathbf{m_D'} \to \epsilon_1 \mathbf{m_D'} - \frac{\mu_2}{2\Lambda} \mathbf{m_D} \qquad \text{and} \qquad \epsilon_2 \mathbf{m_D''} \to \epsilon_2 \mathbf{m_D''} - \frac{\mu_4}{\Lambda} \mathbf{m_D} \tag{3.14}$$

up to contributions with two extra powers of the small L-violating parameters. Thus, in presence of non-zero ϵ_i, it is enough to consider their contribution to the generation of neutrino masses which reads:

$$\hat{m} = \epsilon_1 \mathbf{m_D'^t} \Lambda^{-1} \mathbf{m_D} + \epsilon_1 \mathbf{m_D^t} \Lambda^{-1} \mathbf{m_D'} + \epsilon_2^2 \mathbf{m_D''^t} \Lambda'^{-1} \mathbf{m_D''}. \tag{3.15}$$

Notice that the last term in Eq. (3.15) is suppressed by two powers of ϵ_2 while the others only by one power of ϵ_1. However, ϵ_2 (and μ_3 and μ_4) violates L by one unit while ϵ_1 (and μ_1 and μ_2) by 2. Hence, if the source of L-violation is by one unit it is expected that $\epsilon_1 \sim \epsilon_2^2$. Thus, for full generality, we will keep the last term in Eq. (3.15). The six free parameters encoded in $\mathbf{m_D'}$ and $\mathbf{m_D''}$ allow to give mass to the three mass eigenstates observed in neutrino oscillations as well as the possibility

[1]Notice that, even if μ_1 and μ_3 do not induce neutrino masses at tree level, the L symmetry protecting them is now broken and loop contributions would appear instead [195].

of reproducing any mixing pattern including the, yet unknown, CP-violating phases of Dirac and Majorana types encoded in the PMNS matrix, while leaving $\mathbf{m_D}$, and hence Θ, s and c, mostly unconstrained[2]. One of the three elements of $\mathbf{m_D}$ is, however, fixed by the other two, the values of the light mass eigenstates and the elements of the PMNS matrix when solving for Eq. (3.15) obtaining the following relation:

$$\begin{aligned} Y_\tau \simeq & \frac{1}{\hat{m}_{e\mu}^2 - \hat{m}_{ee}\hat{m}_{\mu\mu}} \left(Y_e \left(\hat{m}_{e\mu}\hat{m}_{\mu\tau} - \hat{m}_{e\tau}\hat{m}_{\mu\mu} \right) + \right. \\ & Y_\mu \left(\hat{m}_{e\mu}\hat{m}_{e\tau} - \hat{m}_{ee}\hat{m}_{\mu\tau} \right) - \sqrt{Y_e^2 \hat{m}_{\mu\mu} - 2 Y_e Y_\mu \hat{m}_{e\mu} + Y_\mu^2 \hat{m}_{ee}} \times \\ & \left. \times \sqrt{\hat{m}_{e\tau}^2 \hat{m}_{\mu\mu} - 2\hat{m}_{e\mu}\hat{m}_{e\tau}\hat{m}_{\mu\tau} + \hat{m}_{ee}\hat{m}_{\mu\tau}^2 + \hat{m}_{e\mu}^2 \hat{m}_{\tau\tau} - \hat{m}_{ee}\hat{m}_{\mu\mu}\hat{m}_{\tau\tau}} \right) , \end{aligned} \tag{3.16}$$

where $\hat{m} = -U^*_{\rm PMNS} m U^\dagger_{\rm PMNS}$ is the mass matrix of the flavour eigenstates. Thus, in our numerical exploration of the parameter space in Section 3.3 we will consider the 9 free parameters summarized in Table 3.1.

An alternative parametrization extensively used in the literature is the so-called Casas-Ibarra parametrization [202]. This parametrization introduces the matrix $R = iM^{-1/2} m_D U_{\rm PMNS} m^{-1/2}$ exploiting the fact that, from Eq. (3.7), R has to be (complex) orthogonal. The main advantage of this parametrization is the ability to easily recover the Yukawa couplings through the heavy mass eigenvalues M and the low energy observables $U_{\rm PMNS}$ and m together with the elements of R as $m_D = -iM^{1/2} R m^{1/2} U^\dagger_{\rm PMNS}$. However, the physical range of the parameters contained in R can be cumbersome and a physical interpretation of their values is not immediately transparent, see Ref. [203] for a detailed discussion. Moreover, these relations only hold at tree level[3]. Thus, when values of R are chosen so as to allow sizable low energy phenomenology through large Yukawas and low M, it is important to check if the pattern displays an approximate $B - L$ symmetry. Otherwise, loop corrections to the unprotected Weinberg operator, that is to $U_{\rm PMNS}$ and m, will exceed present constraints even if their values were correct at tree level. For this reason we rather chose to perform the scan through the parameters summarized in Table 3.1.

[2] In contrast, neglecting the last term in Eq. (3.15) would lead to the more constrained scenario explored in detail in Ref. [196], with a massless neutrino and a mixing pattern in Θ, s and c determined up to an overall factor from the observed neutrino oscillation parameters. This scenario has also been studied in Refs. [197–201]

[3] See Ref. [204] for a generalization of the Casas-Ibarra approach to loop level.

Parameter	$\lvert Y_e\rvert \times \lvert Y_\mu\rvert$	$\lvert Y_e\rvert - \lvert Y_\mu\rvert$	m_1 [eV]	Λ [GeV]	Phases: α_e, α_μ, δ, α_1 & α_2	Osc. data
Range	$(0, 10^{-4})$	$(-0.1, 0.1)$	$(10^{-5}, 1)$	$(10^3, 10^4)$	$(0, 2\pi)$	fixed [127]

Table 3.1: The 9 free parameters of our scan: the modulus and phase of the electron and muon Yukawas $|Y_e|$, $|Y_\mu|$, α_e and α_μ, the Majorana mass scale Λ, the absolute neutrino mass m_1 and the 3 yet unknown CP-violation phases (Dirac and Majorana) in the PMNS mixing matrix: δ, α_1 and α_2. The PMNS mixing angles and mass splittings are fixed to their best fit from the global analysis in Ref. [127].

At energies much below the masses of the heavy neutrinos Λ and Λ' the effects of their mixing Θ manifest dominantly through deviations from unitarity of the lepton mixing matrix N. Since any general matrix can be parametrized as the product of an Hermitian and a Unitary matrix, these deviations from unitarity have been often parametrized as [103]:

$$N = (I - \eta)U_{\text{PMNS}} \tag{3.17}$$

where the small Hermitian matrix η (also called ϵ in other works) corresponds to the coefficient of the only dimension 6 operator obtained at tree level upon integrating out the heavy right-handed neutrinos in a Seesaw scenario [102] and, in our parametrization it would be given from Eqs. (3.5) and (3.10) by:

$$\eta = \frac{1 - \cos\theta}{\theta^2}\Theta\Theta^\dagger. \tag{3.18}$$

3.2 Observables

In this section we introduce the list of observables used for our analysis. While a more comprehensive set could be considered (see for example Ref. [116]), we have rather chosen the most representative of these observables since extending the analysis to the loop level for the whole set would be cumbersome and the dominant constraints as well as the main effects pointed out in [115] are contained in a smaller subset. We will thus present both the 1-loop contributions and the experimental constraints for a total of 13 observables. The loop amplitudes of the processes have been computed exploiting the Goldstone-boson equivalence theorem [205] under the assumption that the mass of the extra neutrinos M_i is larger than the gauge boson masses; i.e. $M_i > M_{W,Z}$. Thus, we have made the simplifying assumption that the most relevant loop corrections are those were the loops are mediated by either the Higgs boson, h, the

Goldstone bosons $\phi^{\pm}$ and ϕ^0 or the heavy Majorana neutrinos. Indeed, this forces the vertexes to involve the potentially large Yukawa couplings (the only couplings that can be relevant at the loop level) and the corrections from including the transverse components are suppressed by $M^2_{W,Z}/M^2_N$. The set of 13 independent observables analyzed in this study is composed of:

- 8 ratios constraining electroweak universality: $R^{\pi}_{\mu e}$, $R^{\pi}_{\tau\mu}$, $R^{W}_{\mu e}$, $R^{W}_{\tau\mu}$, $R^{K}_{\mu e}$, $R^{K}_{\tau\mu}$, $R^{l}_{\mu e}$, $R^{l}_{\tau\mu}$
- The invisible Z width
- The W mass M_W
- 3 rare flavour-changing decays: $\mu \to e\gamma$, $\tau \to \mu\gamma$ and $\tau \to e\gamma$

All of them will be determined as a function of the three most precise electroweak measurements: α, M_Z and G_μ (G_F as measured from μ decay) [128]:

$$\begin{aligned} \alpha &= (7.2973525698 \pm 0.0000000024) \times 10^{-3}, \\ M_Z &= (91.1876 \pm 0.0021)\ \text{GeV}, \\ G_\mu &= (1.1663787 \pm 0.0000006) \times 10^{-5}\ \text{GeV}^{-2}. \end{aligned} \tag{3.19}$$

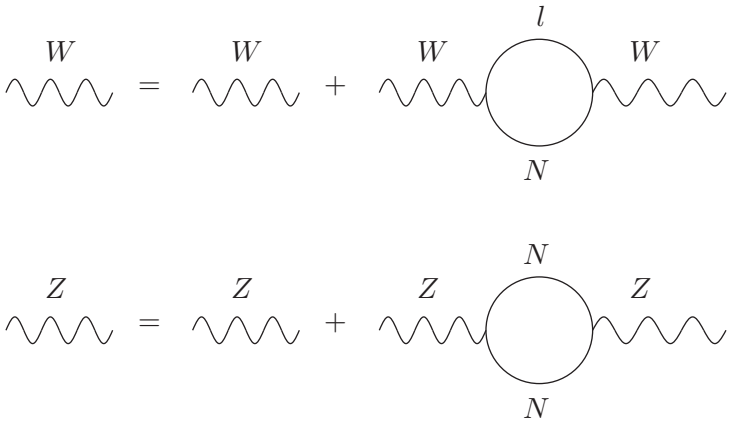

Figure 3.1: 1-loop correction of the new heavy neutrinos to W and Z propagators.

All observables will receive contributions from the loop corrections to the W and Z boson propagators through the diagrams in Fig. 3.1. These contributions are encoded in the flavour-universal corrections $\delta^{\text{univ}}_{W,Z}$ that can be found in Eq. (A.21) in Appendix A. We now list the further corrections exclusive to each of the observables considered:

3.2.1 Muon decay, G_F and M_W

Our input value for G_F is determined through μ decay, but this process will receive corrections both at the tree and the loop level (see Fig. 3.2). Thus, the value determined from μ decay, G_μ, is related to G_F by:

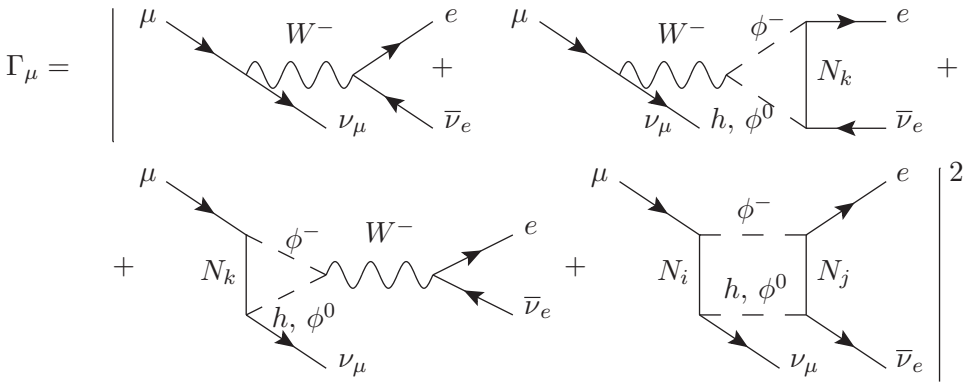

Figure 3.2: 1-loop corrections to μ decay.

$$\Gamma_\mu = \frac{m_\mu^5 G_F^2}{192\pi^3}\left(1 - |\theta_e|^2 - |\theta_\mu|^2 + 2\delta_W^{\text{univ } N} + \delta G\right) \equiv \frac{m_\mu^5 G_\mu^2}{192\pi^3}, \tag{3.20}$$

with

$$\delta G = 2Re[\mathcal{V}_e^W + \mathcal{V}_\mu^{W*} + \delta_e^{\text{CT } W} + \delta_\mu^{\text{CT } W*} + \mathcal{B}_{\mu e}] \tag{3.21}$$

and where $\delta_W^{\text{univ } N}$ is the flavour-universal W propagator correction, $\delta_l^{\text{CT } W}$ and $\mathcal{V}_l^W$ are the flavour-dependent lepton propagator and vertex contributions (see Eqs. (A.9) and (A.11) in Appendix A), and $\mathcal{B}_{\mu e}$ encodes the box diagram contribution computed in Eq. (A.13) in Appendix A.

From Eq. (3.20), we find:

$$G_\mu^2 = G_F^2\left(1 - |\theta_e|^2 - |\theta_\mu|^2 + 2\delta_W^{\text{univ N}} + \delta G\right) . \tag{3.22}$$

The second and third terms in Eq. (3.22) correspond to the tree level correction, the fourth term is the universal 1-loop oblique correction which is given in Eq. (A.21) of Appendix A. This particular expression, when used in an observable mediated by the Z and thus corrected through $2\delta_Z^{\text{univ N}}$, leads to a common correction to these observables given by $1 - |\theta_e|^2 - |\theta_\mu|^2 - 2\alpha T$ (see Eqs. (A.21) and (A.17)). This

common dependence on the tree level and oblique corrections is the source of the cancellation analyzed in Ref. [115].

The the W mass is also correlated to G_F through

$$M_W^2 = \frac{\pi\alpha}{\sqrt{2}G_F s_{\rm W}^2(1-\Delta r)}, \tag{3.23}$$

with $\Delta r = 0.03639 \mp 0.00036 \pm 0.00011$ [128]. Thus, the corrections induced at both the tree and loop levels by the heavy neutrinos from Eq. (3.22) can be probed by the measurement of M_W in LEP and Tevatron [128]:

$$M_W = 80.385 \pm 0.015 \quad \text{GeV}. \tag{3.24}$$

3.2.2 Invisible Z width

The determination of the number of light active neutrinos by LEP through the invisible width of the Z provides a constraint to heavy neutrino mixing already at the tree level. Additional loop corrections are induced through the diagrams in Fig. 3.3 which lead to:

$$\Gamma_{\rm inv} = \sum_{i,j=1}^{3} \frac{G_F M_Z^3 \rho}{24\sqrt{2}\pi} \left(\mathcal{Z}_{ij} + \mathcal{Z}_{ji}\right) , \tag{3.25}$$

where ρ encodes the SM loop corrections to the process and

$$\mathcal{Z}_{ij} = |C_{ij}|^2\left(1+\delta_Z^{\rm univ}\right) + 2Re\left[C_{ij}^*\left(\delta_{ij}^{{\rm CT}\ Z} + \mathcal{V}_{ij}^Z\right)\right] , \tag{3.26}$$

with

$$C_{ij} = \sum_{\alpha=e,\mu,\tau} U_{\alpha i}^* U_{\alpha j} \, . \tag{3.27}$$

and $\delta_{ij}^{{\rm CT}\ Z}$ and $\mathcal{V}_{ij}^Z$ the lepton and vertex corrections shown in Eqs. (A.10) and (A.12) in Appendix A.

Eq. (3.25) is often used to determine the number of active neutrinos N_ν lighter than $M_Z/2$ as:

$$\Gamma_{\rm inv} = \frac{G_F M_Z^3 \rho N_\nu}{12\sqrt{2}\pi} \, , \tag{3.28}$$

The measurement by LEP of $\Gamma_{\rm inv} = (0.4990 \pm 0.0015)$ GeV combined with Eq. (3.28) leads to [128]:

$$N_\nu = 2.990 \pm 0.007 \, . \tag{3.29}$$

We will exploit this result together with Eq. (3.25) to derive constraints on C_{ij} and, hence, on the heavy neutrino mixings.

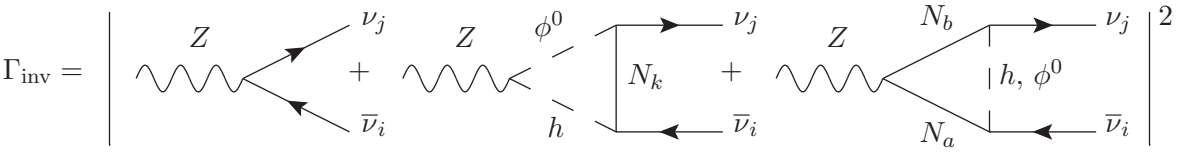

Figure 3.3: 1-loop corrections to the invisible decay of the Z.

3.2.3 Universality ratios

Electroweak coupling universality is strongly constrained through ratios of leptonic decays of K, π, W or charged leptons. In these ratios many uncertainties cancel and a clean constraint can be derived. These observables are corrected both at the tree and loop level, for instance, $R^{\pi}_{\mu e} = \Gamma\left(\pi^- \to \mu\overline{\nu}_\mu\right)/\Gamma\left(\pi^- \to e\overline{\nu}_e\right)$ is corrected by the diagrams in Fig. 3.4.

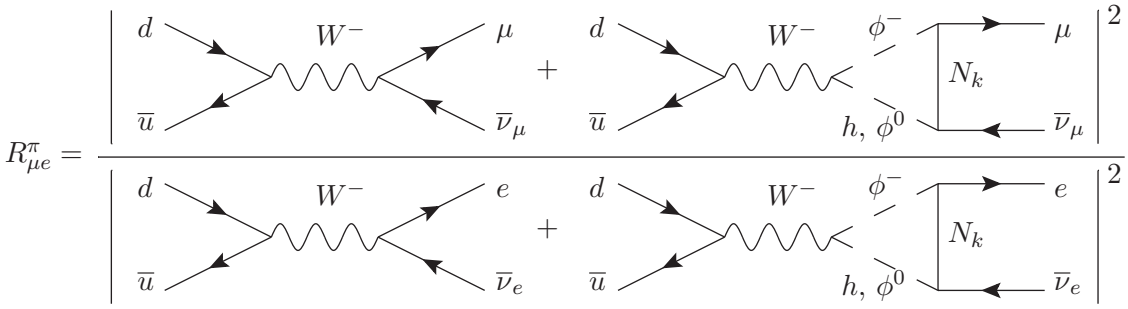

Figure 3.4: 1-loop corrections to weak universality ratios.

Thus, the general expression for the ratio of lepton flavors α and β is given by:

$$R_{\alpha\beta} = R^{SM}_{\alpha\beta}\frac{1-|\theta_\alpha|^2+2\mathrm{Re}\left[\mathcal{V}^W_\alpha+\delta^{\mathrm{CT}\ W}_\alpha\right]}{1-|\theta_\beta|^2+2\mathrm{Re}\left[\mathcal{V}^W_\beta+\delta^{\mathrm{CT}\ W}_\beta\right]}, \tag{3.30}$$

$BR(\pi^+ \to e^+\nu_e)$	$(1.230 \pm 0.004) \times 10^{-4}$
$BR(\pi^+ \to \mu^+\nu_\mu)$	$(99.98770 \pm 0.00004)\,\%$
$BR(\tau^- \to \pi^-\nu_\tau)$	$(10.83 \pm 0.06)\,\%$
$BR(K^+ \to e^+\nu_e)$	$(1.581 \pm 0.008) \times 10^{-5}$
$BR(K^+ \to \mu^+\nu_\mu)$	$(63.55 \pm 0.11)\,\%10^{-5}$
$BR(\tau^- \to K^-\nu_\tau)$	$(7.00 \pm 0.10) \times 10^{-3}$
$BR(W^+ \to e^+\nu_e)$	$(10.71 \pm 0.16)\,\%$
$BR(W^+ \to \mu^+\nu_\mu)$	$(10.63 \pm 0.15)\,\%$
$BR(W^+ \to \tau^+\nu_\tau)$	$(11.38 \pm 0.21)\,\%$
$BR(\tau^- \to \mu^-\overline{\nu}_\mu\nu_\tau)$	$(17.41 \pm 0.04)\,\%$
$BR(\tau^- \to e^-\overline{\nu}_e\nu_\tau)$	$(17.83 \pm 0.04)\,\%$
$\tau_{\pi^\pm}$	$(2.6033 \pm 0.0005) \times 10^{-8}$ s
$\tau_{K^\pm}$	$(1.2380 \pm 0.0021) \times 10^{-8}$ s
τ_τ	$(290.3 \pm 5.0) \times 10^{-15}$ s
τ_μ	$(2.1969811 \pm 0.0000022) \times 10^{-6}$ s
$m_{\pi^\pm}$	139.57018 ± 0.00035 MeV
$m_{K^\pm}$	493.677 ± 0.016 MeV
M_W	80.385 ± 0.0015 MeV
m_e	$0.510998928 \pm 0.000000011$ MeV
m_μ	$105.6583715 \pm 0.0000035$ MeV
m_τ	1776.82 ± 0.16 MeV
$\delta R^\pi_{\mu e}$	(-0.374 ± 0.001)
$\delta R^\pi_{\mu\tau}$	(0.0016 ± 0.0014)
$\delta R^K_{\mu\tau}$	(0.0090 ± 0.0022)

Table 3.2: Input values used for the constraints on weak universality from ratios of meson and charged lepton decays.

where $R_{\alpha\beta}^{SM}$ is the SM value for this ratio, for example, for π decay:

$$R_{\alpha\beta}^{\pi SM} = \left(\frac{m_\alpha \left(m_\pi^2 - m_\alpha^2\right)}{m_\beta \left(m_\pi^2 - m_\beta^2\right)}\right)^2 \frac{1}{1 + \delta R_{\alpha\beta}^{\pi}} \tag{3.31}$$

and where $\delta R_{\alpha\beta}^{\pi}$ are the SM radiative corrections to this process [206]. Notice that the flavour-universal contributions from the W propagator cancel in the ratio.

The predicted values of these ratios are computed through Eqs. (3.30) and (3.31) with data form [128, 130] and compared to the experimental measurements of the decay rates in our global fit. This data is summarized in Table 3.2.

3.2.4 Rare decays

The presence of extra heavy neutrinos beyond the three light ones participating in low energy weak processes induces deviations from unitarity in the PMNS matrix. Thus, the GIM cancellation [136] suppressing flavour-changing processes does not take place and strong constraints on the presence of these extra neutrinos can be derived. Moreover, the extra heavy neutrinos themselves also mediate the flavour-changing processes, such as radiative leptons decays $l_\alpha \to l_\beta \gamma$ in Fig. 3.5. The contribution from both the heavy and light neutrinos is given by:

$$\frac{\Gamma\left(l_\alpha \to l_\beta \gamma\right)}{\Gamma\left(l_\alpha \to l_\beta \nu_\alpha \overline{\nu}_\beta\right)} = \frac{3\alpha}{32\pi} \frac{\left|\sum_{k=1}^{6} U_{\alpha k} U_{k\beta}^{\dagger} F(x_k)\right|^2}{\left(UU^\dagger\right)_{\alpha\alpha}\left(UU^\dagger\right)_{\beta\beta}} \tag{3.32}$$

where $x_k \equiv \frac{M_k^2}{M_W^2}$, and $F(x_k)$ is given by:

$$F(x_k) \equiv \frac{10 - 43x_k + 78x_k^2 - 49x_k^3 + 4x_k^4 + 18x_k^3 \ln x_k}{3(x_k - 1)^4}. \tag{3.33}$$

Thus, for heavy neutrino masses much larger than M_W:

$$\frac{\Gamma\left(l_\alpha \to l_\beta \gamma\right)}{\Gamma\left(l_\alpha \to l_\beta \nu_\alpha \overline{\nu}_\beta\right)} \simeq \frac{3\alpha}{32\pi} |\theta_\alpha \theta_\beta^*|^2 (F(\infty) - F(0))^2. \tag{3.34}$$

The prediction from Eq. (3.32) will be compared with the existing upper bounds from [128]:

$$BR_{\mu e} < 5.7 \times 10^{-13}\,, \tag{3.35}$$
$$BR_{\tau e} < 3.3 \times 10^{-8}\,, \tag{3.36}$$
$$BR_{\tau \mu} < 4.4 \times 10^{-8}\,. \tag{3.37}$$

Notice that these bounds are quoted at the 90% CL so they will be rescaled to 1σ to build the corresponding contribution to the χ^2 function.

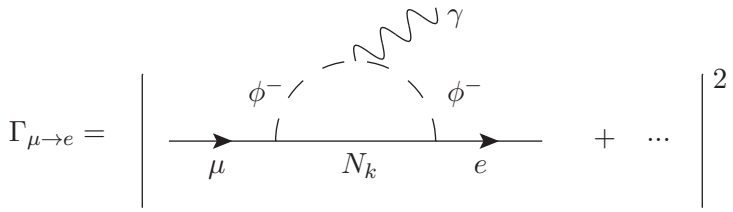

Figure 3.5: Extra neutrino contributions to the $\mu \to e\gamma$ decay.

3.3 Results

3.3.1 Constraints from the global fit

With the 13 observables discussed in Section 3.2 we build a χ^2 function depending on the 9 parameters listed in Table 3.1. Given the large dimensionality of the parameter space, we make use of Markov chain Monte Carlo (MCMC) techniques for efficient parameter exploration. In particular, we implement importance sampling based on the Likelihood obtained from the observables through a Metropolis-Hastings algorithm. The range in which the 9 free parameters are varied is also summarized in Table 3.1. We have run simultaneously 5 different chains through the MCMC algorithm and have verified that good convergence (better than $R - 1 < 0.035$ [207]) for all parameters has been achieved. The results of the runs thus provide a good sample of the χ^2 values in the preferred regions of the parameter space and have been used to marginalize over different subsets of the model parameters. In this way, we will present 2D and 1D frequentist contours on the more phenomenologically relevant parameters of the model. The post-processing of the chains to derive the allowed

confidence regions has been performed with the MonteCUBES [208] user interface.

In Fig. 3.6 we show the results of our MCMC scan for the 2 degrees of freedom constraints of different combinations of the heavy-active mixings θ_α defined in Eq. (3.9). The contours correspond to the 1σ, 90% and 2σ frequentist confidence regions. The upper panels show the bounds in the two combinations we choose to more directly sample (see Table 3.1): $|\theta_e| \times |\theta_\mu|$ and $|\theta_e| - |\theta_\mu|$. The rationale behind this is apparent upon inspection of Fig. 3.6. Indeed, the constraints on the product are more than one order of magnitude smaller than those derived from the difference of the couplings $\sqrt{|\theta_e| \times |\theta_\mu|} \ll ||\theta_e| - |\theta_\mu||$, leading to a very pronounced hyperbolic degeneracy in the panels of the middle row, which contain the same information directly depicted as a function of θ_e and θ_μ. Thus, this particular choice of sampling parameters allowed to scan the hyperbolic degeneracy much more efficiently and speed the convergence of the MCMC. This very strong constraint in $|\theta_e| \times |\theta_\mu|$ stems from the strong bound on $\mu \to e\gamma$ from MEG that, from Eq. (3.34), sets a very stringent limit on $|\theta_\mu \theta_e^*|$.

Finally, the lower panels of Fig. 3.6 contain the constraints derived for the mixing with the τ flavour θ_τ. Notice that Y_τ, and hence θ_τ, was not a free parameter of the fit but was rather obtained from the other two Yukawas and the light neutrino masses and mixings from Eq. (3.16). This is the source of the observed correlation between the values of θ_e and θ_τ. Notice also that, since the particular pattern of light neutrino masses plays an important role in Eq. (3.16), the left (normal hierarchy) and right (inverted hierarchy) panels of Fig. 3.6 display different correlations.

In Fig. 3.7 we show the individual constraints that can be derived on θ_e, θ_μ, and θ_τ (from top to bottom) for a normal (left) and an inverted (right) hierarchy after marginalizing over all other parameters. We generally find a slight improvement of the fit to the observables considered when some amount of mixing is present. In particular, we find that non-zero mixing with the electron is preferred at around the 90% CL by our dataset. Mixing with the tau flavour is also favoured for normal hierarchy due the correlations implied by Eq. (3.16). At the 1σ level, mixing with the μ flavour is significantly constrained due to the preference of some universality bounds (from π and τ decays) for a slightly reduced coupling to the electron with respect to the muon. Thus, since universality constraints are corrected by $1 - |\theta_\alpha|$ for each flavour, a non-zero θ_e is preferred in the fit while θ_μ is kept at small values to satisfy the constraint from $\mu \to e\gamma$. Beyond the 1σ level, the mixing with the electron is allowed to become small and thus the constraint on μ mixing at 2σ is

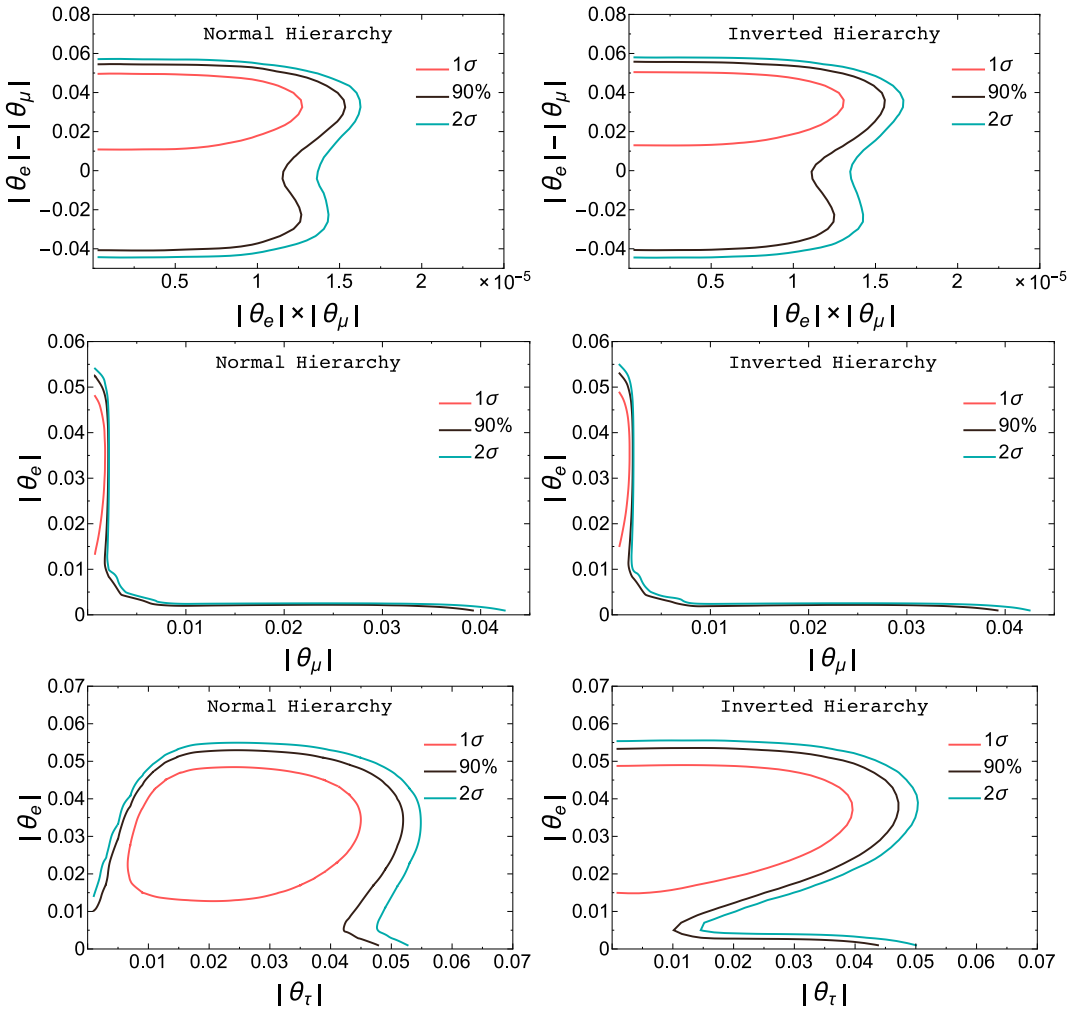

Figure 3.6: Contours for θ_e, θ_μ and θ_τ at 1σ (red), 90% CL (black) and 2σ (blue). The left panels are obtained for normal hierarchy and the right for inverted.

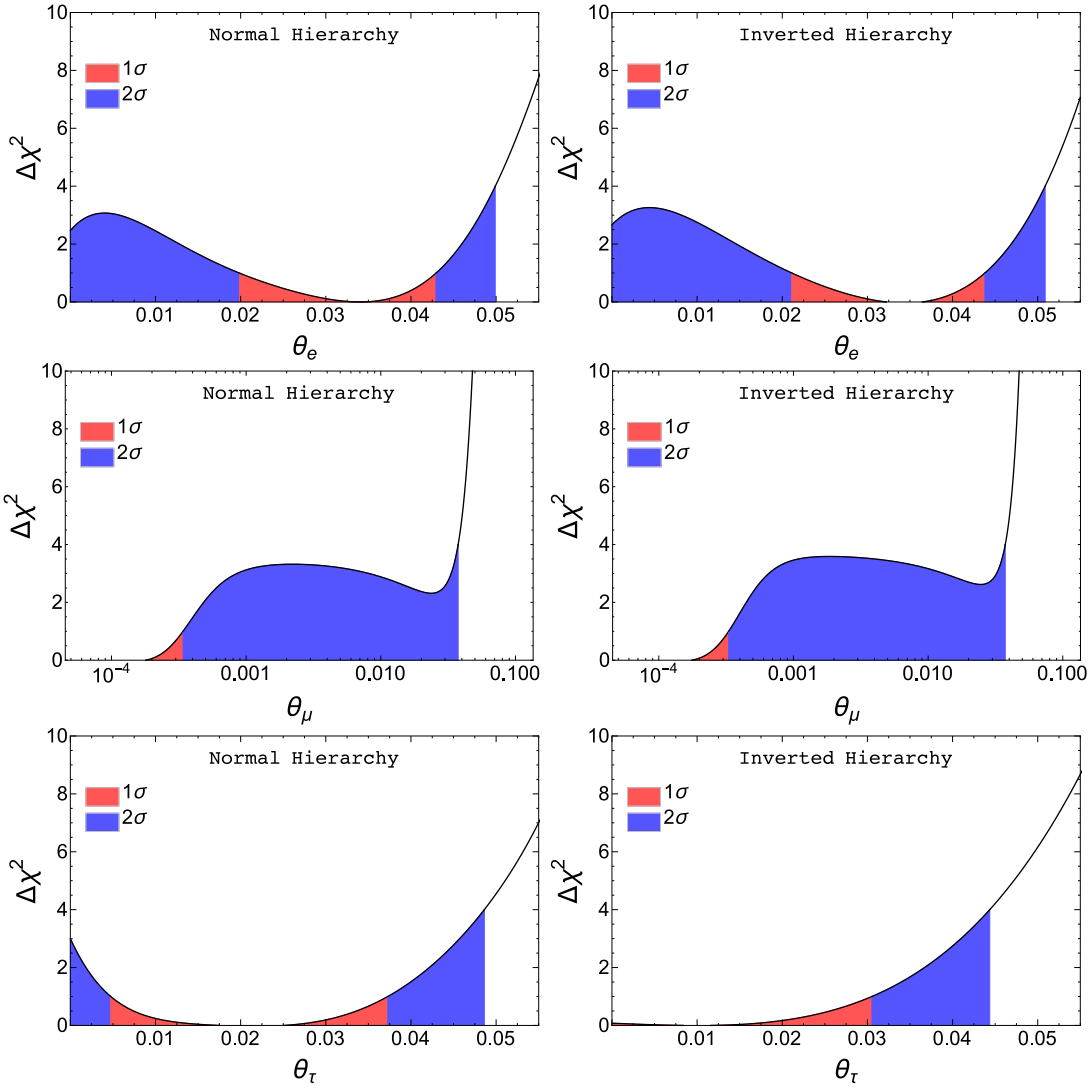

Figure 3.7: $\Delta\chi^2$ (marginalized over all other parameters) for θ_e, θ_μ and θ_τ. Left panels show results for a normal hierarchy and right panels for inverted hierarchy.

much weaker than naively expected from the 1σ region. The limits of the 1 and 2σ regions for the three mixing parameters are summarized in Table 3.3.

	θ_e		θ_μ		θ_τ	
	1σ	2σ	1σ	2σ	1σ	2σ
NH	$0.034^{+0.009}_{-0.014}$	< 0.050	$< 3.2 \cdot 10^{-4}$	< 0.037	$0.018^{+0.019}_{-0.013}$	< 0.049
IH	$0.035^{+0.009}_{-0.014}$	< 0.051	$< 3.3 \cdot 10^{-4}$	< 0.037	< 0.031	< 0.044

Table 3.3: Constraints on θ_e, θ_μ, and θ_τ for normal and inverted hierarchy.

In Fig. 3.8 we show a comparison of the breakdown of the contributions of the different observables to the total χ^2 for the SM (left panel) and our best fit (middle panel) as well as the difference of the two (right panel). It can be seen that some of the existing tension of the SM with the invisible width of the Z can be alleviated by the presence of heavy neutrino mixings and also the agreement between the kinematic determination of M_W and its SM value from G_F, α and M_Z is improved. As already discussed, the universality constraints from π and τ decays are also in better agreement when some mixing with the electron is present. On the other hand, universality tests from kaon decays rather point in the opposite direction. Thus, at the end, the preference for non-vanishing heavy-active mixing is mild and the final improvement of the χ^2 with respect to the SM value is 3.7, not quite reaching the 2σ level. Notice that, even if the number of free parameters in the fit is rather high, the observables actually depend on the combinations $|\theta_e|$, $|\theta_\mu|$ and $|\theta_\tau|$ only (and Λ when loop corrections are relevant). Thus, the reduction by 3.7 of the χ^2 should be attributed to the introduction of 3 (or 4) new parameters rather than 9.

Regarding the importance of the loop effects considered, we have performed a second set of MCMC runs where all loop corrections have been removed. The results of these simulations are essentially identical to the ones stemming from the full computation. By adding to the chain output also the value that the T parameter took in the simulations, we find that its preferred values are $\sim 10^{-7} - 10^{-6}$, negligible with respect to the best fit values of the tree level contributions. In order to understand this apparent lack of relevance of the loop corrections and the T parameter in particular, in direct contrast to the results presented in [115], we will now analyze in further detail the regions of the parameter space in which T could be relevant and

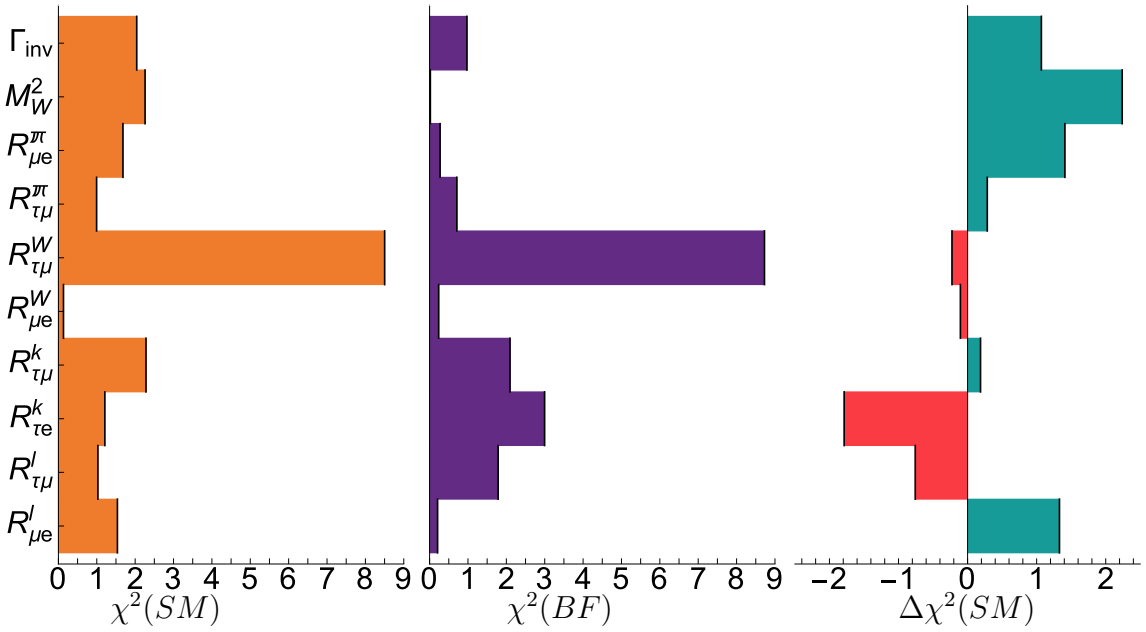

Figure 3.8: Contributions from the different observables to the χ^2. Left plot shows the SM values. Middle plot shows the contributions from three right-handed neutrinos in the best-fit point. Right plot shows $\Delta\chi_i^2 \equiv \chi_i^2(SM) - \chi_i^2(BF)$ for every observable i.

the necessary conditions for the cancellation with the tree level contributions to take place.

3.3.2 The T parameter

The leading contributions (not suppressed by the light neutrino or charged lepton masses) to the T parameter are given by [115]:

$$\alpha T = \frac{\alpha}{8\pi s_{\rm W}^2 M_W^2}\left(\sum_{\alpha,\beta,i,j}\left(U_{\alpha i}^* U_{\alpha j} U_{\beta i} U_{\beta j}^* f_{ij} + U_{\alpha i}^* U_{\alpha j} U_{\beta i}^* U_{\beta j} g_{ij}\right)\right), \tag{3.38}$$

where

$$f_{ij} = \frac{M_i^2 M_j^2}{M_i^2 - M_j^2}\ln\frac{M_i}{M_j} \qquad \text{and} \qquad g_{ij} = \frac{2M_i M_j^3}{M_i^2 - M_j^2}\ln\frac{M_i}{M_j}, \tag{3.39}$$

and where M_i are the neutrino mass eigenvalues. In [209, 210] it was shown that several of the most constraining observables, notably the Z decay to charged leptons and $\sin^2\theta_w^{\rm eff}$ [211], depended on the combination:

$$(NN^\dagger)_{ee}(NN^\dagger)_{\mu\mu} - 2\alpha T \simeq 1 - |\theta_e|^2 - |\theta_\mu|^2 - 2\alpha T. \tag{3.40}$$

Since from Table 3.3 $|\theta_e|^2 + |\theta_\mu|^2 \sim 10^{-3}$, $2\alpha T$ must be of similar order so as to be competitive with the tree contribution. From Eq. (3.38)

$$2\alpha T \simeq \frac{\alpha\Lambda^2|\theta_\alpha|^4}{16\pi s_{\rm W}^2 M_W^2}, \tag{3.41}$$

where Λ is the mass scale of the heavy neutrinos and $\theta_\alpha/\sqrt{2}$ their mixing with the flavour states from Eq. (3.9). Thus, in order for $2\alpha T \sim |\theta_\alpha|^2$ it is necessary that $\Lambda \sim 10 - 100$ TeV. And, since $|\theta_\alpha|^2 \sim |Y_\alpha|^2 v_{\rm EW}^2/2\Lambda^2 \sim 10^{-3}$, then $|Y_\alpha| \sim 1 - 10$, on the very limit of perturbativity but, a priori, an interesting possibility.

Furthermore, notice that the second term in Eq. (3.38) has the typical structure in the elements of the mixing matrix U of L-violating processes, such as, for example, neutrinoless double β decay. Indeed, this term stems from the correction to the Z propagator with two neutrinos running in the loop and a Majorana mass insertion and it is easy to see that it vanishes in the limit of exactly conserved Lepton number, taking all ϵ_i and μ_j to zero. Thus, if $B-L$ is approximately conserved, the first term in Eq. (3.38) dominates the contribution to T. However, it can be shown that the

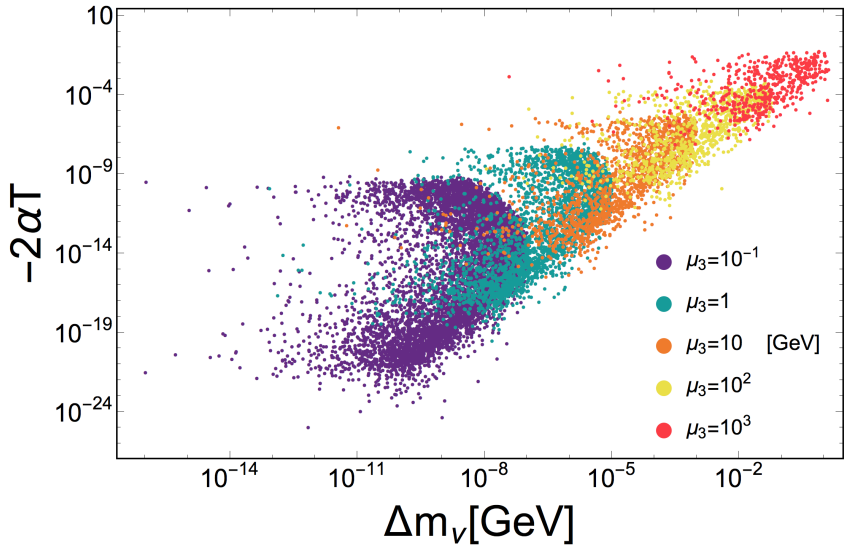

Figure 3.9: T parameter versus 1-loop correction to m_ν for different values of the L-violating parameters μ_1 and μ_3.

matrix f_{ij} is positive semi-definite for three extra heavy neutrinos or less[4] and can then be diagonalized as $f_{ij} = \sum_k V_{ik}\lambda_k V^*_{jk}$, where V is a Unitary matrix and $\lambda_k \geq 0$. Thus, if $B - L$ is approximately conserved:

$$\alpha T \sim \frac{\alpha}{8\pi s_{\rm W}^2 M_W^2} \sum_{\alpha,\beta,i} \left| \sum_k U^*_{\alpha i} U_{\beta i} V_{ik} \sqrt{\lambda_k} \right|^2 \geq 0. \tag{3.42}$$

But from Eq. (3.40) $T < 0$ is mandatory so as to have the cancellation between T and $|\theta_\alpha|^2$ discussed in [115]. Thus, significant violations of $B - L$ are necessary so that the second term in Eq. (3.38), which is allowed to be negative, can dominate over the first.

Notice that, for arbitrary values of the $B - L$-violating parameters ϵ_i and μ_j, Eq. (3.8) is a completely general parametrization of a type-I Seesaw mechanism with three extra right-handed neutrinos. But, given Eq. (3.12), only μ_1 and μ_3 are allowed to be sizable given the present constraints on the light neutrino masses and mixings.

[4]Preliminary explorations indicate that this argument can be generalized to more extra heavy neutrinos.

If $|\mu_1| \gg \Lambda, \Lambda', \mu_3$ a negative T can indeed be obtained:

$$T \simeq \frac{v_{\rm EW}^4}{32\pi s_{\rm W}^2 M_W^2 \mu_1^2} \left(\sum_\alpha |Y_\alpha|^2\right)^2 \left(3 - 4\log\left(\frac{\mu_1}{\Lambda}\right)\right). \tag{3.43}$$

If both μ_1 and μ_3 are simultaneously included and dominate over the L-conserving Λ and Λ' then T is given by:

$$T \simeq \frac{v_{\rm EW}^4}{64\pi s_{\rm W}^2 M_W^2} \left(\sum_\alpha |Y_\alpha|^2\right)^2 \frac{6\mu\mu_1 - (3\mu_1^2 + \mu^2)\log\left(\frac{\mu+\mu_1}{\mu-\mu_1}\right)}{\mu^3\mu_1}, \tag{3.44}$$

where $\mu = \sqrt{\mu_1^2 + 4\mu_3^2}$. In this limit, negative values of T are also easily accessible. However, the price to pay is high, the approximate $B - L$ symmetry protecting the Weinberg operator despite the Yukawas at the very border of perturbativity and the low Seesaw scale, has been strongly broken by μ_1 and μ_3. While this does not induce any dangerous corrections to neutrino masses at tree level, and hence when working with the Casas-Ibarra parametrization as in Ref. [115] the correct masses and mixings seem to be recovered, loop corrections need to also be taken into account since no protecting symmetry can now suppress them. Indeed, the loop contributions mediated by μ_1 and μ_3 to the light neutrino masses are found to be [195, 212–215]:

$$\Delta m_{\nu_{\alpha\beta}} = \frac{Y_\alpha Y_\beta}{32\pi^2\mu}\left(3M_Z^2 f(M_Z) + M_h^2 f(M_h)\right), \tag{3.45}$$

with:

$$f(M) = \frac{(\mu+\mu_1)^2\log\left(\frac{\mu+\mu_1}{2M}\right)}{(\mu+\mu_1)^2 - 4M^2} - \frac{(\mu-\mu_1)^2\log\left(\frac{\mu-\mu_1}{2M}\right)}{(\mu-\mu_1)^2 - 4M^2}. \tag{3.46}$$

These corrections can indeed be sizable and in Fig. 3.9 we show the values that the loop contribution to the light neutrino masses take in order to recover a given value for $-2\alpha T$ for different values of μ_1 and μ_3. From inspection of Eq. (3.46), the limit of vanishing μ_1 would render $f(M) = 0$, keeping under control the loop corrections to neutrino masses[5]. However, from Eq. (3.44), $|\mu_1| > 1.9|\mu_3|$ is necessary for $T < 0$. Indeed, as can be seen in Fig. 3.9, if $-2\alpha T \sim 10^{-3}$ so as to implement the cancellation

[5]In this limit with $\mu_3 \gg \Lambda, \Lambda'$, L-symmetry is recovered with two degenerate neutrinos with mass μ_3 that form a Dirac pair. Hence, the symmetry ensures the stability of ν masses at loop level but conversely drives T to positive values.

between tree and loop level contributions, corrections to the light neutrino masses ranging from ~ 100 keV to ~ 100 MeV, far exceeding present constraints, would be obtained. Thus, we conclude that, while the qualitatively important cancellations described in Ref. [115] can in principle take place and affect the constraints on the heavy-active neutrino mixing for $Y_\alpha \sim 1$ and $\Lambda \sim 10$ TeV, in practice large violations of the protecting $B - L$ symmetry would be required, leading to too large radiative corrections to light neutrino masses.

3.4 Conclusions

In this work we have analyzed in detail the importance of loop corrections when deriving constraints on the mixing between the SM flavour eigenstates and the new heavy neutrinos introduced in Seesaw mechanisms. Although naively the expectation is that radiative corrections involving these new states would be irrelevant given their weaker-than-weak interactions due to their singlet nature and, a priori, suppressed mixings with the SM neutrinos, Seesaw models allow Yukawa couplings to be sizable, even order one. Thus, loop corrections involving Yukawa vertexes, when the loops involve the heavy neutrinos and the Higgs or the W and Z Goldstones, can indeed be sizable as shown in Ref. [115]. In that work, it was shown that, for the low scale Seesaw mechanisms characterized by large Yukawas and low (electroweak) Seesaw scale, the contribution of the new degrees of freedom to the oblique parameters could indeed become as important as the tree level effects in some regions of the parameter space. Moreover, it was observed that several observables shared a common dependence between the T parameter and the tree level contribution, stemming from the modification by these effects of the muon decay through which G_F is determined and subsequently used as input for other observables. Thus, a partial cancellation between these tree and loop level contributions can significantly relax the bounds derived from these observables. Indeed, in Ref. [115] a good fit with sizable mixing was obtained in which the most stringent limits were avoided through this partial cancellation while standing tensions between the SM and some observables like the invisible width of the Z were alleviated.

We have extended the analysis performed in Ref. [115] to include also vertex corrections and not only oblique parameters, since the sizable contributions from the heavy Yukawas do not vanish when taking the light neutrinos and charged lepton masses to zero. We find that, all in all, the oblique parameters do tend to dominate

over the other loop corrections and their contribution could be sizable in some part of the parameter space. However, our MCMC scan shows no preference for any sizable loop corrections and the partial cancellation found in [115] is not reproduced. We then studied in detail the values of the T parameter preferred by data through our MCMC scan and saw that they were not only negligible, but always positive in our results. Indeed, for the cancellation between tree level contributions and the T parameter to take place, the latter must have negative values. We thus studied the necessary conditions for sizable negative values of the T parameter and realized that, not only sizable Yukawas and relatively low Seesaw scales are required, but also large violations of $B-L$. We then identified the only parameters in the mass matrix with three extra heavy neutrinos that could provide the necessary $B-L$ violation required for T to be negative and competitive with tree level contributions, while keeping neutrino masses within their current bounds despite the large Yukawas, low Seesaw scale and loss of protecting $B-L$ symmetry. Finally, we studied how these parameters would contribute to neutrino masses at loop level and found that, for the size of T required for the cancellation to take place, light neutrino masses would range from 10 keV to 100 MeV, effectively ruling out this possibility.

We conclude that loop level corrections are only relevant in a small fraction of the Seesaw parameter space characterized by large Yukawa couplings and low Seesaw scale and that these corrections tend to strengthen the tree level contributions unless large deviations from $B-L$ are present. If $B-L$ is approximately conserved, data thus prefer regions of the parameter space where these loops are irrelevant. On the other hand, if $B-L$ is strongly violated, the cancellation discussed in Ref. [115] can indeed provide a good fit to data with a very relevant role of the loop contributions. However, these large violations of $B-L$ at loop level also lead to too large contributions to the light neutrino masses and hence this possibility is ruled out. We therefore conclude that loop corrections can safely be neglected in analyses of the heavy neutrino mixings in Seesaw mechanisms.

Finally we have also obtained relevant constraints on this mixing when $B-L$ is an approximate symmetry, so as to recover the correct neutrino masses and mixings observed in neutrino oscillation searches. We find a mild ($\sim 90\%$ CL) preference for non-zero mixing with the e flavours with a best fit at $\theta_e = 0.034^{+0.009}_{-0.014}$ or $\theta_e = 0.035^{+0.009}_{-0.014}$ for normal and inverted mass hierarchy respectively. In the case of normal hierarchy, this preference also induces non-zero mixing with the τ flavour $\theta_\tau = 0.018^{+0.019}_{-0.013}$ so as to recover the correct pattern of neutrino masses and mixings. On the other hand, small θ_μ is preferred so as to keep $\mu \to e\gamma$ at acceptable levels

in presence of non-zero θ_e. At the 2σ level the following upper bounds are found: $\theta_e < 0.051$, $\theta_\mu < 0.037$ and $\theta_\tau < 0.049$.

Chapter 4

Testing non-unitarity at a neutrino oscillation experiment

4.1 Non-unitarity and sterile neutrino phenomenology comparison

In this section we will show how, under certain conditions, the phenomenology of non-unitarity and sterile neutrino oscillations are equivalent to leading order in the active-heavy mixing parameters, not only in vacuum but also in matter. If n extra right-handed neutrinos are added to the SM Lagrangian, the full mixing matrix (including both light and heavy states) can be written as

$$\mathcal{U} = \begin{pmatrix} N & \Theta \\ R & S \end{pmatrix} , \tag{4.1}$$

where N represents the 3×3 active-light sub-block (i.e., the PMNS matrix), which will no longer be unitary[1]. Here, Θ is the $3 \times n$ sub-block that includes the mixing between active and heavy states, while the R and S sub-blocks define the mixing of the sterile states with the light and heavy states, respectively. Note that both R and S are only defined up to an unphysical rotation of the sterile states and that neither of them will be involved when considering oscillations among active flavours.

[1]Note that this is true regardless whether the extra states are kinematically accessible or not.

4.1.1 Non-unitarity case

In the case of non-unitarity, only the light states are kinematically accessible and the amplitude for producing one of these states in conjunction with a charged lepton of flavour α in a particular decay is proportional to the mixing matrix element $N^*_{\alpha i}$. In the mass eigenstate basis, the evolution of the produced neutrino state is given by the Hamiltonian [111]

$$H = \frac{1}{2E}\begin{pmatrix} 0 & 0 & 0 \\ 0 & \Delta m^2_{21} & 0 \\ 0 & 0 & \Delta m^2_{31} \end{pmatrix} + N^\dagger \begin{pmatrix} V_{\mathrm{CC}} + V_{\mathrm{NC}} & 0 & 0 \\ 0 & V_{\mathrm{NC}} & 0 \\ 0 & 0 & V_{\mathrm{NC}} \end{pmatrix} N, \tag{4.2}$$

where $V_{\mathrm{CC}} = \sqrt{2} G_F n_e$ and $V_{\mathrm{NC}} = -G_F n_n/\sqrt{2}$ are the charged-current (CC) and neutral-current (NC) matter potentials, respectively. The oscillation evolution matrix S^0 in this basis is now defined as the solution to the differential equation

$$i\dot{S}^0 = HS^0 \tag{4.3}$$

with the initial condition $S^0(0) = I$, I being the identity matrix. For a constant matter potential, this equation has the formal solution

$$S^0 = \exp(-iHL). \tag{4.4}$$

The amplitude for a neutrino in the mass eigenstate j to interact as a neutrino of flavour β is given by the mixing matrix element $N_{\beta j}$, which means that the oscillation probability will be given by

$$P_{\alpha\beta} = |(NS^0N^\dagger)_{\beta\alpha}|^2. \tag{4.5}$$

Here $P_{\alpha\beta}$ denotes the "theoretical" oscillation probabilities (although it should be noted that they do not add up to one), defined as the ratio between the observed number of events divided by the product of the SM-predicted flux times cross section. In other words, $P_{\alpha\beta}$ is the factor that would be needed to obtain the number of events after convolution with the standard model flux and cross sections.

However, in practice neutrino oscillation experiments do not measure $P_{\alpha\beta}$. Most present and future experiments rather determine the flux and cross sections via near detector data and extrapolate to the far detector by correcting for the different

geometries, angular apertures, and detection cross sections. In this scenario, the oscillation probability would then inferred from the ratio

$$\mathcal{P}_{\alpha\beta} = \frac{R_\beta}{R_\alpha}, \tag{4.6}$$

where R_β and R_α are the observed event rates at the far detector and the corresponding extrapolation of the near detector result, respectively. For the near detector, we assume that the phases corresponding to the propagation of the light neutrinos have not yet developed significantly and therefore $S^0 = I$, resulting in the experimentally inferred probability

$$\mathcal{P}_{\alpha\beta} = \frac{\left|(NS^0N^\dagger)_{\beta\alpha}\right|^2}{((NN^\dagger)_{\alpha\alpha})^2}. \tag{4.7}$$

In the SM limit the matrix N becomes unitary and, thus, $NN^\dagger = I$ and $\mathcal{P}_{\alpha\beta} = P_{\alpha\beta}$ as expected.

4.1.2 Sterile neutrino case

In the sterile neutrino scenario, all of the states are kinematically accessible and the full oscillation evolution matrix $\mathcal{S}$, involving both light and heavy states, takes the form

$$\mathcal{S} = \mathcal{U}\mathcal{S}^0\mathcal{U}^\dagger, \tag{4.8}$$

where $\mathcal{S}^0$ is the full $(3+n)\times(3+n)$ evolution matrix expressed in the mass eigenbasis. For vacuum oscillations, we find that $\mathcal{S}^0 = \mathrm{diag}(\exp(-i\Delta m^2_{j1}L/2E))$. Therefore, the active neutrino 3×3 sub-block S can be simplified to

$$S_{\alpha\beta} = \sum_{i\in\text{light}} N_{\alpha i}S^0_{ij}N^*_{\beta j} + \sum_{J\in\text{heavy}} \Theta_{\alpha J}\Theta^*_{\beta J}\Phi_J, \tag{4.9}$$

where α, β stand for active neutrino flavors, Φ_J is the phase factor acquired by the heavy state J as it propagates, and S^0 is defined in the same way as in the non-unitarity case.

In the limit of large mass squared splitting between the light and heavy states (*i.e.*, $\Delta m^2_{iJ}L/E \gg 1$) the oscillations are too fast to be resolved at the detector and only an averaged-out effect is observable. In this averaged-out limit, the cross terms between the first and second term in the evolution matrix average to zero and we

find

$$P_{\alpha\beta} = |S_{\alpha\beta}|^2 = \left| \sum_i N_{\alpha i} S^0_{ij} N^*_{\beta j} \right|^2 + \mathcal{O}(\Theta^4)\,, \tag{4.10}$$

which recovers the same expression as Eq. (4.5) up to the $\mathcal{O}(\Theta^4)$ corrections.[2] Thus, we can conclude that averaged-out sterile neutrino oscillations in vacuum are equivalent to non-unitarity to leading order (this equivalence is indeed lost at higher orders). We will therefore concentrate on this averaged-out limit for the rest of this paper.

For oscillations in the presence of matter, the sterile neutrino oscillations will be subjected to a matter potential that in the flavour basis takes the form

$$\mathcal{H}^f_{\text{mat}} = \begin{pmatrix} V_{3\times3} & 0 \\ 0 & 0 \end{pmatrix}, \tag{4.11}$$

where

$$V_{3\times3} = \begin{pmatrix} V_{\text{CC}} + V_{\text{NC}} & 0 & 0 \\ 0 & V_{\text{NC}} & 0 \\ 0 & 0 & V_{\text{NC}} \end{pmatrix}. \tag{4.12}$$

If the matter potential is small in comparison to the light-heavy energy splitting $\Delta m^2_{iJ}/2E$, the light-heavy mixing in matter will be given by

$$\tilde{\Theta}_{\alpha J} = \Theta_{\alpha J} + \frac{2E}{\Delta m^2_{iJ}} (\delta_{\alpha e} V_{\text{CC}} \Theta_{eJ} + \Theta_{\alpha J} V_{\text{NC}}) \tag{4.13}$$

to first order in perturbation theory. In the limit $\Delta m^2_{iJ}/2E \gg V_{\text{CC}}, V_{\text{NC}}$, we can therefore neglect the difference between the heavy mass eigenstates in vacuum and in matter, and apply Eq. (4.10). Thus, we conclude from this that the matter Hamiltonian in the light sector can be computed in exactly the same way as for the non-unitarity scenario and we therefore find the very same expressions for the "theoretical" probability in Eq. (4.5) as for the non-unitarity case, at leading order in Θ.

[2] Note that this expression is also applicable whenever the light and heavy states decohere due to wave packet separation.

In the case of sterile neutrinos one also needs to consider the impact of the near detector measurements on the extraction of the experimentally measurable probability. In this work we will always assume that the oscillations due to the additional heavy states are averaged out at the far detector. However, this might not be the case at the near detector. Ideally, both sets of observables should be simulated and analyzed together consistently. Nevertheless, the following simplified limiting cases can be identified:

1. The light-heavy oscillations are averaged out already at the near detector. For practical purposes, the oscillation phenomenology in this case is identical to the non-unitarity case and Eq. (4.7) also applies. For the experimental setup of DUNE, that will be studied as an example of these effects in Section 4.5, with a peak neutrino energy of ~ 2.5 GeV and a near detector distance of ~ 0.5 km, this is the case when $\Delta m^2 \gtrsim 100$ eV^2.
2. The light-heavy oscillations have not yet developed at the near detector, but are averaged out at the far detector. In this case, the near detector would measure the SM fluxes and cross sections, and therefore the denominator in Eq. (4.7) would be equal to one. In this case, the experimental probability would coincide with the "theoretical" probability in Eq. (4.5). This scenario is the one implicitly assumed in many phenomenological studies, given the simplicity of Eq. (4.5). However, it is typically only applicable in a very small part of the parameter space, i.e., for very particular values of Δm^2 (which depend on the neutrino energy and on the near and far detector baselines). For DUNE, since the far detector baseline is 1300 km, this would be the case only in the region 0.1 eV$^2 \lesssim \Delta m^2 < 1$ eV^2. This scenario will nevertheless be explored in Sec. 4.5 to highlight its differences relative to the previous one, which is applicable in a larger fraction of the Δm^2 parameter space.
3. The oscillation frequency dictated by the light-heavy frequency matches the near detector distance. In this case, oscillations could be seen at the near detector as a function of neutrino energy, leading to more striking signals. At DUNE, this regime is matched for values of Δm^2 in the range presently favoured by the LSND/MiniBooNE [216,217] and reactor anomalies [218,219] (see [220–222] for recent reviews). This regime at DUNE has been already analized (see for instance Ref. [223]). The sensitivity to this part of the parameter space will be dominated by the dedicated experiments built to explore these anomalies, such as the Fermilab short-baseline neutrino program [224], leaving little room for their averaged-out effects to be observed at the far detectors in long-baseline

oscillation experiments. Therefore, this scenario will not be discussed further.

4.2 Parametrizations

The two most widely used parametrizations to encode these non-unitarity effects stemming from the heavy-active mixing are

$$N = (I - \eta)U' \quad \text{or} \quad N = TU = (I - \alpha)U, \tag{4.14}$$

where η is a Hermitian matrix [102, 103] and T is a lower triangular matrix [161–163, 225]. In Eq. (4.14) both U and U' are unitary matrices that are equivalent to the standard PMNS matrix up to small corrections proportional to the deviations encoded in η and α.

$$\eta = \begin{pmatrix} \eta_{ee} & \eta_{e\mu} & \eta_{e\tau} \\ \eta^*_{e\mu} & \eta_{\mu\mu} & \eta_{\mu\tau} \\ \eta^*_{e\tau} & \eta^*_{\mu\tau} & \eta_{\tau\tau} \end{pmatrix}, \quad \alpha = (1 - T) = \begin{pmatrix} \alpha_{ee} & 0 & 0 \\ \alpha_{\mu e} & \alpha_{\mu\mu} & 0 \\ \alpha_{\tau e} & \alpha_{\tau\mu} & \alpha_{\tau\tau} \end{pmatrix} \tag{4.15}$$

with $\eta_{\alpha\beta}, \alpha_{\alpha\beta} \ll 1$. Note that we choose to label the α matrix elements with flavour indices for notation ease instead of using numbers as in [163]. Furthermore, in [163] the identity matrix is not singled out from α as in our Eq. (4.15) so that the diagonal elements α_{ii} in [163] are close to 1 instead of small. Therefore, in practice, $\alpha_{ii} \to 1 - \alpha_{\alpha\alpha}$. These changes are only cosmetic and the following discussion applies to [163] with the above-mentioned identification.

The deviations from unitarity are directly related to the heavy-active neutrino mixing. For instance, in the hermitian parametrization one can directly identify [164]

$$\eta = \frac{\Theta\Theta^\dagger}{2} \tag{4.16}$$

where $\Theta = m_D^\dagger M^{-1}$ is the heavy-active mixing given by the ratio of the Dirac over the Majorana mass scales. Thus, $(1 - \eta)$ is just the first term in the cosine series correcting the unitary rotation U'. It is also straightforward to obtain the relation between the heavy-active neutrino mixing and the α parameters in the triangular parametrization, if one considers that the heavy-active mixing can also be encoded

by introducing additional complex rotations characterized by new mixing angles θ_{ij}, with $j > 3$. For example,

$$U_{14} = \begin{pmatrix} c_{14} & 0 & 0 & \hat{s}_{14}^* \\ 0 & 1 & 0 & 0 \\ 0 & 0 & 1 & 0 \\ -\hat{s}_{14} & 0 & 0 & c_{14} \end{pmatrix}, \tag{4.17}$$

where $\hat{s}_{ij} = e^{i\delta_{ij}} s_{ij}$, $s_{ij} = \sin\theta_{ij}$ and $c_{ij} = \cos\theta_{ij}$. In the correct order, these extra rotations lead to a lower triangular matrix. For 3 extra neutrinos we can use $U_{36}U_{26}U_{16}U_{35}U_{25}U_{15}U_{34}U_{24}U_{14}$ (where we have not included unphysical rotations among the sterile neutrinos), leading to [161]:

$$\alpha \simeq \begin{pmatrix} \frac{1}{2}\left(s_{14}^2 + s_{15}^2 + s_{16}^2\right) & 0 & 0 \\ \hat{s}_{14}\hat{s}_{24}^* + \hat{s}_{15}\hat{s}_{25}^* + \hat{s}_{16}\hat{s}_{26}^* & \frac{1}{2}\left(s_{24}^2 + s_{25}^2 + s_{26}^2\right) & 0 \\ \hat{s}_{14}\hat{s}_{34}^* + \hat{s}_{15}\hat{s}_{35}^* + \hat{s}_{16}\hat{s}_{36}^* & \hat{s}_{24}\hat{s}_{34}^* + \hat{s}_{25}\hat{s}_{35}^* + \hat{s}_{26}\hat{s}_{36}^* & \frac{1}{2}\left(s_{34}^2 + s_{35}^2 + s_{36}^2\right) \end{pmatrix}, \tag{4.18}$$

which is accurate to second order in the (small) extra mixing angles.

In principle, the two parametrizations should be equally valid. However, the alternative use of each of them seemingly leads to inconsistent results. As an illustrative example, let us compare the ν_μ disappearance probability in the atmospheric regime in the two parametrizations, obtained at linear order in the non-unitarity parameters and for $\theta_{13} = \Delta_{21} = 0$

$$\begin{aligned} \mathcal{P}_{\mu\mu}^{\eta} &= 1 - \left\{\sin^2 2\theta'_{23} - 2\mathrm{Re}[\eta_{\mu\tau}] \sin 4\theta'_{23}\right\} \sin^2\Delta_{31}, \\ \mathcal{P}_{\mu\mu}^{\alpha} &= 1 - \sin^2 2\theta_{23} \sin^2\Delta_{31}, \end{aligned} \tag{4.19}$$

where $\Delta_{ij} = \Delta m_{ij}^2 L/4E$. Here, $\mathcal{P}_{\alpha\beta}$ denotes the "experimental" oscillation probability in vacuum including the normalization factors as discussed in Sec. 4.1.

The naive conclusion derived from Eq. (4.19) is that for the Hermitian parametrization good sensitivity to the non-unitarity parameter $\eta_{\mu\tau}$ is expected in this channel, since it appears at linear order. Conversely, the triangular parametrization does not show this effect. This apparent inconsistency stems from the fact that the unitary matrices U and U' are, in fact, different. This is the case even though these matrices are traditionally identified with the standard unitary PMNS matrix in each

parametrization. However, this identification is only accurate up to the small corrections stemming from the deviations from unitarity. As we will show below, the differences between the two are indeed linear in the non-unitarity parameters, and the two matrices can be easily related to each other. The relevant question is therefore which of these matrices, if any, that more closely matches the one that is determined through the present neutrino oscillation data. Starting from Eq. (4.14) a unitary rotation V can be performed to relate U and U'

$$N = (I - \alpha)U = (I - \eta)VV^\dagger U' \tag{4.20}$$

and therefore

$$I - \alpha = (I - \eta)V \quad \text{and} \quad U = V^\dagger U'. \tag{4.21}$$

From the first relation in Eq. (4.21) the elements of V can be identified as

$$V = I - \begin{pmatrix} 0 & -\eta_{e\mu} & -\eta_{e\tau} \\ \eta^*_{e\mu} & 0 & -\eta_{\mu\tau} \\ \eta^*_{e\tau} & \eta^*_{\mu\tau} & 0 \end{pmatrix} \tag{4.22}$$

at linear order in η. Substituting again in Eq. (4.21) the relations

$$\begin{pmatrix} \alpha_{ee} & 0 & 0 \\ \alpha_{\mu e} & \alpha_{\mu\mu} & 0 \\ \alpha_{\tau e} & \alpha_{\tau\mu} & \alpha_{\tau\tau} \end{pmatrix} = \begin{pmatrix} \eta_{ee} & 0 & 0 \\ 2\eta^*_{e\mu} & \eta_{\mu\mu} & 0 \\ 2\eta^*_{e\tau} & 2\eta^*_{\mu\tau} & \eta_{\tau\tau} \end{pmatrix} \tag{4.23}$$

and

$$U = V^\dagger U' = \left(I + \begin{pmatrix} 0 & -\eta_{e\mu} & -\eta_{e\tau} \\ \eta^*_{e\mu} & 0 & -\eta_{\mu\tau} \\ \eta^*_{e\tau} & \eta^*_{\mu\tau} & 0 \end{pmatrix} \right) U' \tag{4.24}$$

are found. This implies the following mapping between the two sets of mixing angles[3]

[3]Note that, apart from correcting the PMNS mixing angles and CP-phase $\delta_{\rm CP}$ at order η, phase redefinitions of the three charged leptons as well as corrections to the two neutrino Majorana phases are necessary at the same order.

in U' and U:

$$\begin{aligned}
\theta_{12} - \theta'_{12} &= \frac{\mathrm{Re}(s_{23}\eta_{e\tau} - c_{23}\eta_{e\mu})}{c_{13}}, \\
\theta_{13} - \theta'_{13} &= \mathrm{Re}(-s_{23}e^{i\delta_{\mathrm{CP}}}\eta_{e\mu} - c_{23}e^{i\delta_{\mathrm{CP}}}\eta_{e\tau}), \\
\theta_{23} - \theta'_{23} &= -\,\mathrm{Re}(\eta_{\mu\tau}) + \tan\theta_{13}\,\mathrm{Re}\left(c_{23}e^{i\delta_{\mathrm{CP}}}\eta_{e\mu} - s_{23}e^{i\delta_{\mathrm{CP}}}\eta_{e\tau}\right), \\
\delta_{\mathrm{CP}} - \delta'_{\mathrm{CP}} &= \frac{\cos 2\theta_{12}}{s_{12}c_{12}c_{13}}\,\mathrm{Im}\left(s_{23}\eta_{e\tau} - c_{23}\eta_{e\mu}\right) + \frac{1}{s_{13}c_{13}}\,\mathrm{Im}\left(s_{23}e^{i\delta_{\mathrm{CP}}}\eta_{e\mu} + c_{23}e^{i\delta_{\mathrm{CP}}}\eta_{e\tau}\right) \\
&\quad - \frac{\tan\theta_{13}}{s_{23}c_{23}}\,\mathrm{Im}\left(c_{23}^3 e^{i\delta_{\mathrm{CP}}}\eta_{e\mu} + s_{23}^3 e^{i\delta_{\mathrm{CP}}}\eta_{e\tau} + \frac{\eta_{\mu\tau}}{\tan\theta_{13}}\right).
\end{aligned} \tag{4.25}$$

When the relations given in Eqs. 4.23 and 4.25 are taken into account the predictions for the different oscillation channels coincide at leading order in the non-unitarity parameters, as they should. An important conclusion derived from this is that the determination of the mixing angles themselves will generally be affected by non-unitarity corrections. However, the size of these corrections is, at present, negligible compared to the current uncertainties on the determination of the mixing angles themselves. These corrections are parametrization-dependent but, when taken into account and propagated consistently, the predictions derived from both schemes agree.

For neutrino oscillation studies it seems advantageous to adopt the triangular parametrization, since it leads to fewer corrections given its structure. For instance, in the example shown in Eq. (4.19) there are no corrections coming from non-unitarity for this parametrization, and thus the angle θ_{23} in U can be identified with the angle determined in present global fits to a good approximation. Indeed, this is also the case for θ_{12} and θ_{13}, since the $\mathcal{P}_{ee}$ oscillation probabilities in the solar regime (KamLAND) and in the atmospheric regime (Daya Bay, RENO, Double-Chooz) are also independent of any non-unitarity corrections at linear order when the triangular parametrization is considered and when the appropriate normalization is taken into account, see Sec. 4.1.

Thus, the U matrix from the triangular parametrization corresponds, to a good approximation, with the unitary matrix obtained when determining θ_{12}, θ_{23} and θ_{13} through present (disappearance) neutrino oscillation measurements. Since we are here interested in the impact of non-unitarity and sterile neutrinos on neutrino oscillation phenomenology we will therefore use the triangular parametrization in the remainder of this work.

As we will see in Sec. 4.5, the dependence on the diagonal non-unitarity param-

eters $\alpha_{\beta\beta}$ is particularly interesting. Indeed, when the normalization accounting for the new physics effects at the near detector is considered, it effectively cancels any leading order dependence on $\alpha_{\beta\beta}$ in disappearance channels in vacuum. This can be easily understood by introducing the triangular parameterization in Eq. (4.7). Expanding in $\alpha_{\delta\gamma}$ we obtain

$$\mathcal{P}_{\alpha\beta} = \left| (1 + \alpha_{\alpha\alpha} - \alpha_{\beta\beta}) (US^0U^\dagger)_{\alpha\beta} - \sum_{\delta\neq\alpha} \alpha_{\alpha\delta} (US^0U^\dagger)_{\delta\beta} - \sum_{\delta\neq\beta} (US^0U^\dagger)_{\alpha\delta} \alpha^*_{\beta\delta} + \mathcal{O}\left(\alpha^2\right) \right|^2 . \tag{4.26}$$

Therefore, when $\alpha = \beta$ the dependence on $\alpha_{\beta\beta}$ cancels out. This illustrates how relevant the role of the near detectors is regarding the sensitivity to the new physics parameters.

4.3 Non-Standard Interactions

Both types of new physics effects in neutrino oscillations discussed above can be described through the Non-Standard Interaction (NSI) formalism, which parametrizes the new physics effects in neutrino production, detection, and propagation processes in a completely model-independent way. Let us first focus on NSI affecting neutrino production and detection. When these effects are included, the oscillation probability is given by

$$P_{\alpha\beta} = | \left[(1 + \epsilon^d) US^0 U^\dagger (1 + \epsilon^s) \right]_{\beta\alpha} |^2, \tag{4.27}$$

where ϵ^s and ϵ^d are general 3×3 complex matrices which represent the NSI modifications to the production and detection diagrams, respectively. S^0 is defined in Eq. (4.4) with the Hamiltonian H given in Eq. (4.2). The non-unitarity (Eq. (4.5)) and averaged-out sterile neutrino (Eq. (4.10)) effects at production and detection can be mapped to the NSI formalism (Eq. (4.27)) with the identification

$$\epsilon^{s*}_{\beta\alpha} = \epsilon^d_{\alpha\beta} = -\alpha_{\alpha\beta}. \tag{4.28}$$

This mapping can be easily obtained just considering the triangular parameterization, which can be applied in both the non-unitarity and averaged-out sterile neutrino cases, in Eqs. (4.5) or (4.10) and comparing the result to Eq. (4.27).

On the other hand, NSI affecting neutrino propagation are usually described

through the Hamiltonian

$$H = \frac{1}{2E}\begin{pmatrix} 0 & 0 & 0 \\ 0 & \Delta m^2_{21} & 0 \\ 0 & 0 & \Delta m^2_{31} \end{pmatrix} + V_{\rm CC}\, U^\dagger \begin{pmatrix} 1+\epsilon_{ee} & \epsilon_{e\mu} & \epsilon_{e\tau} \\ \epsilon^*_{e\mu} & \epsilon_{\mu\mu} & \epsilon_{\mu\tau} \\ \epsilon^*_{e\tau} & \epsilon^*_{\mu\tau} & \epsilon_{\tau\tau} \end{pmatrix} U, \tag{4.29}$$

in the mass basis, where U is the standard unitary PMNS matrix, and $\epsilon_{\alpha\beta}$ and $\epsilon_{\alpha\alpha}$ are complex and real parameters respectively. In order to understand how the non-unitarity/averaged-out sterile neutrino corrected matter effects can be translated to this parametrization, we introduce the triangular parameterization of N into Eq. (4.2), obtaining the following Hamiltonian at leading order in α

$$H = \frac{1}{2E}\begin{pmatrix} 0 & 0 & 0 \\ 0 & \Delta m^2_{21} & 0 \\ 0 & 0 & \Delta m^2_{31} \end{pmatrix} + \frac{V_{\rm CC}}{2}\, U^\dagger \begin{pmatrix} 2-2\alpha_{ee} & \alpha^*_{\mu e} & \alpha^*_{\tau e} \\ \alpha_{\mu e} & 2\alpha_{\mu\mu} & \alpha^*_{\tau\mu} \\ \alpha_{\tau e} & \alpha_{\tau\mu} & 2\alpha_{\tau\tau} \end{pmatrix} U, \tag{4.30}$$

where approximately equal densities of electrons n_e and neutrons n_n (for the neutral current contribution) in the Earth have been assumed (see also Ref. [112]). Comparing Eqs. (4.30) and (4.29) we find the mapping between the NSI parametrization and the lower triangular parametrization of the non-unitarity and sterile neutrino scenarios

$$\begin{aligned} \epsilon_{ee} &= -\alpha_{ee}, & \epsilon_{\mu\mu} &= \alpha_{\mu\mu}, & \epsilon_{\tau\tau} &= \alpha_{\tau\tau}, \\ \epsilon_{e\mu} &= \frac{1}{2}\alpha^*_{\mu e}, & \epsilon_{e\tau} &= \frac{1}{2}\alpha^*_{\tau e}, & \epsilon_{\mu\tau} &= \frac{1}{2}\alpha^*_{\tau\mu}, \end{aligned} \tag{4.31}$$

which apply for neutrino oscillation experiments in the Earth with constant matter. Note that, in presence of production and detection NSI, the same normalization as for the non-unitarity case discussed in Section 4.1 needs to be taken into account.

4.4 Present constraints on deviations from unitarity

The mapping to NSI described above works both for the non-unitarity and the averaged out sterile neutrino contributions to neutrino oscillations. However, the present

constraints on each of these contributions from other observables are very different. Indeed, PMNS non-unitarity from very heavy extra neutrinos induces modifications of the W and Z couplings that impact precision electroweak and flavour observables [66, 79, 104–114, 116–118]. These modification translate into very strong upper limits on the α parameters. These have been taken from Ref. [79] and are listed in the left column in Table 4.1. The second number quoted in parenthesis for the $\alpha_{\mu e}$ element includes the $\mu \to e\gamma$ observable, which can in principle be evaded [226] for heavy neutrino masses close to M_W and some fine-tuning of the parameters. In this case, the quoted bound is derived from the constraints on the diagonal parameters, through Eq. (4.18).

However, for sterile neutrinos with masses below the electroweak scale these stringent constraints are lost, since all mass eigenstates are kinematically available in the observables used to derive the constraints and unitarity is therefore restored. If the masses of the extra states are in the MeV or GeV range, even stronger constraints can be derived from direct searches at beam-dump experiments as well as from meson and beta decays [170–172]. On the other hand, for masses below the keV scale even the beta decay searches are no longer sensitive, and the only applicable bounds are the much milder constraints stemming from the non-observation of their effects in neutrino oscillation experiments [165, 220, 232]. The sensitivity, or lack thereof, of oscillation experiments to sterile neutrino mixing will depend on the actual value of the sterile neutrino mass, which determines if the corresponding Δm^2 leads to oscillations for the energy and baseline that characterize the experimental setup. As Δm^2 increases, there will be a point at which the sterile neutrino oscillations enter the averaged-out regime. Once oscillations are averaged-out, the constraints derived will become independent of Δm^2 and apply to arbitrarily large values of Δm^2. Limits derived in this regime are summarized in in the middle column of Table 4.1 and apply as long as $\Delta m^2 > 100$ eV^2. They are thus relevant when the sterile neutrino oscillations are in the averaged out regime for both the near and far detectors of the DUNE experiment. Some of these constraints also apply for values of Δm^2 smaller than 100 eV^2. For a more comprehensive breakdown of the available constraints and their ranges of applicability, we refer the interested reader to Appendix B.

Even though the case in which the sterile neutrino oscillations are undeveloped at the near detector, but averaged-out at the far, applies to a significantly smaller fraction of the parameter space, we find it instructive to analyze this scenario as well, since it leads to very different phenomenology and sensitivities, as will be discussed in Section 4.5. For the case of DUNE, this scenario requires $\Delta m^2 \sim 0.1 - 1$ eV^2 and

	"Non-Unitarity"	"Light steriles"	
	$(m >$ EW)	$\Delta m^2 \gtrsim 100$ eV^2	$\Delta m^2 \sim 0.1 - 1$ eV^2
α_{ee}	$1.3 \cdot 10^{-3}$ [79]	$2.4 \cdot 10^{-2}$ [227]	$1.0 \cdot 10^{-2}$ [227]
$\alpha_{\mu\mu}$	$2.2 \cdot 10^{-4}$ [79]	$2.2 \cdot 10^{-2}$ [228]	$1.4 \cdot 10^{-2}$ [229]
$\alpha_{\tau\tau}$	$2.8 \cdot 10^{-3}$ [79]	$1.0 \cdot 10^{-1}$ [228]	$1.0 \cdot 10^{-1}$ [228]
$\lvert\alpha_{\mu e}\rvert$	$6.8 \cdot 10^{-4}$ $(2.4 \cdot 10^{-5})$ [79]	$2.5 \cdot 10^{-2}$ [230]	$1.7 \cdot 10^{-2}$
$\lvert\alpha_{\tau e}\rvert$	$2.7 \cdot 10^{-3}$ [79]	$6.9 \cdot 10^{-2}$	$4.5 \cdot 10^{-2}$
$\lvert\alpha_{\tau\mu}\rvert$	$1.2 \cdot 10^{-3}$ [79]	$1.2 \cdot 10^{-2}$ [231]	$5.3 \cdot 10^{-2}$

Table 4.1: Current upper bounds on the α parameters in the scenarios considered in this work. The limits are shown at 2σ and 95% CL (1 d.o.f.) for the non-unitarity and light sterile neutrino scenarios. The bounds in the middle column apply for $\Delta m^2 \gtrsim 100$ eV^2 and will thus be relevant when the sterile neutrino oscillations are in the averaged-out regimes for both the near and far detectors of most long-baseline experiments. The bounds in the right column apply for $\Delta m^2 \sim 0.1 - 1$ eV^2 and will thus be relevant when the sterile neutrino oscillations are in the averaged-out regime for the far detector, but not for the near detector. The second number quoted in parenthesis for the $\alpha_{\mu e}$ element includes the $\mu \to e\gamma$ observable, which can in principle be evaded [226] , see main text for details. The numbers for the off-diagonal parameters without a reference are obtained indirectly from constraints on the diagonal parameters via $\alpha_{\alpha\beta} \leq 2\sqrt{\alpha_{\alpha\alpha}\alpha_{\beta\beta}}$ (see Eq. (4.18)). See Appendix B for further details.

the corresponding constraints have been compiled in the right column of Table 4.1. Notice that in this range of Δm^2 most constraints come from experiments that would not have reached the averaged-out regime but would rather have oscillations well-matched to their energies and baselines. Thus, the corresponding constraints in this regime oscillate significantly and the value quoted in the table is the most conservative available in that range.

4.5 DUNE sensitivities

In this section we present, as an example, the sensitivities that the proposed DUNE experiment would have to PMNS non-unitarity or, equivalently, to averaged-out sterile neutrino oscillations as discussed in Section 4.1. For this analysis we choose the triangular parametrization of the new physics effects since, as argued in Section 4.2, its unitary part can be more directly mapped to the "standard" PMNS matrix as determined by present experiments through neutrino oscillation disappearance channels. Indeed, production and detection new physics effects in a given channel $P_{\alpha\beta}$ only depend on the elements $\alpha_{\gamma\rho}$ such that $\gamma, \rho \leq \alpha$ or $\gamma, \rho \leq \beta$ when the flavour indices are ordered as $e < \mu < \tau$ [163]. Furthermore, when the new physics affects the near and far detectors in the same manner, the normalization of the oscillation probabilities presented in Eq. (4.7) has to be applied, which effectively cancels any leading order dependence on the new physics parameters $\alpha_{\beta\beta}$ in disappearance channels in vacuum (see Eq. (4.26)). The choice of the facility under study is motivated by the strong matter effects that characterize the DUNE setup and that allow to probe not only the source and detector effects induced by the new physics, but also the matter effects which now provide sensitivity to other $\alpha_{\gamma\rho}$ parameters not necessarily satisfying $\gamma, \rho \leq \alpha$ or $\gamma, \rho \leq \beta$.

The simulation of the DUNE setup was performed with the GLoBES software [233, 234] using the DUNE CDR configuration presented in Ref. [235]. The new physics effects have been implemented in GLoBES via the MonteCUBES [208][4] plug-in, which has also been used to perform a Markov chain Monte Carlo (MCMC) scan of the 15-dimensional parameter space (the 6 standard oscillation parameters plus the 6 moduli of the $\alpha_{\gamma\rho}$ non-zero entries and the 3 phases of the off-diagonal elements). In the fit, the assumed true values for the standard oscillation parameters are set according to their current best-fits from Ref. [127]. The mixing angles and squared-mass splittings are allowed to vary in the simulations, using a Gaussian prior corresponding to their current experimental uncertainties from Ref. [127] centered around their true values. In the case of θ_{13} and θ_{23} the Gaussian priors are implemented on $\sin^2 2\theta$, which is a more accurate description of the present situation and, in the case of θ_{23}, allows to properly account for the octant degeneracy: $\Delta m^2_{21} = (7.50 \pm 0.18) \cdot 10^{-5}\,\text{eV}^2$, $\Delta m^2_{31} = (2.457 \pm 0.049) \cdot 10^{-3}\,\text{eV}^2$, $\theta_{12} = 33.48^\circ \pm 0.77^\circ$, $\sin^2 2\theta_{13} = 0.085 \pm 0.005$, $\sin^2 2\theta_{23} = 0.991 \pm 0.02$. Notice that, as described in Sec-

[4] A new version of the MonteCUBES software implementing the triangular parametrization is available.

tion 4.2, the use of the triangular parametrization allows a direct mapping of the present measurements to the elements of the U matrix. Nevertheless, the present uncertainties adopted in this analysis are still large enough that any correction due to non-unitarity is negligible. The CP-violating phase is left completely free during the simulations, and its true value is set to $\delta_{\rm CP} = -\pi/2$. Finally, a 2 % uncertainty in the PREM matter density profile [236] has also been considered.

We have performed simulations for two distinct new physics scenarios. In the first case (ND averaged) we normalize the oscillation probabilities according to Eq. (4.7). Indeed, as discussed in Section 4.1, at leading order in the new physics parameters this scenario accurately describes both the effects of PMNS non-unitarity from very heavy neutrinos as well as sterile neutrino oscillations that have been averaged out both at the near detector (ND) and far detector. For the DUNE setup, the requirement for having averaged-out oscillations at the near detector translates to the condition $\Delta m^2 >$ few 100 eV^2. The second scenario (ND undeveloped) would correspond to the case where sterile neutrino oscillations are averaged out at the far detector but have not yet developed at the near detector. In this case, no extra normalization is needed and the oscillation probability is directly given by Eq. (4.5). Note that, for the energies and baseline characterizing the DUNE setup, only values of the sterile neutrino masses around $\Delta m^2 \sim 0.1 - 1$ eV^2 roughly satisfy these conditions. However, we find it instructive to study also this regime in order to remark the differences between the two scenarios and the importance of the normalization in Eq. (4.7) that will generally apply in most of the parameter space.

Figures 4.1 and 4.2 show the expected sensitivities to the new physics parameters. These have been obtained by assuming that the true values of all α entries are zero to obtain the corresponding expected number of events, and fitting for the corresponding parameters while marginalizing over all other standard and new physics parameters. The resulting frequentist allowed regions are shown at at 1σ, 90%, and 2σ C.L.

The sensitivities obtained for all parameters fall at least one order of magnitude short of the current bounds on the non-unitarity from heavy neutrino scenario presented in Tab. 4.1. Thus, the standard three-family oscillations explored at DUNE (and the other present and near-future oscillation facilities) will be free from the possible ambiguities that could otherwise be induced by this type of new physics [166, 167, 237, 238]. While these bounds on non-unitarity are too strong for these effects to be probed at present and near-future facilities a Neutrino Factory [168, 169] could be precise enough to explore these effects [103, 164, 239]. The

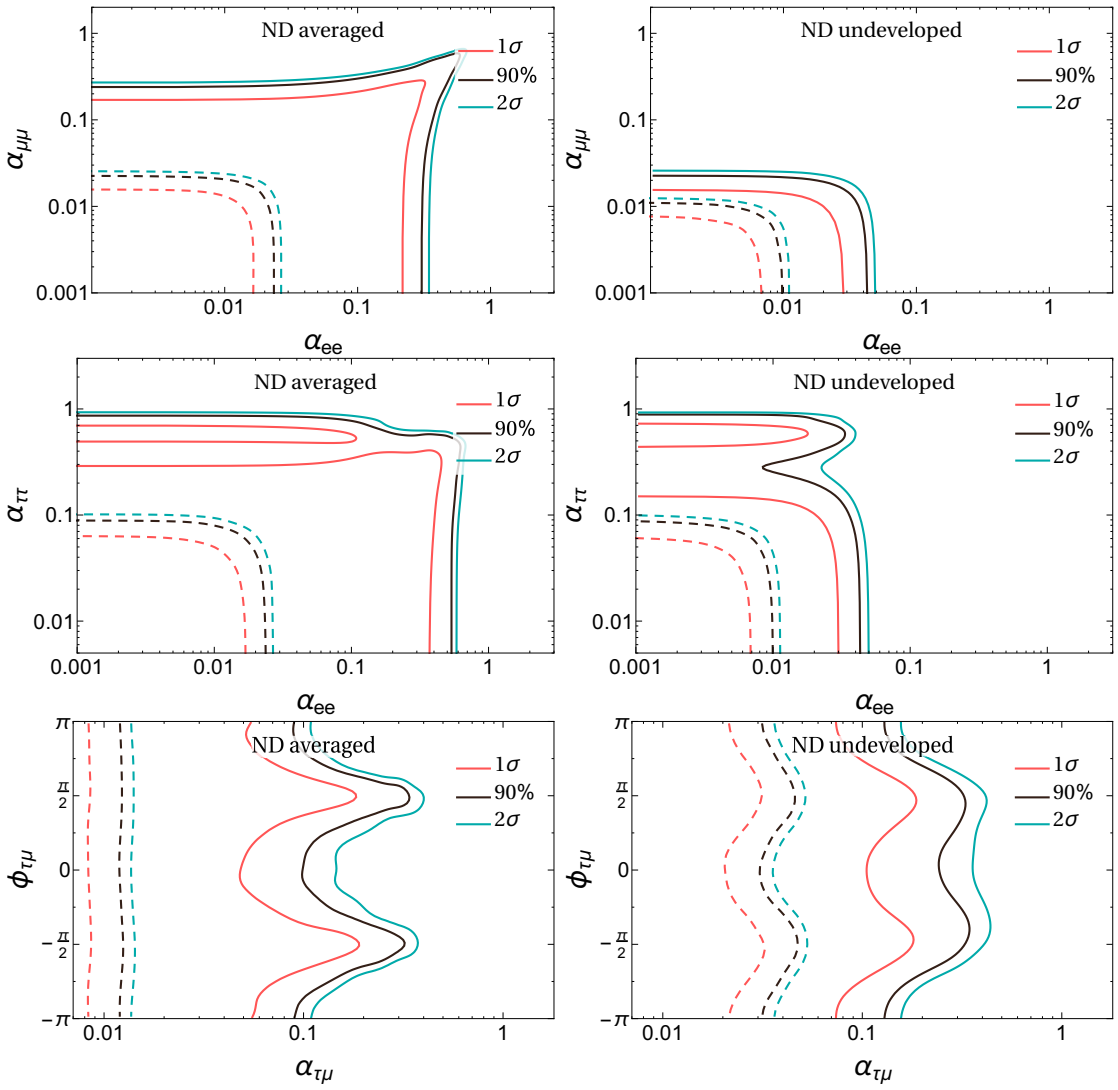

Figure 4.1: Expected frequentist allowed regions at the 1σ, 90% and 2σ C.L. for DUNE. All new physics parameters are assumed to be zero so as to obtain the expected sensitivities. The left panels (ND averaged) correspond to the non-unitarity case, or to the sterile case when the light-heavy oscillations are averaged out in the near and far detectors. The right panels (ND undeveloped) give the sensitivity for the sterile case when the light-heavy oscillations have not yet developed in the near detector, but are averaged out in the far. The solid lines correspond to the analysis of DUNE data alone, while the dashed lines include the present constraints on sterile neutrino mixing from the middle and right columns in Tab. 4.1 for the NS averaged and ND undeveloped scenarios respectively.

situation is slightly different if the results are interpreted in terms of an averaged-out sterile neutrino, since present constraints are weaker in this case. We will therefore focus on this scenario for the rest of our discussion and also study the case in which DUNE data is complemented by our present prior constraints on the sterile neutrino mixing (middle and right columns of Tab. 4.1 for the ND averaged and undeveloped scenarios respectively), since synergies between the data sets may be present. This case is depicted with dashed lines in Figs. 4.1 and 4.2. As an example of such synergy, the sensitivity to the real part of $\alpha_{\tau\mu}$ improves for the ND undeveloped scenario through the combination of DUNE data and the present priors with respect to both datasets independently. Indeed, the prior on its own would give the same bound for the real an imaginary parts (as for the ND averaged case in the left panel) and its value roughly corresponds to the constraint obtained for the the imaginary part of $\alpha_{\tau\mu}$, while the sensitivity to the real part does improve through the combination with DUNE.

Another conclusion that can be drawn from Fig. 4.1 is that the sensitivities to the diagonal parameters α_{ee} and $\alpha_{\mu\mu}$ are significantly stronger for the ND undeveloped (right panels) as compared to the ND averaged scenario (left panels). This was to be expected since the source and detection effects that provide a leading order sensitivity to the diagonal parameters are totally or partially cancelled once the normalization of Eq. (4.7) is included (see Eq. (4.26)). In the disappearance channel both effects cancel in the ratio, while for the appearance channel there is a partial cancellation that only allows the experiment to be sensitive to the combination $\alpha_{ee} - \alpha_{\mu\mu}$. This leads to a pronounced correlation among α_{ee} and $\alpha_{\mu\mu}$, seen in the upper left panel of Fig. 4.1.

From a phenomenological point of view we observe that, if both near and far detectors are affected by the new physics in the same way (as is the case when the sterile neutrino oscillations are averaged out at both detectors, or in the non-unitarity scenario) their effects are more difficult to observe since they cannot be disentangled from the flux and cross section determination at the near detector. Conversely, in the case in which sterile neutrino oscillations have not yet developed at the near detector but are averaged out at the far, the flux determined by both detectors will have a different normalization. Thus, a strong linear sensitivity to α_{ee} and $\alpha_{\mu\mu}$ is obtained from detector and source effects respectively, although there is no improvement over present constraints.

Fig. 4.1 also shows strong correlations in the middle left panel, involving $\alpha_{\tau\tau}$ and α_{ee}. Indeed, sensitivity to $\alpha_{\tau\tau}$ comes through the matter effects, which only

depend on the diagonal entries through their differences $\alpha_{\beta\beta} - \alpha_{\gamma\gamma}$, since a global term of the form of $\alpha_{\gamma\gamma} I$ does not affect neutrino oscillations at leading order in α. In these panels we also observe a large difference between the allowed regions for $\alpha_{\tau\tau}$ once prior constraints on the α parameters are included in the analysis, by comparing the solid and dashed lines. This is due to the lifting of degeneracies involving θ_{23} and the combination $\alpha_{\tau\tau} - \alpha_{\mu\mu}$, and will be discussed in more detail below.

Interesting correlations and degeneracies among the standard and new physics parameters can indeed take place in the averaged-out sterile neutrino scenario [232, 240–242]. In our results, even though the true values of the α parameters were set to zero, some very interesting correlations and degeneracies among θ_{23} and the new physics parameters have been recovered. These are shown in Fig. 4.2, and have been noticed in the context of NSI[5] in Refs. [243–246] (for other works on degeneracies among standard and non-standard parameters in DUNE see *e.g.*, Refs. [247–250]). The first degeneracy appears for the wrong octant of θ_{23}, which would otherwise be correctly determined by the interplay between the appearance and disappearance channels at DUNE (see *e.g.*, Ref. [251]). We have checked that this degeneracy is characterized by non zero values of $\alpha_{\tau e}$ with a non-trivial phase around π. At the same time, positive values of $\alpha_{\mu\mu} - \alpha_{\tau\tau}$ are slightly preferred. From Ref. [246] this degeneracy was expected for the phase of $\phi_{\tau e} = \arg(\alpha_{\tau e}) \sim \pi$ since $\delta_{\rm CP} = -\pi/2$ and strong correlations between these two parameters are required in order to reproduce this degeneracy. Note that this degeneracy is partially lifted in the ND undeveloped scenario (right panels). Indeed, the strong sensitivity that this scenario presents to $\alpha_{\mu\mu}$ translates into very stringent bounds that do not allow the preferred positive values of $\alpha_{\mu\mu} - \alpha_{\tau\tau}$ seen in the left panels for the ND averaged case since the diagonal elements of α are positive (see Eq. (4.18)). Upon the inclusion of prior constraints this degeneracy is lifted in both scenarios.

Interestingly, the second degeneracy involves values of $\theta_{23} \sim \pi/4$, so that it could potentially compromise the capabilities of DUNE to determine the maximality of this mixing angle. This degeneracy takes place for $\alpha_{\mu\mu} - \alpha_{\tau\tau} \sim -0.6$, and large values of $\alpha_{\mu e}$ and $\alpha_{\tau e}$ are also needed. Fortunately, present constraints on these parameters are already strong enough to also rule out this possibility (see Tab. 4.1), so that a clean determination of the maximality of θ_{23} should be possible at DUNE. Moreover, when the current bound on $\alpha_{\tau e}$ from the right column in Tab. 4.1 is added as prior to the simulations, the sensitivity to $\alpha_{\mu e}$ is increased slightly beyond the present prior and the allowed region around $\theta_{23} \sim \pi/4$ is ruled out. This exam-

[5]Note the correspondence between NSI, steriles, and non-unitarity presented in Section 4.3.

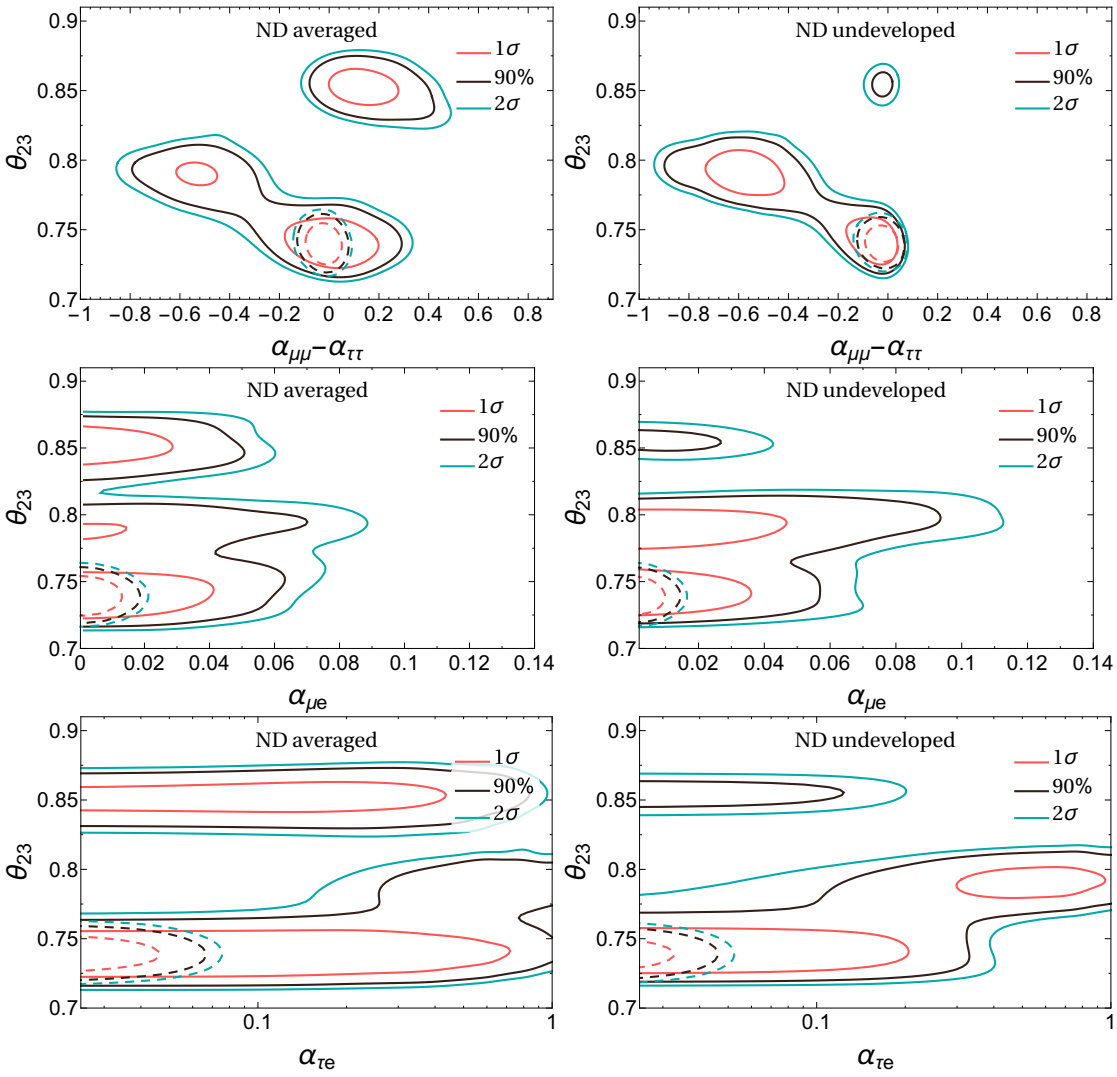

Figure 4.2: Expected frequentist allowed regions at the 1σ, 90% and 2σ CL for DUNE. All new physics parameters are assumed to be zero so as to obtain the expected sensitivities. The left panels (ND averaged) correspond to the non-unitarity case, or to the sterile case when the light-heavy oscillations are averaged out in the near and far detectors. The right panels (ND undeveloped) give the sensitivity for the sterile case when the light-heavy oscillations have not yet developed in the near detector, but are averaged out in the far. The solid lines correspond to the analysis of DUNE data alone, while the dashed lines include the present constraints on sterile neutrino mixing from the middle and right columns in Tab. 4.1 for the ND averaged and ND undeveloped scenarios respectively.

ple shows explicitly the complementarity between current constraints and DUNE sensitivities.

All in all, we find that, upon solving the degeneracies through the inclusion of present priors, DUNE's sensitivity would slightly improve upon the present constraints on $\alpha_{\mu e}$ in the ND averaged case as well as the real part of $\alpha_{\tau\mu}$ for the ND undeveloped scenario. While the potential improvement over present bounds is marginal, this also implies that, at the confidence levels studied in this work, the sensitivities to the standard three neutrino oscillations are rather robust and not significantly compromised by the new physics investigated here.

4.6 Conclusions

The simplest and most natural extension of the Standard Model that can account for our present evidence for neutrino masses and mixings is the addition of right-handed neutrinos to the Standard Model (SM) particle content. Gauge and Lorentz invariance then imply the possible existence of a Majorana mass for these new particles at a scale to be determined by observations. In this work we have studied the impact that two limiting regimes for this new physics scale can have in neutrino oscillation experiments. For very high Majorana masses, beyond the kinematic reach of our experiments, the imprint of these new degrees of freedom at low energies takes the form of unitarity deviations of the PMNS mixing matrix. In the opposite limit, for small Majorana masses, these extra sterile neutrinos are produced and can participate in neutrino oscillations. However, it should be kept in mind that the neutrino oscillation phenomenology discussed here applies also to other types of new physics that could induce unitarity deviations for the PMNS mixing matrix. This includes any model in which heavy fermions mix with the SM neutrinos or charged leptons, as for instance the type-I/type-III seesaw, Left-Right symmetric models, and models with kinematically accessible sterile neutrinos in the averaged-out regime.

Despite being sourced by different underlying physics, we have seen that, when the sterile neutrino oscillations are averaged out (and at leading order in the small heavy-active mixing angles) both limits lead to the same modifications in the neutrino oscillation probabilities. Namely, a modification of the interactions in the source and detector which implies short-distance effects as well as modified matter effects which, contrary to the standard scenario, also involve neutral current interactions. However, the present constraints that apply to these two scenarios are very different.

Indeed, PMNS non-unitarity is bounded at the per mille level, or even better for some elements, through precision electroweak and flavour observables, while sterile neutrino mixing in the averaged-out regime is allowed at the percent level since it can only be probed via oscillation experiments themselves. Thus, PMNS non-unitarity can have no impact in present or near-future oscillation facilities while sterile neutrino mixing could potentially be discovered by them.

We have also noted apparently conflicting results depending on the parametrization used to encode these new physics effects. The source of this apparent inconsistency was found to be the different quantities that are commonly identified with the standard PMNS matrix in each parametrization. The conflict was solved by providing a mapping between the two sets of parameters and by identifying the parametrization for which these PMNS parameters correspond to what is determined experimentally.

The role of the near detector was also explored in depth. Indeed, since present and near future oscillation experiments constrain their fluxes and detection cross sections using near detector data it is important to consider if the new physics affects the near and far detector measurements in the same way. If this is the case, the source and detector short-distance effects cancel to a large extent, since there is no additional handle to separate them from flux and cross-section uncertainties. This is always the case in the non-unitarity scenario and when sterile neutrino oscillations are averaged out both at the near and far detectors. Conversely, if sterile neutrino oscillations have not developed yet at the near detector, the determination of the flux and cross section is free from new physics ambiguities and, when compared with the far detector data, a greater sensitivity to the flavour-conserving new physics effects is obtained. This crucial difference is sometimes overlooked in the present literature. Finally we also provided a mapping of these new physics effects in the popular non-standard interaction (NSI) formalism.

These effects were exemplified through numerical simulations of the proposed DUNE neutrino oscillation experiment. Our simulations confirm that PMNS non-unitarity is indeed beyond the reach of high precision experiments such as DUNE, but that sterile neutrino oscillations could manifest in several possible interesting ways. Indeed, degeneracies between θ_{23} and the new physics parameters, previously identified in the context of NSI, have been found in our simulations. These degeneracies could potentially compromise the capability of DUNE to determine the maximality of θ_{23} as well as its ability to discern its correct octant. We find that current bounds on the new physics parameters are able to lift the degeneracies around

$\theta_{23} \sim \pi/4$.

Through these simulations the importance of correctly accounting for the impact of the near detector was made evident. Indeed, a very significant increase in the sensitivity to the new physics parameters was found for the case in which the near detector is not affected in the same way as the far. This would be the case of sterile neutrino oscillations that are undeveloped at the near detector but averaged out at the far. However, the parameter space for this situation to take place is rather small (for $\Delta m^2 \sim 0.1 - 1$ eV^2). The most common situation would rather be that in which sterile neutrino oscillations are averaged out at both near and far detectors. However, this fact has been usually overlooked in previous literature.

The origin of neutrino masses remains one of our best windows to explore the new physics underlying the open problems of the SM. Its simplest extension to accommodate neutrino masses and mixings offers a multitude of phenomenological consequences that vary depending of the new physics scale introduced and that should be thoroughly explored by future searches. In this work, we have explored the impact of these new physics in neutrino oscillation phenomena. We have found that neutrino oscillation facilities are best suited to probe the lightest new physics scales, i.e., kinematically accessible sterile neutrinos.

Conclusions and Outlook

Despite the remarkable agreement between a wide range of SM predictions and their experimental measurements, the SM has to be extended in order to explain some phenomena that cannot be understood within this model. A very significant example is the overwhelming experimental evidence from the neutrino oscillation phenomena supporting the existence of neutrino masses and mixings, which are absent in the SM. A simple and natural extension, given its symmetry to the quark and charged lepton sectors, to account for neutrino masses is to introduce right-handed neutrinos in the particle content of the SM. Since these extra right-handed neutrinos are singlets under the SM gauge group, a Majorana mass term for these fermions is therefore allowed in the Lagrangian. However, this new mass scale is not related to the Higgs mechanism, and thus no guidance from theoretical grounds exists.

One possibility is that this Majorana scale is above the EW scale but in the 100 GeV-TeV range. Then, the masses of the left-handed neutrinos arise in a simple way after ESB through the Weinberg operator in a low scale SM-Seesaw. In this situation, the presence of the new degrees of freedom will induce deviations from unitarity in the leptonic mixing matrix that appears in the charged current interactions. Thus, processes mediated by the weak currents would be modified, and therefore precision measurements of electroweak and flavor observables become a powerful tool to probe for the existence of heavy Majorana neutrinos.

Following this idea, a global fit to the most complete and updated stringent set of electroweak and flavour observables to constrain the mixing of the extra heavy right-handed neutrinos in a model independent way has been performed in this thesis. On the other hand, at some level, the addition of right-handed neutrinos will also impact neutrino oscillation searches. Therefore, the expected sensitivities of new generation of neutrino oscillation experiments to probe for this New Physics have been analyzed in detail as part of this thesis.

In the following, the main results and conclusions extracted from the present thesis are summarized.

- The most general, updated and comprehensive constraints on the mixing of heavy Seesaw neutrinos with the charged fermions of the SM have been derived through a global fit to precision EW observables, LFV searches and probes on weak lepton universality. These bounds have been computed both for a completely model independent scenario, as well as for the case in which only three extra heavy states are considered, and thus they apply to any extension of the SM with Majorana masses above the EW scale. In the G-SS scenario, at the $1-2\sigma$ level, a mild preference for non-zero mixing in the e and τ sectors of 0.031 and 0.044, respectively, has been found. While at the 2σ level upper bounds of $\sim \mathcal{O}(10^{-2})$ for the diagonal mixing have been derived. Concerning the off-diagonal elements, $\mu \to e\gamma$ sets the most stringent constraint of $\sim \mathcal{O}(10^{-3})$ on the mixing in the $e-\mu$ sector, while the $e-\tau$ and $\mu-\tau$ sectors get an stronger indirect constrain of the percent level from the diagonal bounds via the Schwarz inequality. In the 3N-SS scenario, similar bounds are obtained for all the mixings, the only exception occurring for the μ sector where a stronger constraint of $\sim \mathcal{O}(10^{-4})$ is found due to $\mu \to e\gamma$ and the fact that in this more constrained scenario the Schwarz inequality is turned to an equality.
- The impact of loop level corrections when deriving bounds on the Seesaw mixing in the scenario with three extra right-handed neutrinos has been studied. The main conclusions are that loop level corrections are only relevant in a small fraction of the Seesaw parameter space, characterized by large Yukawa couplings and a low Seesaw scale, and that these corrections tend to strengthen the tree level contributions unless large deviations from $B-L$ are present. If $B-L$ is mildly broken, regions of the parameter space where these contributions from loops are negligible are therefore preferred by data. On the other hand, if $B-L$ is strongly violated, loop corrections could play a crucial role. However, these large violations of $B-L$ at loop level also lead to excessive contributions to the light neutrino masses, and hence this possibility is ruled out. Therefore, loop corrections can safely be neglected in the analysis of the heavy neutrino mixings in Seesaw mechanisms, and therefore the derived bounds in Chapter 2 of the 3N-SS scenario still apply when 1-loop corrections are considered.
- The imprints on neutrino oscillation experiments coming form the addition of right-handed neutrinos to the SM particle content have been studied, taking the DUNE proposal experiment as a benchmark for the discussion of the ex-

pected sensitivities. Two different limits have been analyzed, when the light sterile neutrinos are kinematically accessible in the experiments (bellow the π mass) and when, due to their large mass, the only effect on the oscillations comes from the non-unitarity of the mixing matrix. When the sterile neutrino oscillations are too fast to be resolved (averaged out regime) it has been shown that both limits lead to the same modifications in the neutrino oscillation probabilities (at leading order in the small heavy-active mixing angles). However, the present constraints which apply to these two scenarios are very different. Indeed, and as seen in Chapter 2, the non-unitarity of the PMNS matrix is bounded at the per mille level, or even better for some elements, while the deviations in the mixing matrix produced by sterile neutrinos in the averaged-out regime are allowed at the percent level since it can only be probed via oscillation experiments themselves. Thus, no impact in present or near-future oscillation facilities from non-unitarity is expected while if the sterile neutrinos are light enough to be produced at the source, their mixing could potentially be discovered by neutrino oscillation experiments. Indeed, our simulations confirm that non-unitarity is beyond the reach of high precision experiments such as DUNE, but that sterile neutrino oscillations could manifest in several possible interesting ways. Through these simulations the importance of correctly accounting for the impact of the near detector was also stressed. In particular, a very significant increase in the sensitivity to the New Physics parameters that encode the mixing with e or μ was found for the case in which the near detector is not affected in the same way as the far detector.

In conclusion, one of the main open problems of the SM has been addressed in this thesis: the unknown origin of neutrino masses and their mixing with charged leptons. Even though the regimes at very low energy and above the EW scales have been analyzed in this present work, the Majorana neutrinos could be probed at any scale. It will be extremely relevant to extend these studies to cover other limits, such as neutrinos in Cosmology, searches at future colliders (FCC-ee, ILC), or neutrino production and detection at beam-dump experiments (NA62, DUNE, SHiP). Likewise, significant improvements on the sensitivities of LFV searches like $\mu \to eee$ or $\mu - e$ conversion in nuclei are expected in the near future (Mu3e, COMET, MU2e) and therefore, the studies presented in this thesis should be updated with these sensitive results. Finally, $0\nu\beta\beta$-decay searches are the most promising tool to probe for the Majorana nature of the neutrinos. The quest for the origin of neutrino masses and mixings has started, and with it the hope for progressing in the

understanding of the underlaying fundamental theory beyond the SM.

Conclusiones y Perspectivas

A pesar de la extraordinaria concordancia entre una amplia gama de predicciones del SM y su medida experimental, el SM debe ser extendido para explicar algunos fenómenos que no pueden ser entendidos dentro de este modelo. Un ejemplo muy significante es la apabullante evidencia experimental del fenómeno de oscilación de neutrinos, que sustenta la existencia de masas y mezcla de neutrinos, las cuales no están presentes en el SM. Una simple y natural extensión, dada su simetría con los sectores de quarks y leptones cargados, que explica las masas de los neutrinos, es introducir neutrinos dextrógiros en el contenido de partículas del SM. Debido a que estos neutrinos dextrógiros adicionales son singletes bajo el grupo de gauge del SM, está permitido un término de masa Majorana en el Lagrangiano. Sin embargo, esta nueva escala de masa no está relacionada con el mecanismo de Higgs; y por ello, no existe ninguna pista sobre su valor a partir de fundamentos teóricos.

Una posibilidad es que esta escala de Majorana esté por encima de la escala EW pero en el rango de 100 GeV-TeV. Entonces, las masas de los neutrinos levógiros surgen de forma simple después del EWSB a través del operador de Weinberg en un SM-Seesaw de baja escala. En esta situación, la presencia de los nuevos grados de libertad inducirá desviaciones de la unitariedad de la matriz de mezcla leptónica que aparece en las interacciones de CC. Entonces, los procesos mediados por las corrientes débiles serán modificados, y por lo tanto las medidas de precisión de observables electrodébiles y de sabor se convierten en una herramienta potente para testar la existencia de los neutrinos pesados de Majorana.

Siguiendo esta idea, en esta tesis se ha desarrollado un ajuste global a los datos experimentales del conjunto más completo, actualizado y dominante de observables electrodébiles y de sabor, con el fin de constreñir la mezcla de estos neutrinos dextrógiros pesados adicionales de una forma independiente del modelo. Por otro lado; en algún momento, la incorporación de neutrinos dextrógiros también afectará la búsqueda de oscilaciones de neutrinos. Por ello, como parte de esta tesis se

han analizado las sensitividades esperadas para testar esta Nueva Física en futuras generaciones de experimentos de oscilación de neutrinos.

A continuación se resumen los resultados mas relevantes y las conclusiones extraídas de la presente tesis

- Las cotas mas generales, actualizadas y completas, a la mezcla de los neutrinos pesados del Seesaw con los fermiones cargados del SM han sido derivadas a través de un ajuste global a observables EW de precisión, búsquedas de LFV y tests de universalidad leptónica. Estas cotas han sido calculadas tanto para un escenario completamente independiente del modelo, como para el caso en el que únicamente se consideran tres estados pesados adicionales, y por lo tanto, los resultados aplican a cualquier extensión del SM con masas de Majorana por encima de la escala EW. En el escenario del G-SS, al nivel de $1-2\sigma$, se ha encontrado una ligera preferencia de mezcla no nula en los sectores del e y del τ, con valores de 0.031 y 0.044, respectivamente. Mientras que al nivel de 2σ, se han obtenido cotas superiores a los elementos diagonales de la matriz de mezcla de $\sim \mathcal{O}(10^{-2})$. En cuanto a los elementos no diagonales, la cota mas fuerte de $\sim \mathcal{O}(10^{-3})$ en la mezcla del sector $e-\mu$ proviene de $\mu \to e\gamma$, mientras que los sectores $e-\tau$ y $\mu-\tau$ obtienen cotas indirectas más fuertes, del orden del por ciento, a través de los elementos diagonales vía la desigualdad de Schwarz. En el escenario de 3N-SS, se han obtenido cotas similares para los elementos de la matriz de mezcla, la única excepción ocurre en el sector del μ donde se ha encontrado una cota más fuerte de $\sim \mathcal{O}(10^{-4})$, debido a $\mu \to e\gamma$, y al hecho de que en este escenario más constreñido, la desigualdad de Schwarz se convierte en una igualdad.
- Se ha estudiado el impacto de las correcciones a nivel loop cuando se obtienen cotas a la mezcla del Seesaw en el escenario con tres neutrinos dextrógiros adicionales. Las principales conclusiones son, que las correcciones de los loops únicamente son relevantes en una pequeña fracción del espacio de parámetros del Seesaw, caracterizado por acoplos de Yukawa grandes y escalas del Seesaw bajas, y que estas correcciones tienden a hacer más fuertes las contribuciones a nivel árbol, a no ser que estén presentes desviaciones de $B-L$ muy grandes. Cuando $B-L$ es ligeramente rota, los datos prefieren las regiones del espacio de parámetros en los cuales estas correcciones de los loops son despreciables. Por otro lado, si $B-L$ es fuertemente violada, las correcciones de los loops pueden jugar un papel crucial. Sin embargo, estas violaciones grandes de $B-L$ a nivel loop también conducen a contribuciones excesivas a la masa de los

neutrinos ligeros, y por lo tanto, esta posibilidad está descartada. Por ello, las correcciones de los loops pueden ser despreciadas de forma segura y las cotas derivadas del escenario de 3N-SS en el Capítulo 2, siguen aplicando cuando se consideran las correcciones a 1-loop.

- Se han estudiado las huellas en experimentos de oscilación de neutrinos que vienen de incluir neutrinos dextrógiros en el contenido de partículas del SM, tomando la propuesta del experimento de DUNE como punto de partida para la discusión de las sensitividades esperadas. Dos limites distintos han sido analizados, cuando los neutrinos ligeros son cinemáticamente accesibles en el experimento (por debajo de la masa del π) y cuando, debido a sus grandes masas, los únicos efectos en las oscilaciones vienen de la no unitariedad de la matriz de mezcla. Se ha demostrado que, cuando la oscilación de los neutrinos es demasiado rápida para ser resulta (régimen de oscilaciones promediadas), ambos límites llevan a las mismas modificaciones en las probabilidades de oscilación de los neutrinos (a primer orden en los pequeños ángulos de mezcla neutrino pesado-activo). Sin embargo, las cotas actuales que aplican a ambos límites son muy distintas. De hecho, como se ha visto en el Capítulo 2, la no unitariedad de la matriz PMNS está acotada al nivel del por mil, o incluso mejor para algunos elementos, mientras que las desviaciones en la matriz de mezcla producidas por los neutrinos estériles en el este régimen, están permitidas al nivel del por ciento y por lo tanto, podrían ser testados por los mismos experimentos de oscilaciones. Por ello, no se espera ningún impacto de la no unitariedad en los experimentos de neutrinos actuales ni en los de un futuro próximo, mientras que si los neutrinos estériles son suficientemente ligeros como para ser producidos en la fuente, su mezcla podría ser potencialmente descubierta por experimentos de oscilaciones de neutrinos. De hecho, nuestras simulaciones confirman que la no unitariedad se encuentra más allá del alcance de experimentos de alta precisión tales como DUNE, pero que las oscilaciones de neutrinos estériles podrían manifestarse de varias formas interesantes. También se ha dejado patente a través de estas simulaciones, la importancia de la correcta interpretación de los datos del detector cercano. En particular, se ha encontrado un aumento bastante significativo en la sensitividad a los parámetros de la Nueva Física que codifican la mezcla con el e o con el μ, en el caso en el que el detector cercano no se ve afectado de la misma forma que el detector lejano.

Para concluir, en esta tesis se ha abordado uno de los principales problemas sin resolver del SM: el desconocido origen de las masas de los neutrinos y sus mezclas con los leptones cargados. A pesar de que en el presente trabajo se han analizado los regímenes a muy baja escala y por encima de la escala EW, los neutrinos de Majorana podrían ser testados a cualquier escala. Por lo tanto, sería extremadamente relevante extender estos estudios para cubrir otros limites, como por ejemplo neutrinos en Cosmología, búsquedas en futuros colisionadores (FCC-ee, ILC), o producción y detección de neutrinos en experimentos de blanco fijo (NA62, DUNE, SHiP). Igualmente, se espera que en un futuro próximo (Mu3e, COMET, MU2e) mejoren las sensitividades de búsquedas con LFV tales como $\mu \to eee$ o conversión $\mu - e$ en núcleos, y por lo tanto, los estudios realizados en esta tesis deberían ser actualizados con dichos resultados relevantes. Finalmente, las búsquedas de desintegraciones $0\nu\beta\beta$ son la herramienta más prometedora para testar la naturaleza Majorana de los neutrinos. La búsqueda, del origen de la masa y de la mezcla de los neutrinos ha empezado, y con ella la esperanza de progresar en la comprensión de la teoría fundamental que subyace más allá del SM.

Appendix A: One-loop renormalization

In this Appendix we list the self-energies, counterterms and diagrams that enter in the renormalization of the observables studied in Section 3.2.

Lepton-flavour-dependent counterterms: $\delta_\alpha^{\mathbf{CT}\ W}$ and $\delta^{\mathbf{CT}\ Z}$

The unrenormalized charged lepton fields $l^0_{L\alpha}$ can be written in terms of the renormalized $\hat{l}_{L\alpha}$ ones as

$$l^0_{L\alpha} = \left(\delta_{\alpha\beta} + \frac{1}{2}\delta Z^{\rm l}_{\alpha\beta}\right)\hat{l}_{L\beta}. \tag{A.1}$$

The most general expression for the $l_\beta \to l_\alpha$ transition amplitude between fermionic Dirac states can be written as follows:

$$\Sigma^{\rm lep}_{\alpha\beta}\left(\not{p}\right) = \not{p}P_L\Sigma^L_{\alpha\beta}\left(p^2\right) + \not{p}P_R\Sigma^R_{\alpha\beta}\left(p^2\right) + P_L\Sigma^D_{\alpha\beta}\left(p^2\right) + P_R\Sigma^{D*}_{\alpha\beta}\left(p^2\right)\,, \tag{A.2}$$

where $\Sigma^L = \Sigma^{L\dagger}$ and $\Sigma^R = \Sigma^{R\dagger}$. In the physical observables only the Hermitian part of $\delta Z^{\rm l}$ appears and it is given by

$$\begin{aligned}\delta Z^{\rm lep}_{\alpha\beta} \equiv& \frac{1}{2}\left(\delta Z^{\rm l}_{\alpha\beta} + \delta Z^{\rm l*}_{\beta\alpha}\right)\\ =& -\Sigma^L_{\alpha\beta}\left(m^2_\beta\right) - m_\beta\left[m_\beta\left(\Sigma^{L\prime}_{\alpha\beta}\left(m^2_\beta\right) + \Sigma^{R\prime}_{\alpha\beta}\left(m^2_\beta\right)\right) + \left(\Sigma^{D\prime}_{\alpha\beta}\left(m^2_\beta\right) + \Sigma^{D*\prime}_{\alpha\beta}\left(m^2_\beta\right)\right)\right],\end{aligned} \tag{A.3}$$

with $\Sigma'\left(p^2\right) \equiv {\rm d}\Sigma\left(p^2\right)/{\rm d}p^2$. Therefore, the heavy neutrino contribution to $\delta Z^{\rm lep}$ can be obtained simply computing

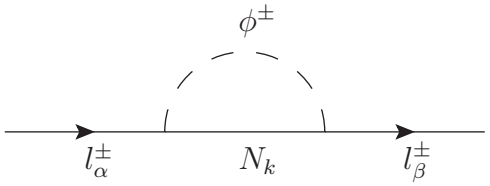

$$= i\Sigma^{\text{lep}}_{\alpha\beta}(\not{p}) \Rightarrow$$

$$\begin{aligned}\Sigma^{\text{lep}}_{\alpha\beta}(\not{p}) = &-\frac{\alpha}{8\pi s^2_{\text{W}} M^2_W}\sum_{k=4}^{6}\Bigg\{M^2_k U_{\beta k}U^*_{\alpha k}\Big[\left(P_L m_\beta + P_R m_\alpha\right)B_0(p^2, M^2_k, M^2_W)\\ &+\not{p}\left(P_R\frac{m_\alpha m_\beta}{M^2_k}+P_L\right)B_1(p^2, M^2_k, M^2_W)\Big]\Bigg\},\end{aligned} \tag{A.4}$$

where B_i (and later B_{ij}, C_{ij}, D_i and D_{ij}) are the Passarino-Veltman integrals [252] using the notation from Ref. [253].

Similarly, the unrenormalized neutrino fields ν^0_{Lj} can also be written in terms of the renormalized ones $\hat{\nu}_{Lj}$ as

$$\nu^0_{Li} = \left(\delta_{ij} + \frac{1}{2}\delta Z^\nu_{ij}\right)\hat{\nu}_{Lj}. \tag{A.5}$$

The transition amplitude between two Majorana states reads

$$\Sigma^{\text{neu}}_{ij}\left(\not{p}\right) = \not{p}P_L\Sigma^L_{ij}\left(p^2\right) + \not{p}P_R\Sigma^{L*}_{ij}\left(p^2\right) + P_L\Sigma^M_{ij}\left(p^2\right) + P_R\Sigma^{M*}_{ij}\left(p^2\right), \tag{A.6}$$

where $\Sigma^L = \Sigma^{R*}$ and $\Sigma^M = \Sigma^{Mt}$. In the Majorana case, the Hermitian part of δZ^ν can be written as

$$\begin{aligned}\delta Z^{\text{neu}}_{ij} \equiv &\frac{1}{2}\left(\delta Z^\nu_{ij} + \delta Z^{\nu*}_{ji}\right)\\ = &-\Sigma^L_{ij}\left(m^2_j\right) - m_j\Big[m_j\Big(\Sigma^{L\prime}_{ij}\left(m^2_j\right) + \Sigma^{L*\prime}_{ij}\left(m^2_j\right)\Big) + \Big(\Sigma^{M\prime}_{ij}\left(m^2_j\right) + \Sigma^{M*\prime}_{ij}\left(m^2_j\right)\Big)\Big].\end{aligned} \tag{A.7}$$

Analogously to the charged lepton case, δZ^{neu} can thus be obtained from the heavy neutrino contribution to the neutrino self energy:

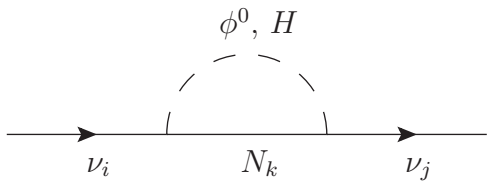

$$= i\Sigma^{\text{neu}}_{ij}(\not{p}) \Rightarrow$$

$$
\begin{aligned}
\Sigma_{ij}^{\rm neu}(\not{p}) = &-\frac{\alpha}{16\pi s_{\rm W}^2 M_W^2}\sum_{k=4}^{6}\Big\{\not{p}P_L\left(M_jC_{jk}^*+M_kC_{jk}\right)\left(M_iC_{ki}^*+M_kC_{ki}\right)\\
&\times\Big[B_1(p^2,M_k^2,M_Z^2)+B_1(p^2,M_k^2,M_h^2)\Big]\\
&+\not{p}P_R\left(M_jC_{jk}+M_kC_{jk}^*\right)\left(M_iC_{ki}+M_kC_{ki}^*\right)\\
&\times\Big[B_1(p^2,M_k^2,M_Z^2)+B_1(p^2,M_k^2,M_h^2)\Big]\\
&+P_LM_k\left(M_jC_{jk}+M_kC_{jk}^*\right)\left(M_kC_{ki}+M_iC_{ki}^*\right)\\
&\times\Big[B_0(p^2,M_k^2,M_Z^2)-B_0(p^2,M_k^2,M_h^2)\Big]\\
&+P_RM_k\left(M_jC_{jk}^*+M_kC_{jk}\right)\left(M_kC_{ki}^*+M_iC_{ki}\right)\\
&\times\Big[B_0(p^2,M_k^2,M_Z^2)-B_0(p^2,M_k^2,M_h^2)\Big]\Big\}.
\end{aligned}
\tag{A.8}
$$

Finally, the lepton-flavour-dependent combinations that will correct and cancel the divergences of 1-loop corrections to the vertex $W\nu l_\alpha$ and $Z\nu\nu$ are respectively:

$$
\delta_\alpha^{{\rm CT}\ W} = \sum_{i=1}^{3}\frac{U_{\alpha i}}{2}\left(\sum_{\beta=1}^{3}\delta Z_{\beta\alpha}^{\rm lep}U_{\beta i}^*+\sum_{j=1}^{6}U_{\alpha j}^*\delta Z_{ij}^{\rm neu}\right) \tag{A.9}
$$

$$
\delta^{{\rm CT}\ Z} = \sum_{k=1}^{6}\left(\delta Z_{ik}^{\rm neu}C_{kj}+\delta Z_{kj}^{\rm neu}C_{ik}\right) \tag{A.10}
$$

Vertex interferences: $\mathcal{V}_\alpha^W$ and $\mathcal{V}_{ij}^Z$

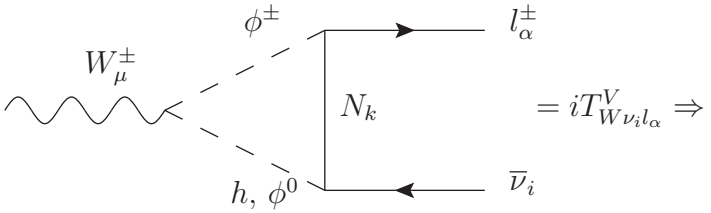

$$
\begin{aligned}
\mathcal{V}_\alpha^W \equiv&\frac{\sum_{i=1}^{3}T_0^*T_{W\nu_i l_\alpha}^V}{\sum_{i=1}^{3}|T_0|^2}\\
=&\frac{\alpha}{8\pi s_{\rm W}^2M_W^2}\sum_{i=1}^{3}\sum_{k=4}^{6}M_k^2U_{\alpha i}U_{\alpha k}^*C_{ki}^*\left[C_{00}(0,0,M_h^2,M_k^2,M_W^2)+C_{00}(0,0,M_Z^2,M_k^2,M_W^2)\right],
\end{aligned}
\tag{A.11}
$$

up to higher order corrections and where T_0 is the corresponding tree level amplitude.

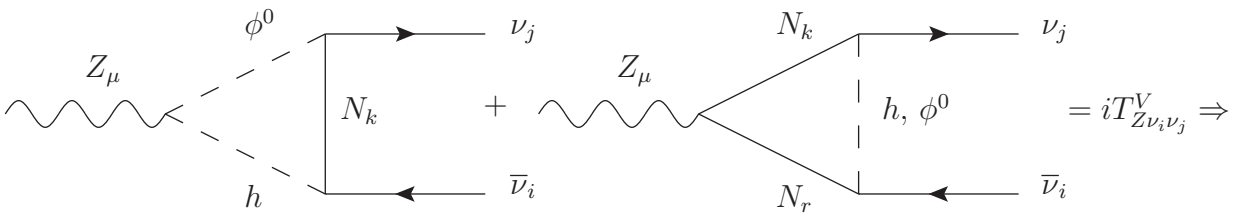

$$
\begin{aligned}
\mathcal{V}^Z_{ij} \equiv & \frac{T_0^* T^V_{Z\nu_i\nu_j}}{|T_0|^2} \\
= & \frac{\alpha}{16\pi s_{\mathrm{W}}^2 M_W^2}\Bigg[\sum_{k,r=4}^{6}\Bigg\{ -2C_{kj}C_{ir}M_kM_r\Big(C_{rk}M_kM_r\Big[C_0(0,M_Z^2,M_h^2,M_k^2,M_r^2) \\
& + C_0(0,M_Z^2,M_Z^2,M_k^2,M_r^2)\Big] + C_{kr}\Big[M_Z^2\big(C_{22}(0,M_Z^2,M_h^2,M_k^2,M_r^2) \\
& + C_{22}(0,M_Z^2,M_Z^2,M_k^2,M_r^2) - C_{21}(0,M_Z^2,M_h^2,M_k^2,M_r^2) - C_{21}(0,M_Z^2,M_Z^2,M_k^2,M_r^2)\big) \\
& + 2\big(C_{00}(0,M_Z^2,M_Z^2,M_k^2,M_r^2) + C_{00}(0,M_Z^2,M_h^2,M_k^2,M_r^2)\big)\Big]\Big)\Bigg\} \\
& + \sum_{k=4}^{6}\Big[4C_{kj}C_{ik}M_k^2\big(C_{00}(0,M_Z^2,M_k^2,M_h^2,M_Z^2) + C_{00}(0,M_Z^2,M_k^2,M_Z^2,M_h^2)\big)\Big]\Bigg],
\end{aligned}
\tag{A.12}
$$

up to higher order corrections and where T_0 is the corresponding tree level amplitude.

Box contribution to μ decay: $\mathcal{B}_{\alpha\beta}$

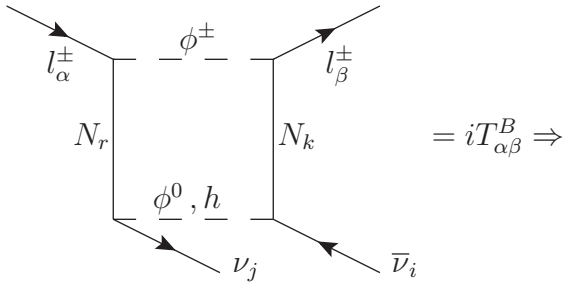

$$
\begin{aligned}
\mathcal{B}_{\alpha\beta} \equiv & \frac{\sum_{i,j=1}^{3} T_0^* T_{\alpha\beta}^B}{\sum_{i,j=1}^{3} |T_0|^2} \\
= & \frac{1}{5} \frac{g^2}{(16\pi)^2 M_W^2} \sum_{i,j=1}^{3} \sum_{k,r=4}^{6} C_{ik} C_{jr} U_{\beta k} U_{\beta i}^* U_{\alpha r}^* U_{\alpha j} M_r^2 M_k^2 \Big\{ 20 \Big[D_{00}(M_h^2) + D_{00}(M_Z^2) \Big] \\
& + m_\alpha^2 \Big[3\big(D_{12}(M_h^2) + D_{12}(M_Z^2) \big) + 2\big(D_{13}(M_h^2) + D_{13}(M_Z^2) \big) \\
& + 3\big(D_2(M_h^2) + D_2(M_Z^2) \big) + 2\big(D_3(M_h^2) + D_3(M_Z^2) \big) \Big] \Big\} ,
\end{aligned}
\tag{A.13}
$$

up to higher order corrections and where T_0 is the corresponding tree level amplitude and using the simplified notation $D_{ij}(M^2) \to D_{ij}(0,0,0,M_r^2,M^2,M_k^2,M_W^2)$. Apart from the explicit sum over final state neutrinos in Eq. (A.13), the integral over the phase space is to be understood in both the numerator and denominator.

Flavour-universal corrections to the gauge boson propagators: $\delta_W^{\text{univ N}}$ and $\delta_Z^{\text{univ N}}$

We label Σ_{WW} and Σ_{ZZ} the terms proportional to $g^{\mu\nu}$ in the W and Z self-energies respectively. Notice that the SM contribution has been subtracted from the total self-energy, as we are interested in the contribution stemming from the new extra neutrinos.

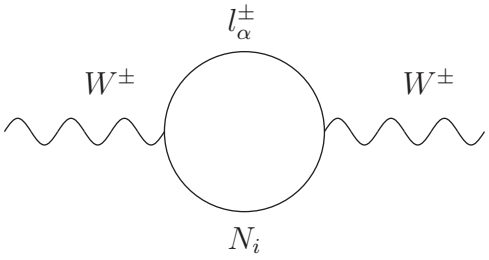

$= i\Sigma_{WW}^{\text{tot}}(p^2) \Rightarrow$

$$
\begin{aligned}
\Sigma_{WW}^{N}(p^2) \equiv & \Sigma_{WW}^{\text{tot}}(p^2) - \Sigma_{WW}^{\text{SM}}(p^2) \\
= & -\frac{\alpha}{4\pi s_{\text{W}}^2} \sum_{\alpha=e,\mu,\tau} \Bigg\{ \sum_{i=1}^{6} |U_{\alpha i}|^2 \Big[2B_{00}(p^2, M_i^2, m_\alpha^2) + p^2 \Big(B_1(p^2, M_i^2, m_\alpha^2) \\
& + B_{11}(p^2, M_i^2, m_\alpha^2) \Big) \Big] - 2B_{00}(p^2, 0, m_\alpha^2) - p^2 \Big(B_1(p^2, 0, m_\alpha^2) + B_{11}(p^2, 0, m_\alpha^2) \Big) \Bigg\}
\end{aligned}
\tag{A.14}
$$

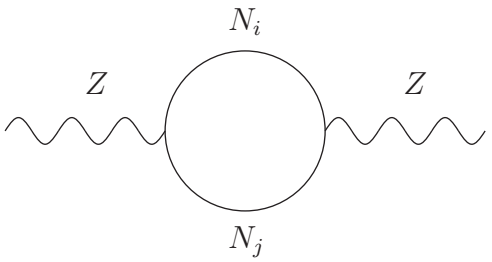

$$= i\Sigma^{\rm tot}_{ZZ}(p^2) \Rightarrow$$

$$\begin{aligned}
\Sigma^{N}_{ZZ}(p^2) \equiv & \Sigma^{\rm tot}_{ZZ}(p^2) - \Sigma^{\rm SM}_{ZZ}(p^2) \\
= & -\frac{\alpha}{8\pi s^2_{\rm W} c^2_{\rm W}} \Bigg\{ \sum_{\alpha,\beta} \sum_{i,j=1}^{6} \Big[U_{\alpha i} U^*_{\alpha j} U_{\beta j} U^*_{\beta i} M_i M_j B_0(p^2, M_i^2, M_j^2) + U_{\alpha j} U^*_{\alpha i} U_{\beta i} U^*_{\beta j} \\
& \times \Big(2B_{00}(p^2, M_i^2, M_j^2) + p^2 \big(B_1(p^2, M_i^2, M_j^2) + B_{11}(p^2, M_i^2, M_j^2) \big) \Big) \Big] \\
& - 3 \Big[2B_{00}(p^2, 0, 0) + p^2 \big(B_1(p^2, 0, 0) + B_{11}(p^2, 0, 0) \big) \Big] \Bigg\}
\end{aligned} \tag{A.15}$$

Notice that both in Eq. (A.14) and in Eq. (A.15) the sums run over all neutrino mass eigenstates (heavy and light) so here M_i can represent both the heavy or the light neutrino masses.

The oblique universal corrections to the electroweak observables can be written as a combination of the three following independent parameters [254, 255]:

$$\alpha S = \frac{4 s^2_{\rm W} c^2_{\rm W}}{M_Z^2} \Big[\hat{\Sigma}^N_{ZZ}(0) + \hat{\Sigma}^N_{\gamma\gamma}(M_Z^2) - \frac{c^2_{\rm W} - s^2_{\rm W}}{c_{\rm W} s_{\rm W}} \hat{\Sigma}^N_{Z\gamma}(M_Z^2) \Big] , \tag{A.16}$$

$$\alpha T = \frac{\hat{\Sigma}^N_{ZZ}(0)}{M_Z^2} - \frac{\hat{\Sigma}^N_{WW}(0)}{M_W^2} , \tag{A.17}$$

$$\alpha U = 4 s^2_{\rm W} c^2_{\rm W} \Big[\frac{1}{c^2_{\rm W}} \frac{\hat{\Sigma}^N_{WW}(0)}{M_W^2} - \frac{\hat{\Sigma}^N_{ZZ}(0)}{M_Z^2} + \frac{s^2_{\rm W}}{c^2_{\rm W}} \frac{\hat{\Sigma}^N_{\gamma\gamma}(M_Z^2)}{M_Z^2} - \frac{2 s_{\rm W}}{c_{\rm W}} \frac{\hat{\Sigma}^N_{Z\gamma}(M_Z^2)}{M_Z^2} \Big] \tag{A.18}$$

and the renormalized self energies are given by:

$$
\begin{aligned}
\hat{\Sigma}^N_{WW}\left(p^2\right) &= \Sigma^N_{WW}\left(p^2\right) - \Sigma^N_{WW}\left(M_W^2\right) + \left(p^2 - M_W^2\right)\left[\frac{c_{\rm W}^2}{s_{\rm W}^2}\mathcal{R} - \Sigma^{N\prime}_{\gamma\gamma}(0)\right], \\
\hat{\Sigma}^N_{ZZ}\left(p^2\right) &= \Sigma^N_{ZZ}\left(p^2\right) - \Sigma^N_{ZZ}\left(M_Z^2\right) + \left(p^2 - M_Z^2\right)\left[\left(\frac{c_{\rm W}^2}{s_{\rm W}^2} - 1\right)\mathcal{R} - \Sigma^{N\prime}_{\gamma\gamma}(0)\right], \\
\hat{\Sigma}^N_{Z\gamma}\left(p^2\right) &= \Sigma^N_{Z\gamma}\left(p^2\right) - \Sigma^N_{Z\gamma}\left(0\right) - p^2\frac{c_{\rm W}}{s_{\rm W}}\mathcal{R}, \\
\hat{\Sigma}^N_{\gamma\gamma}\left(p^2\right) &= \Sigma^N_{\gamma\gamma}\left(p^2\right) - p^2\Sigma^{N\prime}_{\gamma\gamma}\left(0\right), \qquad \text{(A.19)}
\end{aligned}
$$

with

$$
\mathcal{R} = \frac{\Sigma^N_{ZZ}\left(M_Z^2\right)}{M_Z^2} - \frac{\Sigma^N_{WW}\left(M_W^2\right)}{M_W^2} - \frac{2s_{\rm W}}{c_{\rm W}}\frac{\Sigma^N_{Z\gamma}\left(0\right)}{M_Z^2} \qquad \text{(A.20)}
$$

Notice that, in the on-shell renormalization scheme $\hat{\Sigma}^N_{WW}\left(M_W^2\right) = \hat{\Sigma}^N_{ZZ}\left(M_Z^2\right) = \hat{\Sigma}^N_{Z\gamma}\left(0\right) = \hat{\Sigma}^N_{\gamma\gamma}\left(0\right) = 0$. Moreover, there is no contribution to the propagator of the photon from the extra heavy neutrinos and therefore $\Sigma^N_{\gamma\gamma}$ and $\hat{\Sigma}^N_{\gamma\gamma}$ can be set to zero in the previous equations. In addition, there is no correction to $\Sigma_{Z\gamma}$ either, so that $\Sigma^N_{Z\gamma}$ can be set to zero too. The universal oblique counterterms presented in Sec. 3.2 can thus be written as:

$$
\begin{aligned}
\delta_W^{\text{univ N}} &= \frac{\Sigma^N_{WW}\left(0\right) - \Sigma^N_{WW}\left(M_W^2\right)}{M_W^2} - \frac{c_{\rm W}^2}{s_{\rm W}^2}\mathcal{R} = \frac{\hat{\Sigma}^N_{WW}\left(0\right)}{M_W^2} \\
&= \frac{1}{2s_{\rm W}^2}\alpha S - \frac{c_{\rm W}^2}{s_{\rm W}^2}\alpha T - \frac{\cos 2\theta_W}{4s_{\rm W}^4}\alpha U \\
\delta_Z^{\text{univ N}} &= \frac{\Sigma^N_{ZZ}\left(0\right) - \Sigma^N_{ZZ}\left(M_Z^2\right)}{M_Z^2} + \frac{1}{2}\left(1 - \frac{c_{\rm W}^2}{s_{\rm W}^2}\right)\mathcal{R} = \frac{\hat{\Sigma}^N_{ZZ}\left(0\right)}{M_Z^2} \\
&= \frac{1}{2s_{\rm W}^2}\alpha S + \left(1 - \frac{c_{\rm W}^2}{s_{\rm W}^2}\right)\alpha T - \frac{\cos 2\theta_W}{4s_{\rm W}^4}\alpha U. \qquad \text{(A.21)}
\end{aligned}
$$

Appendix B: Current constraints on sterile neutrinos

In this Appendix we summarize and explain in more detail the current constraints on sterile neutrinos that arise from oscillation searches in the averaged out regime and thus apply for arbitrarily large values of Δm^2 as well as those stemming from electroweak and flavour precision observables. Notice that, for the latter, some of the observables only apply above the electroweak scale [79]. Nevertheless, below this scale, stronger constraints from direct searches are available [170–172]. Regarding the oscillation searches, the validity of these constraints will depend on the particular configuration of the experiment used to derive it, which determines when the averaged-out regime is reached. These constraints together with their range of validity are listed in Table B.1.

The strongest constraints on the mixing with electrons (α_{ee}) stem from the BUGEY-3 experiment [227]. At this experiment, oscillations enter the averaged-out regime for $\Delta m^2 \gtrsim 4$ eV^2. Recent competitive constraints on this parameter by the Daya Bay experiment [258] tend to dominate for smaller Δm^2 values and are comparable to the bounds from BUGEY-3 [227] around $\Delta m^2 \gtrsim 0.1$ eV^2. In the range $\Delta m^2 \gtrsim 0.1 - 1$ eV^2 the bound oscillates significantly between $3.0 \cdot 10^{-3}$ and $1.0 \cdot 10^{-2}$: therefore, we quote the latter more conservative bound in the right column of Table B.1.

Current limits on the $\alpha_{\mu\mu}$ and $\alpha_{\tau\tau}$ elements are dominated by the bounds derived from the SK analysis of atmospheric neutrino oscillations [228]. These are derived in the averaged-out regime, which in this case corresponds to $\Delta m^2 \gtrsim 0.1$ eV^2. For $\alpha_{\mu\mu}$, MINOS [229] sets stronger constraints for lower values of Δm^2. Again, these oscillate between $4.4 \cdot 10^{-3}$ and $1.4 \cdot 10^{-2}$ in the range $\Delta m^2 \gtrsim 0.1 - 1$ eV^2. Thus, we quote the more conservative bound in the rightmost column of Table B.1. Regarding

	Applicability range	Bound
α_{ee}	$\Delta m^2 \gtrsim 4$ eV^2	$2.4 \cdot 10^{-2}$ [227]
	$m >$ EW	$1.3 \cdot 10^{-3}$ [79]
$\alpha_{\mu\mu}$	$\Delta m^2 \gtrsim 0.1$ eV^2	$2.2 \cdot 10^{-2}$ [228]
	$m >$ EW	$2.2 \cdot 10^{-4}$ [79]
$\alpha_{\tau\tau}$	$\Delta m^2 \gtrsim 0.1$ eV^2	$1.0 \cdot 10^{-1}$ [228]
	$m >$ EW	$1.3 \cdot 10^{-3}$ [79]
$\lvert\alpha_{\mu e}\rvert$	$\Delta m^2 \gtrsim 4$ eV^2	$3.2 \cdot 10^{-2}$
	$\Delta m^2 \gtrsim 10$ eV^2	$2.8 \cdot 10^{-2}$ [256]
	$\Delta m^2 \gtrsim 100$ eV^2	$2.5 \cdot 10^{-2}$ [230]
	$\Delta m^2 \gtrsim 1000$ eV^2	$2.3 \cdot 10^{-2}$ [257]
	$m >$ EW	$6.8 \cdot 10^{-4}$ [79]
$\lvert\alpha_{\tau e}\rvert$	$\Delta m^2 \gtrsim 4$ eV^2	$6.9 \cdot 10^{-2}$
	$m >$ EW	$2.7 \cdot 10^{-3}$ [79]
$\lvert\alpha_{\tau\mu}\rvert$	$\Delta m^2 \gtrsim 0.1$ eV^2	$6.6 \cdot 10^{-2}$
	$\Delta m^2 \gtrsim 100$ eV^2	$1.2 \cdot 10^{-2}$ [231]
	$m >$ EW	$1.2 \cdot 10^{-3}$ [79]

Table B.1: Summary of the current experimental constraints in the averaged-out regime, applicable to sterile neutrinos above a certain mass range. The bounds on the off-diagonal elements which do not have a reference have been obtained indirectly from the bounds on the diagonal elements at that scale, using $\alpha_{\alpha\beta} \leq 2\sqrt{\alpha_{\alpha\alpha}\alpha_{\beta\beta}}$ (see Eq. (4.18)).

$\alpha_{\tau\tau}$, MINOS [259] has similar constraints to the ones from SK atmospherics. Stronger limits are obtained in the global fit in Ref. [260] but only for $\Delta m^2 = 6$ eV^2 and not

in the averaged-out limit.

For the off-diagonal elements, the strongest limit for $\alpha_{\mu e}$ stems from the null results of appearance searches by NuTeV [257] $|\alpha_{e\mu}| < 2.3 \cdot 10^{-2}$, valid once they enter the averaged-out regime for $\Delta m^2 \gtrsim 1000$ eV^2. Nevertheless, similar bounds from NOMAD [230] $|\alpha_{e\mu}| < 2.5 \cdot 10^{-2}$ and KARMEN [256] $|\alpha_{e\mu}| < 2.8 \cdot 10^{-2}$ apply for $\Delta m^2 \gtrsim 100$ eV^2 and $\Delta m^2 \gtrsim 10$ eV^2 respectively. NOMAD [231] also gives the most stringent constraints for $\alpha_{\tau\mu}$, valid for $\Delta m^2 \gtrsim 100$ eV^2. For $\alpha_{\tau e}$, the strongest bounds are derived from those on the diagonal elements through $\alpha_{\alpha\beta} \leq 2\sqrt{\alpha_{\alpha\alpha}\alpha_{\beta\beta}}$ (see Eq. (4.18)). Finally, for very light sterile neutrinos, $\Delta m^2 \sim 0.1$ eV^2, all the direct constraints on the off-diagonal elements from NuTeV, NOMAD and KARMEN fade away. In this case, the strongest bounds are obtained indirectly from the diagonal elements via $\alpha_{\alpha\beta} \leq 2\sqrt{\alpha_{\alpha\alpha}\alpha_{\beta\beta}}$.

Bibliography

[1] S. L. Glashow, "Partial Symmetries of Weak Interactions," *Nucl. Phys.* **22** (1961) 579–588.

[2] M. Gell-Mann, "A Schematic Model of Baryons and Mesons," *Phys. Lett.* **8** (1964) 214–215.

[3] G. Zweig, "An SU(3) model for strong interaction symmetry and its breaking. Version 2," in *Developments in the quark theory of hadrons. vol. 1. 1964 - 1978*, D. Lichtenberg and S. P. Rosen, eds., pp. 22–101. 1964. http://inspirehep.net/record/4674/files/cern-th-412.pdf.

[4] S. Weinberg, "A Model of Leptons," *Phys. Rev. Lett.* **19** (1967) 1264–1266.

[5] A. Salam, "Weak and Electromagnetic Interactions," *Conf. Proc.* **C680519** (1968) 367–377.

[6] F. Englert and R. Brout, "Broken Symmetry and the Mass of Gauge Vector Mesons," *Phys. Rev. Lett.* **13** (1964) 321–323.

[7] P. W. Higgs, "Broken Symmetries and the Masses of Gauge Bosons," *Phys. Rev. Lett.* **13** (1964) 508–509.

[8] G. S. Guralnik, C. R. Hagen, and T. W. B. Kibble, "Global Conservation Laws and Massless Particles," *Phys. Rev. Lett.* **13** (1964) 585–587.

[9] **ATLAS** Collaboration, G. Aad *et al.*, "Observation of a new particle in the search for the Standard Model Higgs boson with the ATLAS detector at the LHC," *Phys. Lett.* **B716** (2012) 1–29, arXiv:1207.7214 [hep-ex].

[10] **CMS** Collaboration, S. Chatrchyan *et al.*, "Observation of a new boson at a mass of 125 GeV with the CMS experiment at the LHC," *Phys. Lett.* **B716** (2012) 30–61, arXiv:1207.7235 [hep-ex].

[11] **WMAP** Collaboration, C. L. Bennett *et al.*, "Nine-Year Wilkinson Microwave Anisotropy Probe (WMAP) Observations: Final Maps and

Results," *Astrophys. J. Suppl.* **208** (2013) 20, arXiv:1212.5225 [astro-ph.CO].

[12] **Planck** Collaboration, P. A. R. Ade *et al.*, "Planck 2015 results. XIII. Cosmological parameters," *Astron. Astrophys.* **594** (2016) A13, arXiv:1502.01589 [astro-ph.CO].

[13] M. Fukugita and T. Yanagida, "Baryogenesis Without Grand Unification," *Phys. Lett.* **B174** (1986) 45.

[14] A. D. Sakharov, "Violation of CP Invariance, c Asymmetry, and Baryon Asymmetry of the Universe," *Pisma Zh. Eksp. Teor. Fiz.* **5** (1967) 32–35. [Usp. Fiz. Nauk161,61(1991)].

[15] M. B. Gavela, P. Hernandez, J. Orloff, O. Pene, and C. Quimbay, "Standard model CP violation and baryon asymmetry. Part 2: Finite temperature," *Nucl. Phys.* **B430** (1994) 382–426, arXiv:hep-ph/9406289 [hep-ph].

[16] V. A. Kuzmin, V. A. Rubakov, and M. E. Shaposhnikov, "On the Anomalous Electroweak Baryon Number Nonconservation in the Early Universe," *Phys. Lett.* **155B** (1985) 36.

[17] R. Davis, Jr., D. S. Harmer, and K. C. Hoffman, "Search for neutrinos from the sun," *Phys. Rev. Lett.* **20** (1968) 1205–1209.

[18] B. T. Cleveland, T. Daily, R. Davis, Jr., J. R. Distel, K. Lande, C. K. Lee, P. S. Wildenhain, and J. Ullman, "Measurement of the solar electron neutrino flux with the Homestake chlorine detector," *Astrophys. J.* **496** (1998) 505–526.

[19] A. I. Abazov *et al.*, "Search for neutrinos from sun using the reaction Ga-71 (electron-neutrino e-) Ge-71," *Phys. Rev. Lett.* **67** (1991) 3332–3335.

[20] K. Lande *et al.*, "The Homestake solar neutrino program," *Nucl. Phys. Proc. Suppl.* **77** (1999) 13–19.

[21] **Super-Kamiokande** Collaboration, S. Fukuda *et al.*, "Determination of solar neutrino oscillation parameters using 1496 days of Super-Kamiokande I data," *Phys. Lett.* **B539** (2002) 179–187, arXiv:hep-ex/0205075 [hep-ex].

[22] **GNO** Collaboration, T. A. Kirsten, "Progress in GNO," *Nucl. Phys. Proc. Suppl.* **118** (2003) 33–38. [,33(2003)].

[23] **SNO** Collaboration, Q. R. Ahmad *et al.*, "Measurement of the rate of $\nu_e + d \to p + p + e^-$ interactions produced by ^8B solar neutrinos at the Sudbury Neutrino Observatory," *Phys. Rev. Lett.* **87** (2001) 071301,

arXiv:nucl-ex/0106015 [nucl-ex].

[24] **SNO** Collaboration, Q. R. Ahmad *et al.*, "Direct evidence for neutrino flavor transformation from neutral current interactions in the Sudbury Neutrino Observatory," *Phys. Rev. Lett.* **89** (2002) 011301, arXiv:nucl-ex/0204008 [nucl-ex].

[25] **SNO** Collaboration, Q. R. Ahmad *et al.*, "Measurement of day and night neutrino energy spectra at SNO and constraints on neutrino mixing parameters," *Phys. Rev. Lett.* **89** (2002) 011302, arXiv:nucl-ex/0204009 [nucl-ex].

[26] **SNO** Collaboration, S. N. Ahmed *et al.*, "Measurement of the total active B-8 solar neutrino flux at the Sudbury Neutrino Observatory with enhanced neutral current sensitivity," *Phys. Rev. Lett.* **92** (2004) 181301, arXiv:nucl-ex/0309004 [nucl-ex].

[27] **Super-Kamiokande** Collaboration, J. Hosaka *et al.*, "Solar neutrino measurements in super-Kamiokande-I," *Phys. Rev.* **D73** (2006) 112001, arXiv:hep-ex/0508053 [hep-ex].

[28] **Super-Kamiokande** Collaboration, J. P. Cravens *et al.*, "Solar neutrino measurements in Super-Kamiokande-II," *Phys. Rev.* **D78** (2008) 032002, arXiv:0803.4312 [hep-ex].

[29] **Borexino** Collaboration, G. Bellini *et al.*, "Measurement of the solar 8B neutrino rate with a liquid scintillator target and 3 MeV energy threshold in the Borexino detector," *Phys. Rev.* **D82** (2010) 033006, arXiv:0808.2868 [astro-ph].

[30] **Super-Kamiokande** Collaboration, K. Abe *et al.*, "Solar neutrino results in Super-Kamiokande-III," *Phys. Rev.* **D83** (2011) 052010, arXiv:1010.0118 [hep-ex].

[31] F. Kaether, W. Hampel, G. Heusser, J. Kiko, and T. Kirsten, "Reanalysis of the GALLEX solar neutrino flux and source experiments," *Phys. Lett.* **B685** (2010) 47–54, arXiv:1001.2731 [hep-ex].

[32] **SNO** Collaboration, B. Aharmim *et al.*, "Combined Analysis of all Three Phases of Solar Neutrino Data from the Sudbury Neutrino Observatory," *Phys. Rev.* **C88** (2013) 025501, arXiv:1109.0763 [nucl-ex].

[33] G. Bellini *et al.*, "Precision measurement of the 7Be solar neutrino interaction rate in Borexino," *Phys. Rev. Lett.* **107** (2011) 141302, arXiv:1104.1816

[hep-ex].

[34] **BOREXINO** Collaboration, G. Bellini *et al.*, "Neutrinos from the primary proton–proton fusion process in the Sun," *Nature* **512** no. 7515, (2014) 383–386.

[35] **NUSEX** Collaboration, M. Aglietta *et al.*, "Experimental study of atmospheric neutrino flux in the NUSEX experiment," *Europhys. Lett.* **8** (1989) 611–614.

[36] **Kamiokande** Collaboration, Y. Fukuda *et al.*, "Atmospheric muon-neutrino / electron-neutrino ratio in the multiGeV energy range," *Phys. Lett.* **B335** (1994) 237–245.

[37] **Frejus** Collaboration, K. Daum *et al.*, "Determination of the atmospheric neutrino spectra with the Frejus detector," *Z. Phys.* **C66** (1995) 417–428.

[38] R. Becker-Szendy *et al.*, "Neutrino measurements with the IMB detector," *Nucl. Phys. Proc. Suppl.* **38** (1995) 331–336.

[39] **Super-Kamiokande** Collaboration, Y. Fukuda *et al.*, "Evidence for oscillation of atmospheric neutrinos," *Phys. Rev. Lett.* **81** (1998) 1562–1567, arXiv:hep-ex/9807003 [hep-ex].

[40] **Kamiokande** Collaboration, S. Hatakeyama *et al.*, "Measurement of the flux and zenith angle distribution of upward through going muons in Kamiokande II + III," *Phys. Rev. Lett.* **81** (1998) 2016–2019, arXiv:hep-ex/9806038 [hep-ex].

[41] **Super-Kamiokande** Collaboration, S. Fukuda *et al.*, "Tau neutrinos favored over sterile neutrinos in atmospheric muon-neutrino oscillations," *Phys. Rev. Lett.* **85** (2000) 3999–4003, arXiv:hep-ex/0009001 [hep-ex].

[42] **Soudan-2** Collaboration, W. A. Mann, "New results on atmospheric neutrinos from Soudan 2," *Nucl. Phys. Proc. Suppl.* **91** (2001) 134–140, arXiv:hep-ex/0007031 [hep-ex]. [,134(2000)].

[43] **MACRO** Collaboration, M. Ambrosio *et al.*, "Matter effects in upward going muons and sterile neutrino oscillations," *Phys. Lett.* **B517** (2001) 59–66, arXiv:hep-ex/0106049 [hep-ex].

[44] **Super-Kamiokande** Collaboration, Y. Ashie *et al.*, "Evidence for an oscillatory signature in atmospheric neutrino oscillation," *Phys. Rev. Lett.* **93** (2004) 101801, arXiv:hep-ex/0404034 [hep-ex].

[45] **IceCube** Collaboration, M. G. Aartsen *et al.*, "Determining neutrino

oscillation parameters from atmospheric muon neutrino disappearance with three years of IceCube DeepCore data," *Phys. Rev.* **D91** no. 7, (2015) 072004, arXiv:1410.7227 [hep-ex].

[46] **KamLAND** Collaboration, T. Araki *et al.*, "Measurement of neutrino oscillation with KamLAND: Evidence of spectral distortion," *Phys. Rev. Lett.* **94** (2005) 081801, arXiv:hep-ex/0406035 [hep-ex].

[47] **KamLAND** Collaboration, A. Gando *et al.*, "Constraints on θ_{13} from A Three-Flavor Oscillation Analysis of Reactor Antineutrinos at KamLAND," *Phys. Rev.* **D83** (2011) 052002, arXiv:1009.4771 [hep-ex].

[48] **RENO** Collaboration, H. Seo, "New Results from RENO," *PoS* **NUFACT2014** (2015) 040.

[49] **Double Chooz** Collaboration, M. Ishitsuka, "First results with two detectors from Double Chooz," in *Proceedings, 51st Rencontres de Moriond on Electroweak Interactions and Unified Theories: La Thuile, Italy, March 12-19, 2016*, pp. 157–164, ARISF. ARISF, 2016. http://inspirehep.net/record/1591235/files/1589812_157-164.pdf.

[50] **Daya Bay** Collaboration, F. P. An *et al.*, "Measurement of electron antineutrino oscillation based on 1230 days of operation of the Daya Bay experiment," *Phys. Rev.* **D95** no. 7, (2017) 072006, arXiv:1610.04802 [hep-ex].

[51] **K2K** Collaboration, M. H. Ahn *et al.*, "Indications of neutrino oscillation in a 250 km long baseline experiment," *Phys. Rev. Lett.* **90** (2003) 041801, arXiv:hep-ex/0212007 [hep-ex].

[52] **K2K** Collaboration, M. H. Ahn *et al.*, "Measurement of Neutrino Oscillation by the K2K Experiment," *Phys. Rev.* **D74** (2006) 072003, arXiv:hep-ex/0606032 [hep-ex].

[53] **MINOS** Collaboration, D. G. Michael *et al.*, "Observation of muon neutrino disappearance with the MINOS detectors and the NuMI neutrino beam," *Phys. Rev. Lett.* **97** (2006) 191801, arXiv:hep-ex/0607088 [hep-ex].

[54] **MINOS** Collaboration, P. Adamson *et al.*, "Measurement of Neutrino and Antineutrino Oscillations Using Beam and Atmospheric Data in MINOS," *Phys. Rev. Lett.* **110** no. 25, (2013) 251801, arXiv:1304.6335 [hep-ex].

[55] **MINOS** Collaboration, P. Adamson *et al.*, "Electron neutrino and antineutrino appearance in the full MINOS data sample," *Phys. Rev. Lett.*

110 no. 17, (2013) 171801, arXiv:1301.4581 [hep-ex].

[56] **NOvA** Collaboration, P. Adamson *et al.*, "First measurement of muon-neutrino disappearance in NOvA," *Phys. Rev.* **D93** no. 5, (2016) 051104, arXiv:1601.05037 [hep-ex].

[57] **NOvA** Collaboration, P. Adamson *et al.*, "First measurement of electron neutrino appearance in NOvA," *Phys. Rev. Lett.* **116** no. 15, (2016) 151806, arXiv:1601.05022 [hep-ex].

[58] **T2K** Collaboration, K. Iwamoto, "Recent Results from T2K and Future Prospects," *PoS* **ICHEP2016** (2016) 517.

[59] **T2K** Collaboration, K. Abe *et al.*, "Combined Analysis of Neutrino and Antineutrino Oscillations at T2K," *Phys. Rev. Lett.* **118** no. 15, (2017) 151801, arXiv:1701.00432 [hep-ex].

[60] J. A. Casas, J. R. Espinosa, and I. Hidalgo, "Implications for new physics from fine-tuning arguments. 1. Application to SUSY and seesaw cases," *JHEP* **11** (2004) 057, arXiv:hep-ph/0410298 [hep-ph].

[61] P. Minkowski, "$\mu \to e\gamma$ at a rate of one out of 10^9 muon decays?," *Phys. Lett.* **B67** (1977) 421.

[62] R. N. Mohapatra and G. Senjanovic, "Neutrino mass and spontaneous parity nonconservation," *Phys. Rev. Lett.* **44** (1980) 912.

[63] T. Yanagida, "Horizontal gauge symmetry and masses of neutrinos,". In Proceedings of the Workshop on the Baryon Number of the Universe and Unified Theories, Tsukuba, Japan.

[64] M. Gell-Mann, P. Ramond, and R. Slansky, "Complex Spinors and Unified Theories.". Print-80-0576 (CERN).

[65] M. Magg and C. Wetterich, "Neutrino Mass Problem and Gauge Hierarchy," *Phys. Lett.* **94B** (1980) 61–64.

[66] J. Schechter and J. W. F. Valle, "Neutrino Masses in SU(2) x U(1) Theories," *Phys. Rev.* **D22** (1980) 2227.

[67] C. Wetterich, "Neutrino Masses and the Scale of B-L Violation," *Nucl. Phys.* **B187** (1981) 343–375.

[68] G. Lazarides, Q. Shafi, and C. Wetterich, "Proton Lifetime and Fermion Masses in an SO(10) Model," *Nucl. Phys.* **B181** (1981) 287–300.

[69] R. N. Mohapatra and G. Senjanovic, "Neutrino Masses and Mixings in Gauge Models with Spontaneous Parity Violation," *Phys. Rev.* **D23** (1981) 165.

[70] R. Foot, H. Lew, X. G. He, and G. C. Joshi, "Seesaw Neutrino Masses Induced by a Triplet of Leptons," *Z. Phys.* **C44** (1989) 441.

[71] E. Ma, "Pathways to naturally small neutrino masses," *Phys. Rev. Lett.* **81** (1998) 1171–1174, arXiv:hep-ph/9805219 [hep-ph].

[72] E. Ma and D. P. Roy, "Heavy triplet leptons and new gauge boson," *Nucl. Phys.* **B644** (2002) 290–302, arXiv:hep-ph/0206150 [hep-ph].

[73] T. Hambye, Y. Lin, A. Notari, M. Papucci, and A. Strumia, "Constraints on neutrino masses from leptogenesis models," *Nucl. Phys.* **B695** (2004) 169–191, arXiv:hep-ph/0312203 [hep-ph].

[74] B. Bajc and G. Senjanovic, "Seesaw at LHC," *JHEP* **08** (2007) 014, arXiv:hep-ph/0612029 [hep-ph].

[75] B. Bajc, M. Nemevsek, and G. Senjanovic, "Probing seesaw at LHC," *Phys. Rev.* **D76** (2007) 055011, arXiv:hep-ph/0703080 [hep-ph].

[76] I. Dorsner and P. Fileviez Perez, "Upper Bound on the Mass of the Type III Seesaw Triplet in an SU(5) Model," *JHEP* **06** (2007) 029, arXiv:hep-ph/0612216 [hep-ph].

[77] P. Fileviez Perez, "Supersymmetric Adjoint SU(5)," *Phys. Rev.* **D76** (2007) 071701, arXiv:0705.3589 [hep-ph].

[78] E. Fernandez-Martinez, J. Hernandez-Garcia, J. Lopez-Pavon, and M. Lucente, "Loop level constraints on Seesaw neutrino mixing," *JHEP* **10** (2015) 130, arXiv:1508.03051 [hep-ph].

[79] E. Fernandez-Martinez, J. Hernandez-Garcia, and J. Lopez-Pavon, "Global constraints on heavy neutrino mixing," *JHEP* **08** (2016) 033, arXiv:1605.08774 [hep-ph].

[80] M. Blennow, P. Coloma, E. Fernandez-Martinez, J. Hernandez-Garcia, and J. Lopez-Pavon, "Non-Unitarity, sterile neutrinos, and Non-Standard neutrino Interactions," *JHEP* **04** (2017) 153, arXiv:1609.08637 [hep-ph].

[81] Y. Nambu, "Quasiparticles and Gauge Invariance in the Theory of Superconductivity," *Phys. Rev.* **117** (1960) 648–663.

[82] J. Goldstone, "Field Theories with Superconductor Solutions," *Nuovo Cim.* **19** (1961) 154–164.

[83] J. Goldstone, A. Salam, and S. Weinberg, "Broken Symmetries," *Phys. Rev.* **127** (1962) 965–970.

[84] N. Cabibbo, "Unitary Symmetry and Leptonic Decays," *Phys. Rev. Lett.* **10**

(1963) 531–533. [,648(1963)].

[85] M. Kobayashi and T. Maskawa, "CP Violation in the Renormalizable Theory of Weak Interaction," *Prog. Theor. Phys.* **49** (1973) 652–657.

[86] B. Pontecorvo, "Mesonium and anti-mesonium," *Sov. Phys. JETP* **6** (1957) 429. [Zh. Eksp. Teor. Fiz.33,549(1957)].

[87] Z. Maki, M. Nakagawa, and S. Sakata, "Remarks on the unified model of elementary particles," *Prog. Theor. Phys.* **28** (1962) 870–880.

[88] B. Pontecorvo, "Neutrino Experiments and the Problem of Conservation of Leptonic Charge," *Sov. Phys. JETP* **26** (1968) 984–988. [Zh. Eksp. Teor. Fiz.53,1717(1967)].

[89] V. N. Gribov and B. Pontecorvo, "Neutrino astronomy and lepton charge," *Phys. Lett.* **28B** (1969) 493.

[90] L.-L. Chau and W.-Y. Keung, "Comments on the Parametrization of the Kobayashi-Maskawa Matrix," *Phys. Rev. Lett.* **53** (1984) 1802.

[91] C. Giunti, C. W. Kim, and U. W. Lee, "When do neutrinos really oscillate?: Quantum mechanics of neutrino oscillations," *Phys. Rev.* **D44** (1991) 3635–3640.

[92] C. Giunti, "Neutrino wave packets in quantum field theory," *JHEP* **11** (2002) 017, arXiv:hep-ph/0205014 [hep-ph].

[93] E. K. Akhmedov and J. Kopp, "Neutrino oscillations: Quantum mechanics vs. quantum field theory," *JHEP* **04** (2010) 008, arXiv:1001.4815 [hep-ph]. [Erratum: JHEP10,052(2013)].

[94] L. Wolfenstein, "Neutrino Oscillations in Matter," *Phys. Rev.* **D17** (1978) 2369–2374.

[95] S. P. Mikheev and A. Yu. Smirnov, "Resonance Amplification of Oscillations in Matter and Spectroscopy of Solar Neutrinos," *Sov. J. Nucl. Phys.* **42** (1985) 913–917. [Yad. Fiz.42,1441(1985)].

[96] I. Esteban, M. C. Gonzalez-Garcia, M. Maltoni, I. Martinez-Soler, and T. Schwetz, "Updated fit to three neutrino mixing: exploring the accelerator-reactor complementarity," *JHEP* **01** (2017) 087, arXiv:1611.01514 [hep-ph].

[97] C. Kraus *et al.*, "Final results from phase II of the Mainz neutrino mass search in tritium beta decay," *Eur. Phys. J.* **C40** (2005) 447–468, arXiv:hep-ex/0412056 [hep-ex].

[98] **Troitsk** Collaboration, V. N. Aseev *et al.*, "An upper limit on electron antineutrino mass from Troitsk experiment," *Phys. Rev.* **D84** (2011) 112003, arXiv:1108.5034 [hep-ex].

[99] S. Weinberg, "Baryon and Lepton Nonconserving Processes," *Phys.Rev.Lett.* **43** (1979) 1566–1570.

[100] K. S. Babu and V. S. Mathur, "Radiatively Induced Seesaw Mechanism for Neutrino Masses," *Phys. Rev.* **D38** (1988) 3550.

[101] K. S. Babu and E. Ma, "Natural Hierarchy of Radiatively Induced Majorana Neutrino Masses," *Phys. Rev. Lett.* **61** (1988) 674.

[102] A. Broncano, M. B. Gavela, and E. E. Jenkins, "The effective Lagrangian for the seesaw model of neutrino mass and leptogenesis," *Phys. Lett.* **B552** (2003) 177–184, arXiv:hep-ph/0210271.

[103] E. Fernandez-Martinez, M. B. Gavela, J. Lopez-Pavon, and O. Yasuda, "CP-violation from non-unitary leptonic mixing," *Phys. Lett.* **B649** (2007) 427–435, arXiv:hep-ph/0703098.

[104] R. E. Shrock, "New Tests For, and Bounds On, Neutrino Masses and Lepton Mixing," *Phys. Lett.* **B96** (1980) 159–164.

[105] R. E. Shrock, "General Theory of Weak Leptonic and Semileptonic Decays. 1. Leptonic Pseudoscalar Meson Decays, with Associated Tests For, and Bounds on, Neutrino Masses and Lepton Mixing," *Phys. Rev.* **D24** (1981) 1232.

[106] R. E. Shrock, "General Theory of Weak Processes Involving Neutrinos. 2. Pure Leptonic Decays," *Phys. Rev.* **D24** (1981) 1275.

[107] P. Langacker and D. London, "Mixing Between Ordinary and Exotic Fermions," *Phys.Rev.* **D38** (1988) 886.

[108] S. M. Bilenky and C. Giunti, "Seesaw type mixing and $\nu_\mu \to \nu_\tau$ oscillations," *Phys.Lett.* **B300** (1993) 137–140, arXiv:hep-ph/9211269 [hep-ph].

[109] E. Nardi, E. Roulet, and D. Tommasini, "Limits on neutrino mixing with new heavy particles," *Phys.Lett.* **B327** (1994) 319–326, arXiv:hep-ph/9402224 [hep-ph].

[110] D. Tommasini, G. Barenboim, J. Bernabeu, and C. Jarlskog, "Nondecoupling of heavy neutrinos and lepton flavor violation," *Nucl.Phys.* **B444** (1995) 451–467, arXiv:hep-ph/9503228 [hep-ph].

[111] S. Antusch, C. Biggio, E. Fernandez-Martinez, M. Gavela, and J. Lopez-Pavon, "Unitarity of the Leptonic Mixing Matrix," *JHEP* **0610**

(2006) 084, arXiv:hep-ph/0607020 [hep-ph].

[112] S. Antusch, J. P. Baumann, and E. Fernandez-Martinez, "Non-Standard Neutrino Interactions with Matter from Physics Beyond the Standard Model," *Nucl.Phys.* **B810** (2009) 369–388, arXiv:0807.1003 [hep-ph].

[113] C. Biggio, "The Contribution of fermionic seesaws to the anomalous magnetic moment of leptons," *Phys. Lett.* **B668** (2008) 378–384, arXiv:0806.2558 [hep-ph].

[114] R. Alonso, M. Dhen, M. Gavela, and T. Hambye, "Muon conversion to electron in nuclei in type-I seesaw models," *JHEP* **1301** (2013) 118, arXiv:1209.2679 [hep-ph].

[115] E. Akhmedov, A. Kartavtsev, M. Lindner, L. Michaels, and J. Smirnov, "Improving Electro-Weak Fits with TeV-scale Sterile Neutrinos," *JHEP* **1305** (2013) 081, arXiv:1302.1872 [hep-ph].

[116] S. Antusch and O. Fischer, "Non-unitarity of the leptonic mixing matrix: Present bounds and future sensitivities," *JHEP* **1410** (2014) 94, arXiv:1407.6607 [hep-ph].

[117] A. Abada and T. Toma, "Electric Dipole Moments of Charged Leptons with Sterile Fermions," *JHEP* **02** (2016) 174, arXiv:1511.03265 [hep-ph].

[118] A. Abada and T. Toma, "Electron electric dipole moment in Inverse Seesaw models," arXiv:1605.07643 [hep-ph].

[119] M. Blennow and E. Fernandez-Martinez, "Parametrization of Seesaw Models and Light Sterile Neutrinos," *Phys.Lett.* **B704** (2011) 223–229, arXiv:1107.3992 [hep-ph].

[120] A. Broncano, M. B. Gavela, and E. E. Jenkins, "Neutrino Physics in the Seesaw Model," *Nucl. Phys.* **B672** (2003) 163–198, arXiv:hep-ph/0307058.

[121] S. Antusch, S. Blanchet, M. Blennow, and E. Fernandez-Martinez, "Non-unitary Leptonic Mixing and Leptogenesis," *JHEP* **01** (2010) 017, arXiv:0910.5957 [hep-ph].

[122] J. Kersten and A. Y. Smirnov, "Right-Handed Neutrinos at CERN LHC and the Mechanism of Neutrino Mass Generation," *Phys.Rev.* **D76** (2007) 073005, arXiv:0705.3221 [hep-ph].

[123] A. Abada, C. Biggio, F. Bonnet, M. B. Gavela, and T. Hambye, "Low energy effects of neutrino masses," *JHEP* **12** (2007) 061, arXiv:0707.4058 [hep-ph].

[124] R. Adhikari and A. Raychaudhuri, "Light neutrinos from massless texture and below TeV seesaw scale," *Phys. Rev.* **D84** (2011) 033002, arXiv:1004.5111 [hep-ph].

[125] S. Antusch and O. Fischer, "Testing sterile neutrino extensions of the Standard Model at future lepton colliders," *JHEP* **05** (2015) 053, arXiv:1502.05915 [hep-ph].

[126] C.-H. Lee, P. S. Bhupal Dev, and R. N. Mohapatra, "Natural TeV-scale left-right seesaw mechanism for neutrinos and experimental tests," *Phys. Rev.* **D88** no. 9, (2013) 093010, arXiv:1309.0774 [hep-ph].

[127] M. Gonzalez-Garcia, M. Maltoni, and T. Schwetz, "Updated fit to three neutrino mixing: status of leptonic CP violation," *JHEP* **1411** (2014) 052, arXiv:1409.5439 [hep-ph].

[128] **Particle Data Group** Collaboration, K. A. Olive *et al.*, "Review of Particle Physics," *Chin. Phys.* **C38** (2014) 090001.

[129] **SLD Electroweak Group, DELPHI, ALEPH, SLD, SLD Heavy Flavour Group, OPAL, LEP Electroweak Working Group, L3** Collaboration, S. Schael *et al.*, "Precision electroweak measurements on the Z resonance," *Phys. Rept.* **427** (2006) 257–454, arXiv:hep-ex/0509008 [hep-ex].

[130] A. Pich, "Precision Tau Physics," *Prog. Part. Nucl. Phys.* **75** (2014) 41–85, arXiv:1310.7922 [hep-ph].

[131] J. C. Hardy and I. S. Towner, "Superallowed $0^+ \to 0^+$ nuclear decays: 2014 critical survey, with precise results for V_{ud} and CKM unitarity," *Phys. Rev.* **C91** no. 2, (2015) 025501, arXiv:1411.5987 [nucl-ex].

[132] S. Aoki *et al.*, "Review of lattice results concerning low-energy particle physics," *Eur. Phys. J.* **C74** (2014) 2890, arXiv:1310.8555 [hep-lat].

[133] **FlaviaNet Working Group on Kaon Decays** Collaboration, M. Antonelli *et al.*, "An Evaluation of $|V_{us}|$ and precise tests of the Standard Model from world data on leptonic and semileptonic kaon decays," *Eur. Phys. J.* **C69** (2010) 399–424, arXiv:1005.2323 [hep-ph].

[134] M. Moulson, "Experimental determination of V_{us} from kaon decays," in *8th International Workshop on the CKM Unitarity Triangle (CKM2014) Vienna, Austria, September 8-12, 2014*. 2014. arXiv:1411.5252 [hep-ex]. http://inspirehep.net/record/1328784/files/arXiv:1411.5252.pdf.

[135] **Heavy Flavor Averaging Group (HFAG)** Collaboration, Y. Amhis *et al.*, "Averages of b-hadron, c-hadron, and τ-lepton properties as of summer 2014," arXiv:1412.7515 [hep-ex].

[136] S. L. Glashow, J. Iliopoulos, and L. Maiani, "Weak Interactions with Lepton-Hadron Symmetry," *Phys. Rev.* **D2** (1970) 1285–1292.

[137] **CMS** Collaboration, V. Khachatryan *et al.*, "Search for Lepton-Flavour-Violating Decays of the Higgs Boson," *Phys. Lett.* **B749** (2015) 337–362, arXiv:1502.07400 [hep-ex].

[138] **ATLAS** Collaboration, G. Aad *et al.*, "Search for lepton-flavour-violating $H \to \tau\mu$ decays of the Higgs boson with the ATLAS detector," *JHEP* **11** (2015) 211, arXiv:1508.03372 [hep-ex].

[139] A. M. Baldini *et al.*, "MEG Upgrade Proposal," arXiv:1301.7225 [physics.ins-det].

[140] **SuperB** Collaboration, M. Bona *et al.*, "SuperB: A High-Luminosity Asymmetric e^+e^- Super Flavor Factory. Conceptual Design Report," arXiv:0709.0451 [hep-ex].

[141] **ATLAS** Collaboration, G. Aad *et al.*, "Search for the lepton flavor violating decay $Z \to e\mu$ in pp collisions at $\sqrt{s}$TeV with the ATLAS detector," *Phys. Rev.* **D90** no. 7, (2014) 072010, arXiv:1408.5774 [hep-ex].

[142] A. Abada, V. De Romeri, S. Monteil, J. Orloff, and A. M. Teixeira, "Indirect searches for sterile neutrinos at a high-luminosity $Z-$factory," *JHEP* **04** (2015) 051, arXiv:1412.6322 [hep-ph].

[143] **L3** Collaboration, O. Adriani *et al.*, "Search for lepton flavor violation in Z decays," *Phys. Lett.* **B316** (1993) 427–434.

[144] **OPAL** Collaboration, R. Akers *et al.*, "A Search for lepton flavor violating Z^0-decays," *Z. Phys.* **C67** (1995) 555–564.

[145] **DELPHI** Collaboration, P. Abreu *et al.*, "Search for lepton flavor number violating Z^0-decays," *Z. Phys.* **C73** (1997) 243–251.

[146] **CMS** Collaboration, C. Collaboration, "Search for lepton-flavour-violating decays of the Higgs boson to etau and emu at $\sqrt{s} = 8$ TeV,".

[147] **SINDRUM** Collaboration, U. Bellgardt *et al.*, "Search for the Decay $\mu^+ \to e^+e^+e^-$," *Nucl. Phys.* **B299** (1988) 1–6.

[148] A. Blondel *et al.*, "Research Proposal for an Experiment to Search for the Decay $\mu \to eee$," arXiv:1301.6113 [physics.ins-det].

[149] K. Hayasaka *et al.*, "Search for Lepton Flavor Violating τ Decays into Three Leptons with 719 Million Produced $\tau^+\tau^-$ Pairs," *Phys. Lett.* **B687** (2010) 139–143, arXiv:1001.3221 [hep-ex].

[150] R. K. Kutschke, "The Mu2e Experiment at Fermilab," in *Proceedings, 31st International Conference on Physics in collisions (PIC 2011)*. 2011. arXiv:1112.0242 [hep-ex]. http://inspirehep.net/record/1079590/files/arXiv:1112.0242.pdf.

[151] **SINDRUM II** Collaboration, C. Dohmen *et al.*, "Test of lepton flavor conservation in $\mu \to e$ conversion on titanium," *Phys. Lett.* **B317** (1993) 631–636.

[152] R. J. Barlow, "Tau lepton physics. Proceedings, 11th International Workshop, TAU 2010, Manchester, UK, September 13-17, 2010," *Nucl. Phys. Proc. Suppl.* **218** (2011) 44–49.

[153] J. I. Illana, M. Jack, and T. Riemann, "Predictions for $Z \to \mu\tau$ and related reactions," in *5th Workshop of the 2nd ECFA - DESY Study on Physics and Detectors for a Linear Electron - Positron Collider Obernai, France, October 16-19, 1999*, pp. 490–524. 1999. arXiv:hep-ph/0001273 [hep-ph]. http://www-library.desy.de/cgi-bin/showprep.pl?LC-TH-2000-007. [,490(1999)].

[154] A. Pilaftsis, "Lepton flavor nonconservation in H^0 decays," *Phys. Lett.* **B285** (1992) 68–74.

[155] E. Arganda, A. M. Curiel, M. J. Herrero, and D. Temes, "Lepton flavor violating Higgs boson decays from massive seesaw neutrinos," *Phys. Rev.* **D71** (2005) 035011, arXiv:hep-ph/0407302 [hep-ph].

[156] E. Arganda, M. J. Herrero, X. Marcano, and C. Weiland, "Imprints of massive inverse seesaw model neutrinos in lepton flavor violating Higgs boson decays," *Phys. Rev.* **D91** no. 1, (2015) 015001, arXiv:1405.4300 [hep-ph].

[157] A. Ilakovac and A. Pilaftsis, "Flavor violating charged lepton decays in seesaw-type models," *Nucl. Phys.* **B437** (1995) 491, arXiv:hep-ph/9403398 [hep-ph].

[158] R. Kitano, M. Koike, and Y. Okada, "Detailed calculation of lepton flavor violating muon electron conversion rate for various nuclei," *Phys. Rev.* **D66** (2002) 096002, arXiv:hep-ph/0203110 [hep-ph]. [Erratum: Phys. Rev.D76,059902(2007)].

[159] T. Suzuki, D. F. Measday, and J. P. Roalsvig, "Total Nuclear Capture Rates for Negative Muons," *Phys. Rev.* **C35** (1987) 2212.

[160] T. Ohlsson, "Status of non-standard neutrino interactions," *Rept. Prog. Phys.* **76** (2013) 044201, arXiv:1209.2710 [hep-ph].

[161] Z.-z. Xing, "Correlation between the Charged Current Interactions of Light and Heavy Majorana Neutrinos," *Phys. Lett.* **B660** (2008) 515–521, arXiv:0709.2220 [hep-ph].

[162] Z.-z. Xing, "A full parametrization of the 6×6 flavor mixing matrix in the presence of three light or heavy sterile neutrinos," *Phys. Rev.* **D85** (2012) 013008, arXiv:1110.0083 [hep-ph].

[163] F. J. Escrihuela, D. V. Forero, O. G. Miranda, M. Tortola, and J. W. F. Valle, "On the description of non-unitary neutrino mixing," arXiv:1503.08879 [hep-ph].

[164] S. Antusch, M. Blennow, E. Fernandez-Martinez, and J. Lopez-Pavon, "Probing non-unitary mixing and CP-violation at a Neutrino Factory," *Phys. Rev.* **D80** (2009) 033002, arXiv:0903.3986 [hep-ph].

[165] S. Parke and M. Ross-Lonergan, "Unitarity and the Three Flavour Neutrino Mixing Matrix," arXiv:1508.05095 [hep-ph].

[166] O. G. Miranda, M. Tortola, and J. W. F. Valle, "New ambiguity in probing CP violation in neutrino oscillations," arXiv:1604.05690 [hep-ph].

[167] S.-F. Ge, P. Pasquini, M. Tortola, and J. W. F. Valle, "Measuring the Leptonic CP Phase in Neutrino Oscillations with Non-Unitary Mixing," arXiv:1605.01670 [hep-ph].

[168] S. Geer, "Neutrino beams from muon storage rings: Characteristics and physics potential," *Phys. Rev.* **D57** (1998) 6989–6997, arXiv:hep-ph/9712290 [hep-ph]. [Erratum: Phys. Rev.D59,039903(1999)].

[169] A. De Rujula, M. B. Gavela, and P. Hernandez, "Neutrino oscillation physics with a neutrino factory," *Nucl. Phys.* **B547** (1999) 21–38, arXiv:hep-ph/9811390 [hep-ph].

[170] A. Atre, T. Han, S. Pascoli, and B. Zhang, "The Search for Heavy Majorana Neutrinos," *JHEP* **05** (2009) 030, arXiv:0901.3589 [hep-ph].

[171] O. Ruchayskiy and A. Ivashko, "Experimental bounds on sterile neutrino mixing angles," *JHEP* **06** (2012) 100, arXiv:1112.3319 [hep-ph].

[172] M. Drewes and B. Garbrecht, "Experimental and cosmological constraints on

heavy neutrinos," arXiv:1502.00477 [hep-ph].

[173] A. de Gouvêa and A. Kobach, "Global Constraints on a Heavy Neutrino," *Phys. Rev.* **D93** no. 3, (2016) 033005, arXiv:1511.00683 [hep-ph].

[174] F. F. Deppisch, P. S. Bhupal Dev, and A. Pilaftsis, "Neutrinos and Collider Physics," *New J. Phys.* **17** no. 7, (2015) 075019, arXiv:1502.06541 [hep-ph].

[175] A. D. Dolgov and F. L. Villante, "BBN bounds on active sterile neutrino mixing," *Nucl. Phys.* **B679** (2004) 261–298, arXiv:hep-ph/0308083 [hep-ph].

[176] M. Cirelli, G. Marandella, A. Strumia, and F. Vissani, "Probing oscillations into sterile neutrinos with cosmology, astrophysics and experiments," *Nucl. Phys.* **B708** (2005) 215–267, arXiv:hep-ph/0403158 [hep-ph].

[177] A. Melchiorri, O. Mena, S. Palomares-Ruiz, S. Pascoli, A. Slosar, and M. Sorel, "Sterile Neutrinos in Light of Recent Cosmological and Oscillation Data: A Multi-Flavor Scheme Approach," *JCAP* **0901** (2009) 036, arXiv:0810.5133 [hep-ph].

[178] S. Hannestad, I. Tamborra, and T. Tram, "Thermalisation of light sterile neutrinos in the early universe," *JCAP* **1207** (2012) 025, arXiv:1204.5861 [astro-ph.CO].

[179] O. Ruchayskiy and A. Ivashko, "Restrictions on the lifetime of sterile neutrinos from primordial nucleosynthesis," *JCAP* **1210** (2012) 014, arXiv:1202.2841 [hep-ph].

[180] A. Mirizzi, N. Saviano, G. Miele, and P. D. Serpico, "Light sterile neutrino production in the early universe with dynamical neutrino asymmetries," *Phys. Rev.* **D86** (2012) 053009, arXiv:1206.1046 [hep-ph].

[181] T. D. Jacques, L. M. Krauss, and C. Lunardini, "Additional Light Sterile Neutrinos and Cosmology," *Phys. Rev.* **D87** no. 8, (2013) 083515, arXiv:1301.3119 [astro-ph.CO]. [Erratum: Phys. Rev.D88,no.10,109901(2013)].

[182] N. Saviano, A. Mirizzi, O. Pisanti, P. D. Serpico, G. Mangano, and G. Miele, "Multi-momentum and multi-flavour active-sterile neutrino oscillations in the early universe: role of neutrino asymmetries and effects on nucleosynthesis," *Phys. Rev.* **D87** (2013) 073006, arXiv:1302.1200 [astro-ph.CO].

[183] M. Archidiacono, N. Fornengo, C. Giunti, S. Hannestad, and A. Melchiorri,

"Sterile neutrinos: Cosmology versus short-baseline experiments," *Phys. Rev.* **D87** no. 12, (2013) 125034, arXiv:1302.6720 [astro-ph.CO].

[184] A. Mirizzi, G. Mangano, N. Saviano, E. Borriello, C. Giunti, G. Miele, and O. Pisanti, "The strongest bounds on active-sterile neutrino mixing after Planck data," *Phys. Lett.* **B726** (2013) 8–14, arXiv:1303.5368 [astro-ph.CO].

[185] P. Hernandez, M. Kekic, and J. Lopez-Pavon, "Low-scale seesaw models versus N_{eff}," *Phys. Rev.* **D89** no. 7, (2014) 073009, arXiv:1311.2614 [hep-ph].

[186] A. C. Vincent, E. F. Martinez, P. Hernández, M. Lattanzi, and O. Mena, "Revisiting cosmological bounds on sterile neutrinos," *JCAP* **1504** no. 04, (2015) 006, arXiv:1408.1956 [astro-ph.CO].

[187] P. Hernandez, M. Kekic, and J. Lopez-Pavon, "$N_{\rm eff}$ in low-scale seesaw models versus the lightest neutrino mass," *Phys. Rev.* **D90** no. 6, (2014) 065033, arXiv:1406.2961 [hep-ph].

[188] S. Antusch and O. Fischer, "Probing the non-unitarity of the leptonic mixing matrix at the CEPC," arXiv:1604.00208 [hep-ph].

[189] S. Antusch, E. Cazzato, and O. Fischer, "Displaced vertex searches for sterile neutrinos at future lepton colliders," arXiv:1604.02420 [hep-ph].

[190] J. Schechter and J. W. F. Valle, "Neutrino Decay and Spontaneous Violation of Lepton Number," *Phys. Rev.* **D25** (1982) 774.

[191] A. Donini, P. Hernandez, J. Lopez-Pavon, M. Maltoni, and T. Schwetz, "The minimal 3+2 neutrino model versus oscillation anomalies," *JHEP* **07** (2012) 161, arXiv:1205.5230 [hep-ph].

[192] R. Mohapatra and J. Valle, "Neutrino Mass and Baryon Number Nonconservation in Superstring Models," *Phys.Rev.* **D34** (1986) 1642.

[193] J. Bernabeu, A. Santamaria, J. Vidal, A. Mendez, and J. Valle, "Lepton Flavor Nonconservation at High-Energies in a Superstring Inspired Standard Model," *Phys.Lett.* **B187** (1987) 303.

[194] M. Malinsky, J. Romao, and J. Valle, "Novel supersymmetric SO(10) seesaw mechanism," *Phys.Rev.Lett.* **95** (2005) 161801, arXiv:hep-ph/0506296 [hep-ph].

[195] J. Lopez-Pavon, S. Pascoli, and C.-f. Wong, "Can heavy neutrinos dominate neutrinoless double beta decay?," *Phys.Rev.* **D87** no. 9, (2013) 093007,

arXiv:1209.5342 [hep-ph].

[196] M. B. Gavela, T. Hambye, D. Hernandez, and P. Hernandez, "Minimal Flavour Seesaw Models," *JHEP* **09** (2009) 038, arXiv:0906.1461 [hep-ph].

[197] H. Zhang and S. Zhou, "The Minimal Seesaw Model at the TeV Scale," *Phys. Lett.* **B685** (2010) 297–301, arXiv:0912.2661 [hep-ph].

[198] M. Malinsky, T. Ohlsson, Z.-z. Xing, and H. Zhang, "Non-unitary neutrino mixing and CP violation in the minimal inverse seesaw model," *Phys. Lett.* **B679** (2009) 242–248, arXiv:0905.2889 [hep-ph].

[199] A. Ibarra, E. Molinaro, and S. T. Petcov, "TeV Scale See-Saw Mechanisms of Neutrino Mass Generation, the Majorana Nature of the Heavy Singlet Neutrinos and $(\beta\beta)_{-}0\nu$-Decay," *JHEP* **09** (2010) 108, arXiv:1007.2378 [hep-ph].

[200] A. Ibarra, E. Molinaro, and S. T. Petcov, "Low Energy Signatures of the TeV Scale See-Saw Mechanism," *Phys. Rev.* **D84** (2011) 013005, arXiv:1103.6217 [hep-ph].

[201] C. G. Cely, A. Ibarra, E. Molinaro, and S. T. Petcov, "Higgs Decays in the Low Scale Type I See-Saw Model," *Phys. Lett.* **B718** (2013) 957–964, arXiv:1208.3654 [hep-ph].

[202] J. A. Casas and A. Ibarra, "Oscillating neutrinos and $\mu \to e, \gamma$," *Nucl. Phys.* **B618** (2001) 171–204, arXiv:hep-ph/0103065.

[203] J. A. Casas, J. M. Moreno, N. Rius, R. Ruiz de Austri, and B. Zaldivar, "Fair scans of the seesaw. Consequences for predictions on LFV processes," *JHEP* **03** (2011) 034, arXiv:1010.5751 [hep-ph].

[204] J. Lopez-Pavon, E. Molinaro, and S. T. Petcov, "Radiative Corrections to Light Neutrino Masses in Low Scale Type I Seesaw Scenarios and Neutrinoless Double Beta Decay," arXiv:1506.05296 [hep-ph].

[205] J. M. Cornwall, D. N. Levin, and G. Tiktopoulos, "Derivation of Gauge Invariance from High-Energy Unitarity Bounds on the s Matrix," *Phys. Rev.* **D10** (1974) 1145. [Erratum: Phys. Rev.D11,972(1975)].

[206] R. Decker and M. Finkemeier, "Short and long distance effects in the decay $\tau \to \pi\nu_\tau(\gamma)$," *Nucl. Phys.* **B438** (1995) 17–53, arXiv:hep-ph/9403385 [hep-ph].

[207] A. Gelman and D. B. Rubin, "Inference from Iterative Simulation Using Multiple Sequences," *Statist.Sci.* **7** (1992) 457–472.

[208] M. Blennow and E. Fernandez-Martinez, "Neutrino oscillation parameter sampling with MonteCUBES," *Comput.Phys.Commun.* **181** (2010) 227–231, arXiv:0903.3985 [hep-ph].

[209] W. Loinaz, N. Okamura, T. Takeuchi, and L. Wijewardhana, "The NuTeV anomaly, neutrino mixing, and a heavy Higgs boson," *Phys.Rev.* **D67** (2003) 073012, arXiv:hep-ph/0210193 [hep-ph].

[210] W. Loinaz, N. Okamura, S. Rayyan, T. Takeuchi, and L. Wijewardhana, "The NuTeV anomaly, lepton universality, and nonuniversal neutrino gauge couplings," *Phys.Rev.* **D70** (2004) 113004, arXiv:hep-ph/0403306 [hep-ph].

[211] **SLD Heavy Flavor Group, DELPHI, ALEPH, OPAL, LEP Electroweak Working Group, L3 Collaborations** Collaboration, LEP, "A Combination of preliminary electroweak measurements and constraints on the standard model," arXiv:hep-ex/0212036 [hep-ex].

[212] A. Pilaftsis, "Radiatively induced neutrino masses and large Higgs neutrino couplings in the standard model with Majorana fields," *Z. Phys.* **C55** (1992) 275–282, arXiv:hep-ph/9901206 [hep-ph].

[213] W. Grimus and L. Lavoura, "One-loop corrections to the seesaw mechanism in the multi-Higgs-doublet standard model," *Phys. Lett.* **B546** (2002) 86–95, arXiv:hep-ph/0207229 [hep-ph].

[214] D. Aristizabal Sierra and C. E. Yaguna, "On the importance of the 1-loop finite corrections to seesaw neutrino masses," *JHEP* **08** (2011) 013, arXiv:1106.3587 [hep-ph].

[215] P. S. B. Dev and A. Pilaftsis, "Minimal Radiative Neutrino Mass Mechanism for Inverse Seesaw Models," *Phys. Rev.* **D86** (2012) 113001, arXiv:1209.4051 [hep-ph].

[216] **LSND** Collaboration, A. Aguilar *et al.*, "Evidence for neutrino oscillations from the observation of $\overline{\nu}_e$ appearance in a $\overline{\nu}_\mu$ beam," *Phys. Rev.* **D64** (2001) 112007, arXiv:hep-ex/0104049.

[217] **MiniBooNE** Collaboration, A. A. Aguilar-Arevalo *et al.*, "Improved Search for $\bar{\nu}_\mu \to \bar{\nu}_e$ Oscillations in the MiniBooNE Experiment," *Phys. Rev. Lett.* **110** (2013) 161801, arXiv:1303.2588 [hep-ex].

[218] G. Mention, M. Fechner, T. Lasserre, T. Mueller, D. Lhuillier, *et al.*, "The Reactor Antineutrino Anomaly," *Phys.Rev.* **D83** (2011) 073006,

arXiv:1101.2755 [hep-ex].

[219] P. Huber, "On the determination of anti-neutrino spectra from nuclear reactors," arXiv:1106.0687 [hep-ph].

[220] J. Kopp, P. A. N. Machado, M. Maltoni, and T. Schwetz, "Sterile Neutrino Oscillations: The Global Picture," *JHEP* **05** (2013) 050, arXiv:1303.3011 [hep-ph].

[221] C. Giunti, "Light Sterile Neutrinos: Status and Perspectives," *Nucl. Phys.* **B908** (2016) 336–353, arXiv:1512.04758 [hep-ph].

[222] G. H. Collin, C. A. Argüelles, J. M. Conrad, and M. H. Shaevitz, "Sterile Neutrino Fits to Short Baseline Data," *Nucl. Phys.* **B908** (2016) 354–365, arXiv:1602.00671 [hep-ph].

[223] S. Choubey and D. Pramanik, "Constraints on Sterile Neutrino Oscillations using DUNE Near Detector," *Phys. Lett.* **B764** (2017) 135–141, arXiv:1604.04731 [hep-ph].

[224] **LAr1-ND, ICARUS-WA104, MicroBooNE** Collaboration, M. Antonello *et al.*, "A Proposal for a Three Detector Short-Baseline Neutrino Oscillation Program in the Fermilab Booster Neutrino Beam," arXiv:1503.01520 [physics.ins-det].

[225] Y.-F. Li and S. Luo, "Neutrino Oscillation Probabilities in Matter with Direct and Indirect Unitarity Violation in the Lepton Mixing Matrix," *Phys. Rev.* **D93** no. 3, (2016) 033008, arXiv:1508.00052 [hep-ph].

[226] D. V. Forero, S. Morisi, M. Tortola, and J. W. F. Valle, "Lepton flavor violation and non-unitary lepton mixing in low-scale type-I seesaw," *JHEP* **09** (2011) 142, arXiv:1107.6009 [hep-ph].

[227] Y. Declais, J. Favier, A. Metref, H. Pessard, B. Achkar, *et al.*, "Search for neutrino oscillations at 15-meters, 40-meters, and 95-meters from a nuclear power reactor at Bugey," *Nucl.Phys.* **B434** (1995) 503–534.

[228] **Super-Kamiokande** Collaboration, K. Abe *et al.*, "Limits on sterile neutrino mixing using atmospheric neutrinos in Super-Kamiokande," *Phys. Rev.* **D91** (2015) 052019, arXiv:1410.2008 [hep-ex].

[229] **MINOS** Collaboration, P. Adamson *et al.*, "A search for sterile neutrinos mixing with muon neutrinos in MINOS," *Submitted to: Phys. Rev. Lett.* (2016) , arXiv:1607.01176 [hep-ex].

[230] **NOMAD** Collaboration, P. Astier *et al.*, "Search for nu(mu) —¿ nu(e)

oscillations in the NOMAD experiment," *Phys. Lett.* **B570** (2003) 19–31, arXiv:hep-ex/0306037 [hep-ex].

[231] **NOMAD** Collaboration, P. Astier *et al.*, "Final NOMAD results on muon-neutrino —¿ tau-neutrino and electron-neutrino —¿ tau-neutrino oscillations including a new search for tau-neutrino appearance using hadronic tau decays," *Nucl. Phys.* **B611** (2001) 3–39, arXiv:hep-ex/0106102 [hep-ex].

[232] D. Dutta, R. Gandhi, B. Kayser, M. Masud, and S. Prakash, "Capabilities of long-baseline experiments in the presence of a sterile neutrino," arXiv:1607.02152 [hep-ph].

[233] P. Huber, M. Lindner, and W. Winter, "Simulation of long-baseline neutrino oscillation experiments with GLoBES (General Long Baseline Experiment Simulator)," *Comput. Phys. Commun.* **167** (2005) 195, arXiv:hep-ph/0407333 [hep-ph].

[234] P. Huber, J. Kopp, M. Lindner, M. Rolinec, and W. Winter, "New features in the simulation of neutrino oscillation experiments with GLoBES 3.0: General Long Baseline Experiment Simulator," *Comput. Phys. Commun.* **177** (2007) 432–438, arXiv:hep-ph/0701187 [hep-ph].

[235] **DUNE** Collaboration, T. Alion *et al.*, "Experiment Simulation Configurations Used in DUNE CDR," arXiv:1606.09550 [physics.ins-det].

[236] A. M. Dziewonski and D. L. Anderson, "Preliminary reference earth model," *Phys. Earth Planet. Interiors* **25** (1981) 297–356.

[237] S. Verma and S. Bhardwaj, "Probing Non-unitary CP Violation effects in Neutrino Oscillation Experiments," arXiv:1609.06412 [hep-ph].

[238] D. Dutta, P. Ghoshal, and S. Roy, "Effect of Non Unitarity on Neutrino Mass Hierarchy determination at DUNE, NOνA and T2K," arXiv:1609.07094 [hep-ph].

[239] D. Meloni, T. Ohlsson, W. Winter, and H. Zhang, "Non-standard interactions versus non-unitary lepton flavor mixing at a neutrino factory," *JHEP* **04** (2010) 041, arXiv:0912.2735 [hep-ph].

[240] J. M. Berryman, A. de Gouvêa, K. J. Kelly, and A. Kobach, "Sterile neutrino at the Deep Underground Neutrino Experiment," *Phys. Rev.* **D92** no. 7, (2015) 073012, arXiv:1507.03986 [hep-ph].

[241] S. K. Agarwalla, S. S. Chatterjee, and A. Palazzo, "Physics Reach of DUNE with a Light Sterile Neutrino," *JHEP* **09** (2016) 016, arXiv:1603.03759 [hep-ph].

[242] S. K. Agarwalla, S. S. Chatterjee, and A. Palazzo, "Octant of θ_{23} in danger with a light sterile neutrino," arXiv:1605.04299 [hep-ph].

[243] P. Coloma, "Non-Standard Interactions in propagation at the Deep Underground Neutrino Experiment," *JHEP* **03** (2016) 016, arXiv:1511.06357 [hep-ph].

[244] A. de Gouvêa and K. J. Kelly, "Non-standard Neutrino Interactions at DUNE," *Nucl. Phys.* **B908** (2016) 318–335, arXiv:1511.05562 [hep-ph].

[245] M. Blennow, S. Choubey, T. Ohlsson, D. Pramanik, and S. K. Raut, "A combined study of source, detector and matter non-standard neutrino interactions at DUNE," *JHEP* **08** (2016) 090, arXiv:1606.08851 [hep-ph].

[246] S. K. Agarwalla, S. S. Chatterjee, and A. Palazzo, "Degeneracy between θ_{23} octant and neutrino non-standard interactions at DUNE," arXiv:1607.01745 [hep-ph].

[247] M. Masud and P. Mehta, "Nonstandard interactions and resolving the ordering of neutrino masses at DUNE and other long baseline experiments," *Phys. Rev.* **D94** no. 5, (2016) 053007, arXiv:1606.05662 [hep-ph].

[248] M. Masud and P. Mehta, "Nonstandard interactions spoiling the CP violation sensitivity at DUNE and other long baseline experiments," *Phys. Rev.* **D94** (2016) 013014, arXiv:1603.01380 [hep-ph].

[249] M. Masud, A. Chatterjee, and P. Mehta, "Probing CP violation signal at DUNE in presence of non-standard neutrino interactions," *J. Phys.* **G43** no. 9, (2016) 095005, arXiv:1510.08261 [hep-ph].

[250] P. Coloma and T. Schwetz, "Generalized mass ordering degeneracy in neutrino oscillation experiments," *Phys. Rev.* **D94** no. 5, (2016) 055005, arXiv:1604.05772 [hep-ph]. [Erratum: Phys. Rev.D95,no.7,079903(2017)].

[251] V. De Romeri, E. Fernandez-Martinez, and M. Sorel, "Neutrino oscillations at DUNE with improved energy reconstruction," arXiv:1607.00293 [hep-ph].

[252] G. Passarino and M. J. G. Veltman, "One Loop Corrections for e^+e^- Annihilation Into $\mu^+\mu^-$ in the Weinberg Model," *Nucl. Phys.* **B160** (1979) 151.

[253] R. K. Ellis, Z. Kunszt, K. Melnikov, and G. Zanderighi, "One-loop

calculations in quantum field theory: from Feynman diagrams to unitarity cuts," *Phys. Rept.* **518** (2012) 141–250, arXiv:1105.4319 [hep-ph].

[254] M. E. Peskin and T. Takeuchi, "A New constraint on a strongly interacting Higgs sector," *Phys. Rev. Lett.* **65** (1990) 964–967.

[255] M. E. Peskin and T. Takeuchi, "Estimation of oblique electroweak corrections," *Phys. Rev.* **D46** (1992) 381–409.

[256] **KARMEN** Collaboration, B. Armbruster *et al.*, "Upper limits for neutrino oscillations muon-anti-neutrino —¿ electron-anti-neutrino from muon decay at rest," *Phys. Rev.* **D65** (2002) 112001, arXiv:hep-ex/0203021 [hep-ex].

[257] **NuTeV** Collaboration, S. Avvakumov *et al.*, "A Search for $\nu_\mu \to \nu_e$ and $\overline{\nu}_\mu \to \overline{\nu}_e$ oscillations at NuTeV," *Phys. Rev. Lett.* **89** (2002) 011804, arXiv:hep-ex/0203018 [hep-ex].

[258] **Daya Bay** Collaboration, F. P. An *et al.*, "Improved Search for a Light Sterile Neutrino with the Full Configuration of the Daya Bay Experiment," *Phys. Rev. Lett.* **117** no. 15, (2016) 151802, arXiv:1607.01174 [hep-ex].

[259] **MINOS** Collaboration, P. Adamson *et al.*, "Active to sterile neutrino mixing limits from neutral-current interactions in MINOS," *Phys. Rev. Lett.* **107** (2011) 011802, arXiv:1104.3922 [hep-ex].

[260] G. H. Collin, C. A. Argüelles, J. M. Conrad, and M. H. Shaevitz, "First Constraints on the Complete Neutrino Mixing Matrix with a Sterile Neutrino," arXiv:1607.00011 [hep-ph].